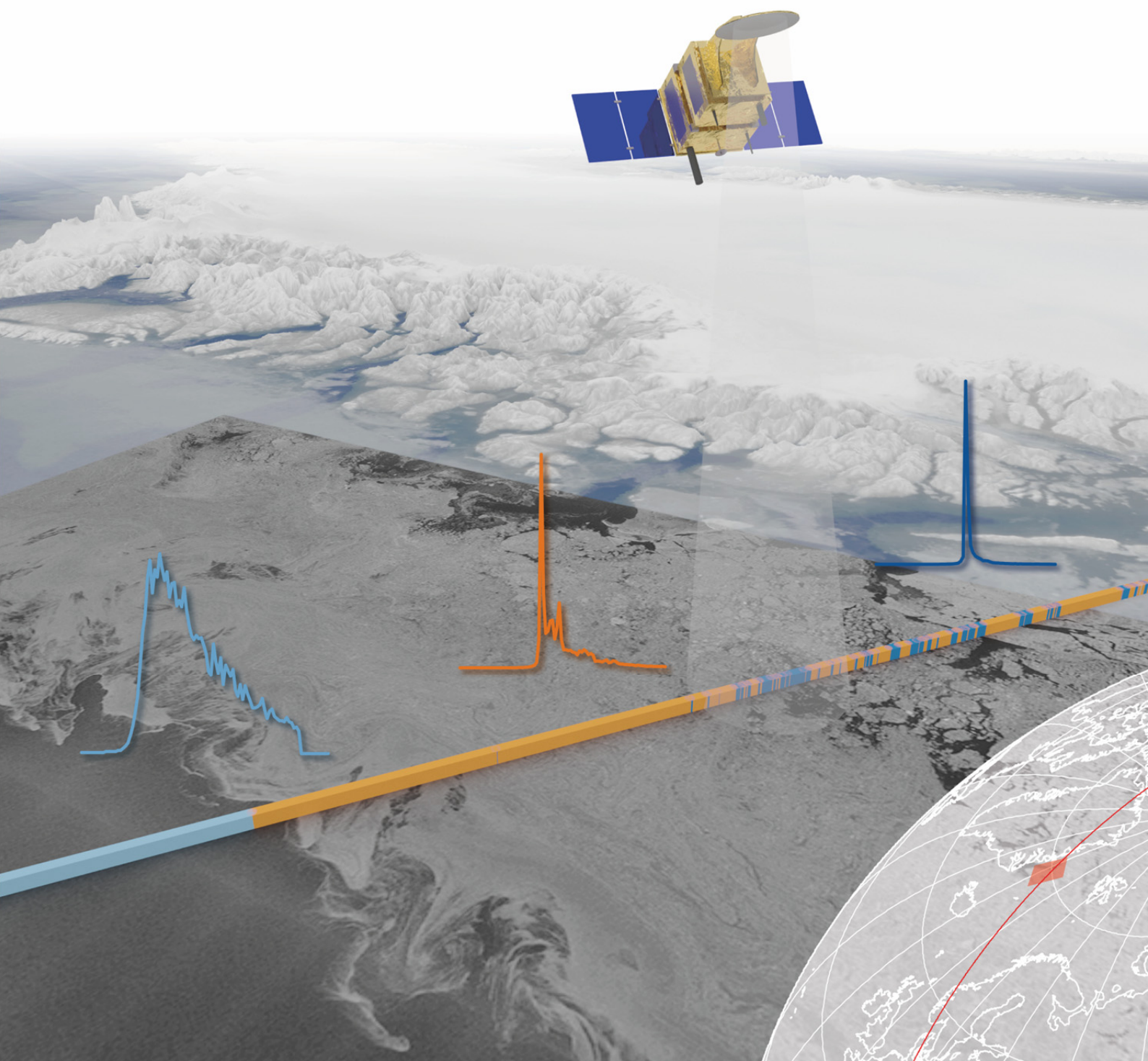


Annual Report 2016

Deutsches Geodätisches Forschungsinstitut
der Technischen Universität München
(DGFI-TUM)



Front cover:

Altimetry-based open water detection in sea-ice regions and its validation based on SAR images. The picture shows the SARAL satellite in March 2015 as it passes over the Greenland Sea. Three examples of its radar observations, so-called waveforms (line plots), are displayed. They are reflected by the ocean (left), sea-ice (middle) and enclosed open water areas (right). The small coloured bars indicate the measurement locations along the satellite track and the colour-coded waveform classification results (light blue: open ocean; orange: sea ice; blue: lead/polynya). The SAR image displayed over parts of the ocean was recorded by Sentinel-1 almost simultaneously with the altimetry measurements and illustrates the spatial distribution of sea-ice (light grey: ice; dark grey: water). This work is part of the DFG project NEG-OCEAN. More information can be found in Section 2.2 of this report.

Technische Universität München
Ingenieurfaculty Bau Geo Umwelt
Deutsches Geodätisches Forschungsinstitut (DGFI-TUM)

Arcisstr. 21
D - 80333 München

www.dgfi.tum.de

Contents

Preface	1
1 Research Area Reference Systems	4
1.1 Analysis of Space-Based Microwave Observations	5
1.2 Analysis of Satellite Laser Ranging Observations	7
1.3 Computation of Satellite Orbits	9
1.4 Determination of Reference Frames	12
2 Research Area Satellite Altimetry	21
2.1 Multi-Mission Altimetry	21
2.2 Sea Surface	23
2.3 Inland Altimetry	33
3 Cross-Cutting Research Topics	40
3.1 Atmosphere	40
3.2 Regional Gravity Field	49
3.3 Standards and Conventions	55
4 Information Services and Scientific Transfer	60
4.1 Internet representation	60
4.2 Membership in scientific bodies	63
4.3 Publications	67
4.4 Posters and oral presentations	70
4.5 Participation in meetings, symposia, conferences	77
4.6 Guests	80
5 Projects	81
6 Personnel	83
6.1 Lectures and courses at universities	83
6.2 Lectures at seminars and schools	83
6.3 Thesis supervision	83
6.4 Conferral of Doctorates	84
6.5 TUM Graduate School	84
6.6 Scientific Awards	84

Preface

The Institute

Since 2015, the Deutsches Geodätisches Forschungsinstitut (DGFI-TUM) is a research institute of the Technical University of Munich (TUM) where it is part of the Chair of Geodetic Geodynamics within TUM's Faculty of Civil, Geo and Environmental Engineering (BGU).

DGFI-TUM's scientific activities are oriented towards geodetic basic research with the ambition to provide a comprehensive and long-term valid metric of the Earth system for science and practice at highest precision and consistency.

Originally established in 1952 as an independent research facility at the Bavarian Academy of Sciences and Humanities (BAW) in Munich, the institute has a history of 65 years. It has continuously been involved in various national and international research activities of which many were of high significance for the scientific advancement of geodesy. DGFI's participation in geodetic-astronomical observations and electro-optical distance measurements for the determination of the German and European triangulation, its involvement in the first worldwide network of satellite triangulation, and its contribution to the development of dynamical methods of satellite geodesy for precise orbit determination, point positioning and gravity field modelling belonged to the early milestones.

A central aspect of DGFI's research has always been the precise determination of the Earth's time-variable surface geometry. For the solid Earth, this involves in particular the realization of global and regional horizontal and vertical terrestrial reference systems and of the celestial reference system. With respect to water surfaces, the institute has significantly extended its capacities for the precise determination of the sea level and water stages of lakes, rivers and wetlands using satellite altimetry over the past years.

DGFI-TUM's strategic focus is reflected by its organization into the two research areas *Reference Systems* and *Satellite Altimetry* (Fig. 1). The two research areas are complemented by three overarching research topics that cover the investigation of the state and dynamics of the atmosphere (with a strong focus on ionospheric disturbances), the determination of high resolution regional gravity fields, and the establishment of unique standards and conventions for geodetic data analysis worldwide.

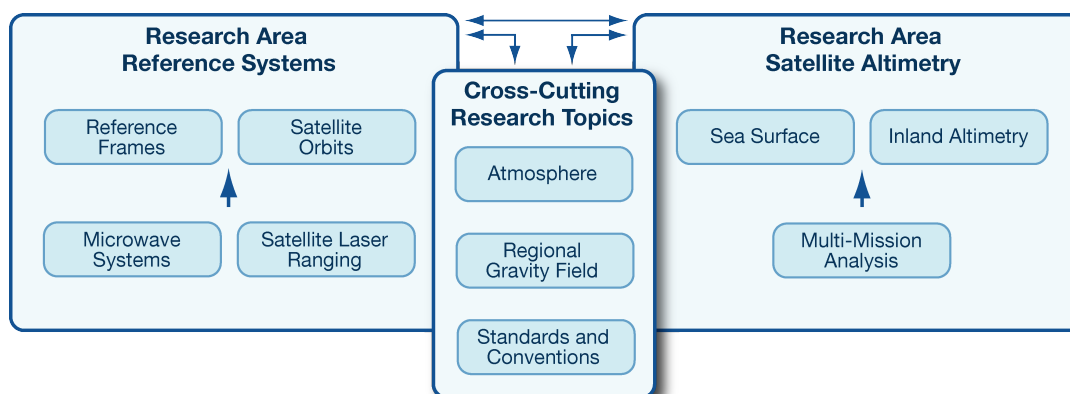


Fig. 1: Research Areas of the DGFI-TUM

National and international involvement

In strong international and interdisciplinary collaboration, the DGFI-TUM processes, analyses and combines observations from all relevant space-geodetic observing systems and complementary data sources at the highest level of scientific knowledge. The institute operates several worldwide distributed GNSS stations and contributes to the scientific data processing of the Geodetic Observatories Wettzell (Germany) and AGGO (Argentina) in the frame of the Forschungsgruppe Satellitengeodäsie (FGS).

The DGFI-TUM is involved in various internationally coordinated research activities and collaborates intensively within the framework of the international scientific organizations IUGG (International Union of Geodesy and Geophysics), IAU (International Astronomical Union) and IAG (International Association of Geodesy). In particular, the institute recognizes the outstanding role of IAG's Scientific Services that form the backbone of national and international spatial data infrastructure. In this context, the DGFI-TUM operates data centers, analysis centers and research centers and has taken leading positions and supporting functions in IAG's Commissions, Projects, Working and Study Groups. Several scientists of the DGFI-TUM collaborate at key positions in international scientific organizations (see Section 4.2), and thus contribute to shaping the future direction of international geodetic research. In IAG's Global Geodetic Observing System (GGOS) that coordinates the generation of high-quality science data products under predefined standards and conventions, the DGFI-TUM has a position of particular importance by chairing the GGOS Bureau of Products and Standards (Section 3.2).

The DGFI-TUM also participates in research programmes of the European Union (EU) and the European Space Agency (ESA), and it cooperates in activities of the United Nations (UN). In this regard, the institute is currently involved in the implementation of a UN Resolution for a Global Geodetic Reference Frame (GGRF) and provides an IAG representative to the UN Working Group for the GGRF.

Research highlights of particular public interest

During the year 2016, several research results of the DGFI-TUM attained good visibility in the scientific community and in the media. Particular public interest was generated by the following activities and publications.

- Determination of a new conventional value for the geoid reference potential W_0 : In the framework of IAG's Global Geodetic Observing System, the DGFI-TUM is chairing the GGOS Focus Area 1 (Unified Height System) that promotes the definition and realization of a global vertical reference system with homogeneous consistency and long-term stability. In this context, the DGFI-TUM coordinated the GGOS Working Group on Vertical Datum Standardization for the term 2011–2015. The main purpose of this working group was to determine an updated value for the gravity potential W_0 of the geoid to be introduced as the conventional reference level of a global height system. In 2016, scientists from the DGFI-TUM together with several international partners published the updated value for W_0 and the computation strategy in the article *A conventional value for the geoid reference potential W_0* (Journal of Geodesy, 2016, doi: 10.1007/s00190-016-0913-x). The IAG adopted this value officially in its Resolution No. 1 (2015) as the conventional W_0 value for the definition and realization of the International Height Reference System (IHRF). More information can be found on page 19.

- Release of the new DGFI-TUM realization DTRF2014 of the International Terrestrial Reference System (ITRS): In its role as an ITRS Combination Centre within the International Earth Rotation and Reference Systems Service (IERS), the DGFI-TUM took the responsibility for providing realizations of the Earth's fundamental coordinate system ITRS in regular intervals. An up-to-date ITRS realization at mm-accuracy and long-term stability is an indispensable requirement, e.g., for the use of global navigation and positioning systems, for surveying, and for the computation of spacecraft and satellite orbits. Furthermore, it is the backbone for Earth system research by providing the metrological basis and uniform reference for monitoring processes in the context of global change (e.g., ice melting, sea level rise) over long time spans. The DTRF2014 is DGFI-TUM's new realization of the ITRS. It comprises 3D-positions and velocities of 1712 globally distributed geodetic observing stations and includes six additional years of data compared to our previous realization. Additionally, for the first time, non-tidal atmospheric and hydrological signals are considered in the DTRF2014 station position time series. Concomitant with the publication of the DTRF2014 (*The new DGFI-TUM realization of the ITRS: DTRF2014 (data)*, doi:[10.1594/PANGAEA.864046](https://doi.org/10.1594/PANGAEA.864046)) a press release was placed that met with a positive media response. Among others, a television report was broadcasted by the Bayerischer Rundfunk. Read more about the DTRF2014 in Section 1.4 of this report.
- Data grid for GOCE gravity field measurements sheds new light on the Earth's structure: In the widely recognized study *Satellite gravity gradient grids for geophysics* (Nature Scientific Reports, 2016, doi: [10.1038/srep21050](https://doi.org/10.1038/srep21050)) scientists from the DGFI-TUM reported about an innovative mathematical representation of the observation data of ESA's gravity satellite GOCE that allows for resolving geophysical structures deep below the Earth's surface. In combination with geophysical models of the Earth's interior the data enables conclusions regarding density and thickness of different tectonic plates and thus can provide additional information to the tectonic model. A press release related to this publication received a broad response in national and international media. More information can be found in Section 3.2.
- The Johannes B. Ortner-Stiftung of the Technical University of Munich acknowledged DGFI-TUM's research associate Dr. Marco Limberger in recognition of outstanding scientific achievements for his dissertation with the title *Ionosphere modeling from GPS radio occultations and complimentary data based on B-splines*. The prize was given to him in appreciation of his important contribution to the four-dimensional modelling of the ionospheric electron content using an innovative mathematical-physical model. The model can be adapted to geodetic observations that are distributed heterogeneously with respect to space and time at inhomogeneous quality. Details on DGFI-TUM's activities in ionosphere research are presented in Section 3.1.



1 Research Area Reference Systems

Since many years, the topic “Reference Systems” is a key research field of DGFI-TUM. The work in this research area relies on the space geodetic observation techniques Very Long Baseline Interferometry (VLBI), Satellite and Lunar Laser Ranging (SLR/LLR), Global Navigation Satellite Systems (GNSS), and Doppler Orbitography and Radiopositioning Integrated by Satellite (DORIS). The data of these geometric techniques provide the basis for the determination of highly accurate geodetic reference frames as a fundamental requirement for precise positioning, navigation, and for quantifying smallest geometric variations in space and time, e.g., to measure global change phenomena and for supplying near real-time warning systems.

As a part of the Forschungsgruppe Satellitengeodäsie (FGS), DGFI-TUM contributes to the complete processing chain from operation of observing stations, data acquisition and provision, development of procedures and theoretical models, data analysis and combination, and parameter determination. Among the institute’s core products are highly accurate regional and global realisations of three-dimensional geodetic reference systems that are determined from the combination of the above-mentioned space geodetic observation techniques.

This research area is divided into four research topics:

- 1.1 Analysis of space-based microwave observations
- 1.2 Analysis of satellite laser ranging observations
- 1.3 Computation of satellite orbits
- 1.4 Determination of reference frames

The work benefits from DGFI-TUM’s engagement in the international scientific services of the International Association of Geodesy (IAG). Mostly by virtue of long-term commitments, DGFI-TUM operates data centres, analysis centres, and research centres within the IAG. This ensures the direct access to the original data of the space geodetic techniques and to the products generated by the scientific services. Table 1.1 summarises the activities that are closely related to this research area. The responsibilities require an operational analysis of SLR, VLBI and GNSS data and a timely generation of geodetic products. The DGFI-TUM software packages DOGS (DGFI Orbit and Geodetic Parameter Estimation Software) need to be updated regularly according to the latest versions of conventions, models and processing standards (i.e., DOGS-OC for SLR, OCCAM/DOGS-RI for VLBI and the combination software DOGS-CS).

Table 1.1: Long-term commitments of DGFI-TUM in IAG Services that are related to this research area.

IAG Service	DGFI-TUM Commitments
International Earth Rotation and Reference Systems Service (IERS)	International Terrestrial Reference System (ITRS) ITRS Combination Centre
International GNSS Service (IGS)	Regional Network Associate Analysis Centre for SIRGAS (RNAAC-SIR), Tide Gauge Monitoring Working Group (TIGA)
International Laser Ranging Service (ILRS)	Global Data and Operation Centre (EDC), Analysis Centre
International VLBI Service for Geodesy and Astrometry (IVS)	Analysis Centre, Combination Centre (together with BKG)

1.1 Analysis of Space-Based Microwave Observations

VLBI data analysis

As one of the operational analysis centres of the IVS, DGFI-TUM regularly submits constraint-free normal equations of 24-hour VLBI sessions for the IVS rapid and quarterly products. Besides, a reprocessing was started in 2013 to include the estimation of source positions. Table 1.2 shows all 362 sessions that were analysed in 2016 including the so-called VLBI Calibrator Survey (VCS-II) sessions with more than 300 sources per session. Considering previous years, 1929 consistently analysed sessions for the time span from March 2003 to December 2016 were available at the end of 2016.

All routine VLBI analyses were still performed with OCCAM. Besides, a new software called DOGS-RI (Radio Interferometry) that strictly follows IERS Conventions 2010 was developed. After intensive internal comparisons with OCCAM, DOGS-RI participated in the “VLBI Analysis Software Comparison Campaign 2015” on the basis of computed theoretical delays (Klopotek et al. 2016). DOGS-RI was among the six software packages that could achieve a sub-mm agreement in terms of RMS differences.

After a new SINEX (solution independent exchange format) interface had been implemented, first solutions could be provided to the IVS Combination Centre. Based on sessions from 2016, session-wise comparisons with the IVS combined solution could not reveal systematic differences. Before DGFI-TUM can switch to the new software, data back to 2003 has to be processed with DOGS-RI to rule out long-term systematic effects.

Monitoring of regional deformations with GNSS

Geodetic techniques, especially GNSS, allow to measure large- and small-scale displacements at high spatial and temporal resolutions. Some examples are surface deformations associated to natural hazards (like volcano eruptions, seismic effects, landslides, subsidence, etc.), man-made structures (dams, buildings, bridges, mines, etc.), tectonic features (plate motion, surface deformation, slow-slip interactions, etc.), vertical movements (mountain building, global

Table 1.2: Number of VLBI sessions analysed in 2016 using OCCAM.

Session type	2003	2004	2011	2012	2013	2014	2015	2016	Total
AOV	–	–	–	–	–	–	–	2	2
APSG	2	–	–	–	–	–	1	1	4
AUS	–	–	–	–	–	–	–	1	1
EUROPE	3	2	–	–	–	–	2	5	12
IVS-CRF	3	1	–	–	–	–	–	3	7
IVS-E3	1	5	–	–	–	–	–	–	6
IVS-OHIG	–	1	–	–	–	–	3	2	6
IVS-R1	40	35	–	–	–	–	6	48	129
IVS-R4	39	33	–	–	1	1	9	44	127
IVS-R&D	8	3	–	–	–	–	2	3	16
IVS-T2	6	8	1	–	–	–	4	4	23
VCS-II	–	–	–	–	–	6	2	–	8
VLBA	7	8	–	–	–	–	1	5	21
Total	109	96	1	–	1	7	30	118	362

isostatic adjustment, uplift/subsidence), and small signals of surface deformations caused by oceanic, hydrologic, or atmospheric loading. Based on the analysis of precise station position time series, DGFI-TUM investigates the best possible strategy to consistently model three main components: (1) a linear component to derive horizontal and vertical displacement fields that serve as basis for monitoring regional surface deformations; (2) earthquake-related discontinuities to identify deformation patterns associated with inter-seismic, co-seismic and post-seismic effects; and (3) seasonal components to infer transient surface deformations caused by atmospheric and hydrologic loading. As examples, Fig. 1.1 and Fig. 1.2 show the surface crustal deformation after the 2010 earthquakes in Latin America and the seasonal deformation caused by hydrological loads at selected SIRGAS stations, respectively. The former is based on the least squares collocation approach with empirically determined covariance functions using a multi-year velocity solution for a network of 456 continuously operating GNSS stations as the input data. The latter is based on a numerical solution of the static equilibrium equation for an elastic medium (i.e. the Earth's crust) characterised by an elastic parameter. The elastic parameter relies on the combination of the Poisson's ratio and the Young's modulus. This strategy combines loosely constrained weekly GNSS normal equations (which describe the geometric displacements) with monthly grids of equivalent water height values provided by GRACE (which are assumed to describe the hydrologic load). Thus, the solution of the normal equations leads to the common adjustment of seven parameters per GNSS station; namely, three position coordinates at a certain epoch, three constant velocity coordinates, and one elastic parameter.

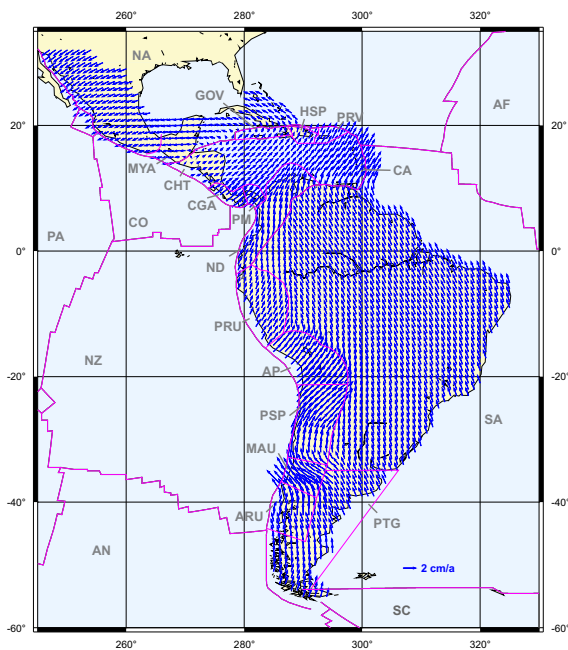


Fig. 1.1: Crustal deformation and surface kinematics after the 2010 earthquakes in Latin America (see Sánchez and Drewes 2016a and b). Tectonic plates: AF: Africa, AN: Antarctica, AP: Altiplano, CA: Caribbean, CO: Cocos, EA: Easter Island, GP: Galapagos, JZ: Juan Fernandez, NA: North America, ND: North Andes, NZ: Nazca, PA: Pacific, PM: Panama, RI: Rivera, SA: South America, SC: Scotia. Orogenes and tectonic blocks: GOV: Gonave, HSP: Hispaniola, PRV: Puerto Rico and Virgin Islands, MAY: Maya, CHT: Chortis, CGA: Chorotega, PRU: Peru, PSP: Puna-Sierras Pampeanas, MAU: El Maule, ARU: Araucania, PTG: Patagonia.

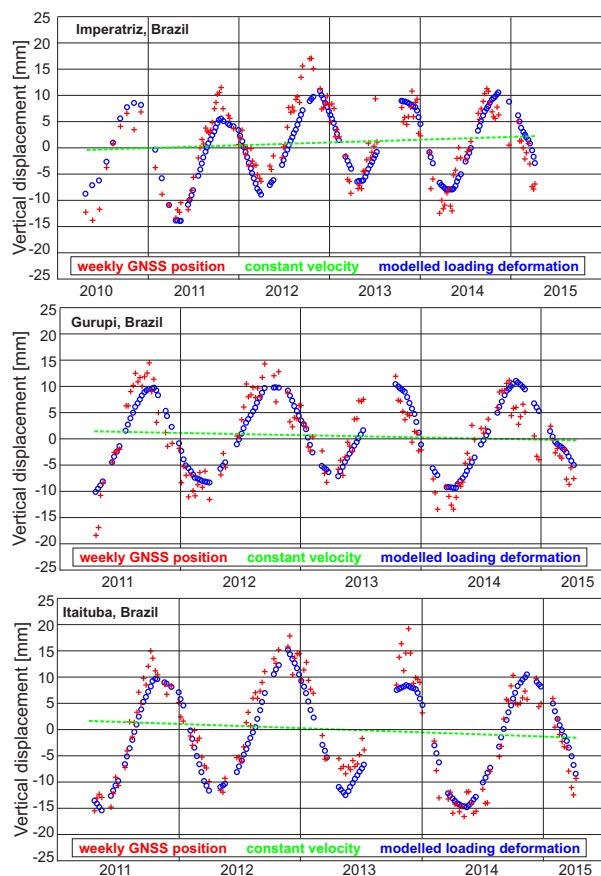


Fig. 1.2: Hydrologic loading deformation modelled by combining GNSS geometric movements and GRACE-inferred equivalent water heights at the normal equation level.

Complementary, DGFI-TUM operates different continuously measuring GNSS stations (four along the Bavarian Alps, three in Bolivia, three in Chile, and two in Peru). The operation of these stations is supported by local partner institutions, who take care of the appropriate functioning of the equipment and the opportune data delivery to the DGFI-TUM, where the data are centralised and posteriorly distributed to the processing centres. DGFI-TUM regularly processes these data in the frame of several projects like modelling of regional deformations (as shown before), computation of the regional reference frame SIRGAS, GNSS monitoring of tide gauges, and vertical datum unification in South America. These stations additionally contribute to the IGS Tide Gauge Benchmark Working Group (TIGA), see Schöne et al. (2016), the IGS Multi-GNSS Experiment (MGEX), and the regional densification of the ITRF in Latin America.

1.2 Analysis of Satellite Laser Ranging Observations

SLR data management

Since the foundation of the International Laser Ranging Service (ILRS) in 1998, the EUROLAS Data Centre (EDC) acts as one of two global ILRS data centres: the EDC at DGFI-TUM and the Crustal Dynamics Data Information System (CDDIS) at NASA. The EDC, as ILRS Operation Center (OC) and ILRS Data Center (DC) has to ensure the quality of submitted data sets by checking their format (Schwatke, 2016a). Furthermore, a daily and hourly data exchange with the NASA OC and CDDIS is performed. All data sets and products are publicly available for the ILRS community via ftp (<ftp://edc.dgfi.tum.de>) and website (<http://edc.dgfi.tum.de>). In 2016, the design of the EDC website has been changed to the cooperate design of the TUM (Schwatke, 2016b).

EDC is running several mail lists for the exchange of information, data and results. The Consolidated Prediction Format (CPF) files (50856 in 2016) of 93 satellites are sent automatically to the SLR stations and stored at the ftp server. Mailing lists such as SLR-Mail (77 messages in 2016), SLR-Report (1171 in 2016), Urgent and Rapid-Service-Mail (23 in 2016) are maintained by EDC. In 2016, 41 SLR stations observed 102 satellites. There were 14 new satellite missions tracked by SLR stations, namely Compass-IS2, Galileo-207, Galileo-208, Galileo-209, Galileo-210, Galileo-211, Galileo-212, Galileo-213, Galileo-214, Glonass-135, Glonass-136, IRNSS-1E, IRNSS-1F, and Lomonosov.

SLR quality control

System biases have plagued SLR since the times of the first SLR measurements in 1964. Long and short term biases can degrade the quality of SLR products. To keep track and possibly reduce these error sources, the ILRS has established a new service, the Quality Control Board (ILRS/QCB), as a joint activity of the Analysis Standing Committee (ASC) and the Network and Engineering Standing Committee (NESC). The goal is to quickly provide feedback to the tracking station operators in case of unexpected data anomalies to support them in maintaining the data quality. The board meets monthly via teleconference or in person.

DGFI-TUM performs the daily processing of station biases on a pass-by-pass basis for most of the relevant geodetic satellites. Weekly files per satellite are available from our website (ilrs.dgfi.tum.de/quality/weekly_biases/). Additionally, the website contains time series of biases for all tracking stations. These graphics contain the pass by pass biases and mean values over 100 passes. These mean values are smoother and allow a better identification of trends in the bias behaviour. Presently, we use the new terrestrial reference frames ITRF2014 and

DTRF2104 together with the old SLRF2008 to compute the biases. Results are presented in different subdirectories. Figure 1.3 shows an example for the station Yarragadee using DTRF2014 coordinates. The behaviour of the mean bias for the three satellites is similar with a small offset only. In case of bias anomalies the station is contacted via the ILRS Rapid Service Mail. In 2015, 22 bias alerts were issued by the Quality Control (Q/C) Centres.

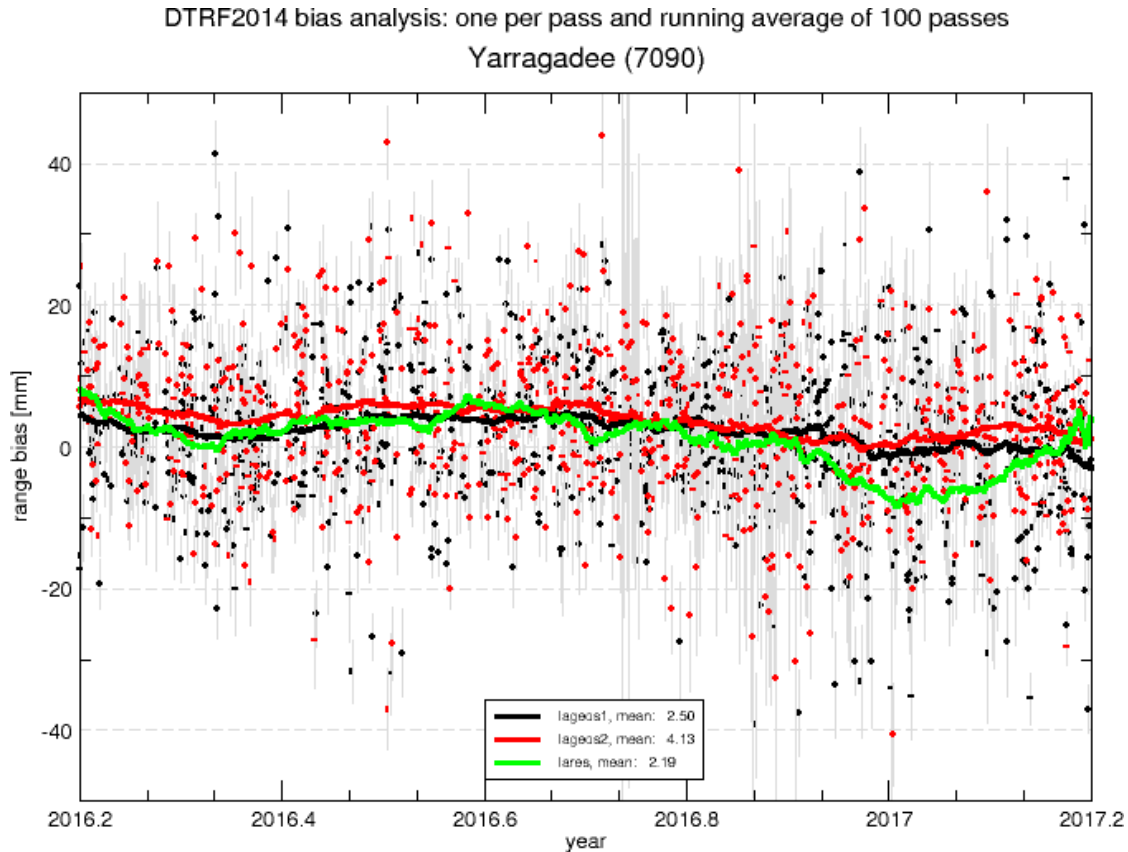


Fig. 1.3: An example of the station bias plots available at the DGFI-TUM web site.

SLR data analysis

DGFI-TUM is one of presently six active analysis centres (AC) of the ILRS Analysis Standing Committee (ILRS/ASC). It contributes with solutions for station coordinates and Earth orientation parameters (EOPs) on the basis of weekly arcs. The ILRS/AC provides two different product series, on a daily basis, mainly for the rapid EOP service and weekly for reference frames and EOPs. The weekly products also include orbits in the "sp3-format" to the Lageos and Etalon satellites. Additionally, DGFI-TUM contributes to the pilot projects of the ILRS/ASC on the estimation of range biases for all stations and the replacement of the SLRF2008 reference frame by the ITRF2014, including post-seismic deformations.

The ILRS and the other geometric services have been asked by the ITRS Centre to evaluate the latest ITRF solutions of the three ITRS Combination Centres: the ITRF2014 (IGN, France), the JTRF2014 (JPL, USA) and DTRF2014 (DGFI-TUM, Germany). In its function as an ILRS analysis centre, DGFI-TUM has decided to compare the three ITRS realizations by computing different SLR solutions. Among these comparisons, the orbits of non-spherical satellites were computed to test the orbit fits. The results of these comparisons are reported in Sect. 1.3.

1.3 Computation of Satellite Orbits

Impact of TRF realizations on precise orbit determination (POD)

To quantify the impact of TRF realizations on the orbits of near-Earth satellites (spherical satellites at high altitudes and non-spherical satellites at low altitudes), the DTRF2014 and ITRF2014 have been used for precise orbit determination by SLR observations within the DOGS-OC software. In case of the Low Earth Orbiters (LEOs), Jason-2 orbits (3.5-day resolution) have been computed between 20th July 2008 and 1st March 2015 using these terrestrial reference frame (TRF) realizations as fixed a priori TRFs. As a reference, the SLRF2008 was used in the POD process. In all solutions, equal background models were used for the POD to ensure that orbit differences are only caused by the different used TRF realizations. In addition to the station coordinates, the Earth orientation parameters (EOP) were fixed to IERS EOP 08 C04 (IAU2000A).

Using DTRF2014 instead of SLRF2008 reduces (improves) SLR RMS fits from 2.42 to 2.24 cm, i.e., by about 7.4%. Furthermore, the mean of SLR fits is reduced as compared with the POD using the SLRF2008 (from 0.62 to -0.37 mm, Fig. 1.4). DTRF2014 improves the SLR RMS fits by about 1.4%, compared to the results based on the ITRF2014 (2.24 cm instead of 2.28 cm). In comparison to the results based on the ITRF2014, the DTRF2014 reduces the mean of SLR fits and the offset (from 0.76 to -0.37 mm, Fig. 1.4).

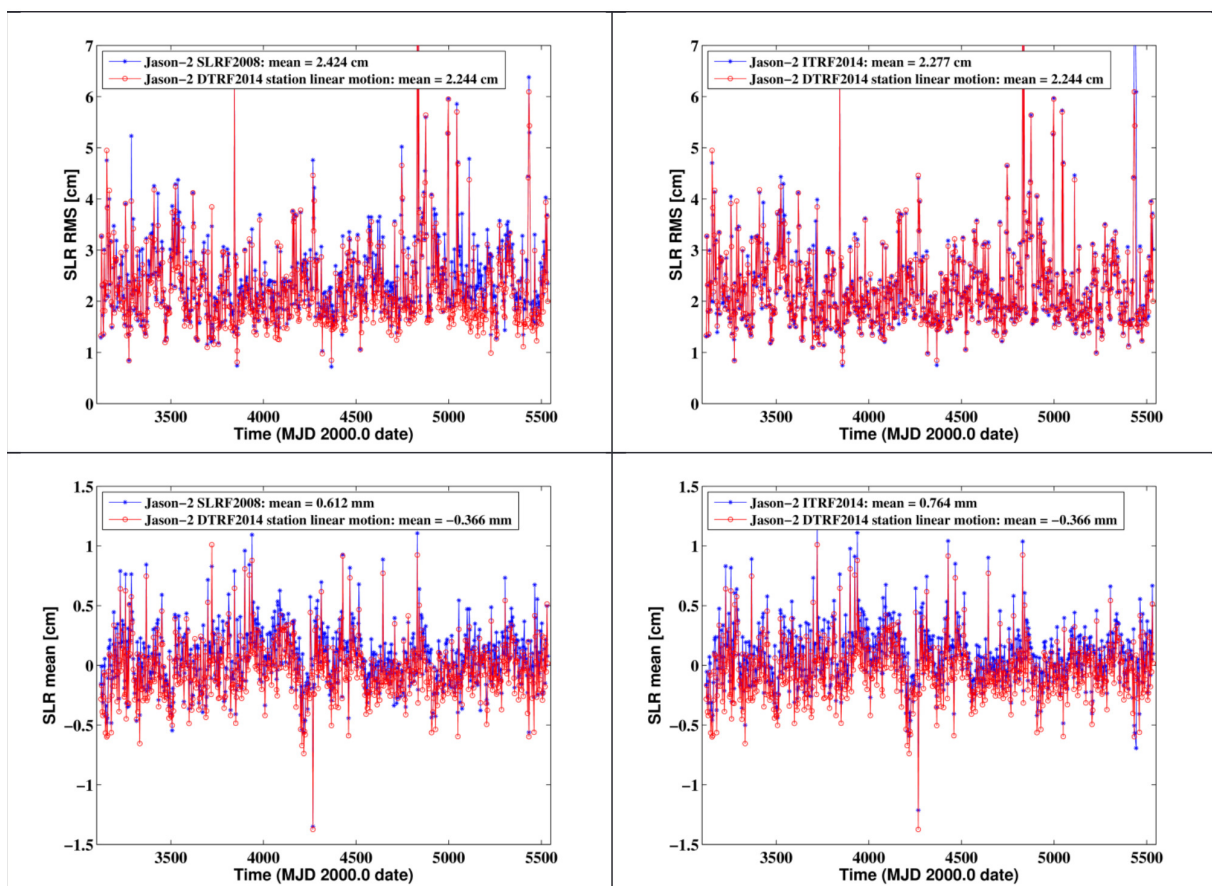


Fig. 1.4: RMS (top) and mean (bottom) fits of SLR observations for Jason-2 orbit from 20 July 2008 to 1 March 2015 derived using DTRF2014 and SLRF2008 (left) and DTRF2014 and ITRF2014 (right) terrestrial reference frame realizations.

For spherical satellites at higher altitudes, we used SLR observations and analysed weekly estimated range biases for stable (core) stations of the SLR network.

The ITRS realizations are used in two different time intervals:

- Interpolation time period (1993.0 – 2015.0),
- Extrapolation time period (2015.0 – 2017.0).

The JTRF2014 is only available in the interpolation time period. With the DTRF2014, ITRF2014 and SLRF2008 solution, all station coordinates (including those of stations affected by post-seismic deformations) can be extrapolated with the conventional (linear) velocities. Fig. 1.5 shows the mean weekly biases for the core stations of the ILRS. The largest mean biases are obtained for the SLRF2008 whereas the results of the other three ITRS realizations are comparable. In general, the SLRF2008 causes the largest range biases in the extrapolation time period (see Fig. 1.6). The comparison of the ITRF2014 and DTRF2014 results shows that the DTRF2014 solution causes some smaller biases for stations in Europe, whereas the ITRF2014 performs slightly better on the southern hemisphere.

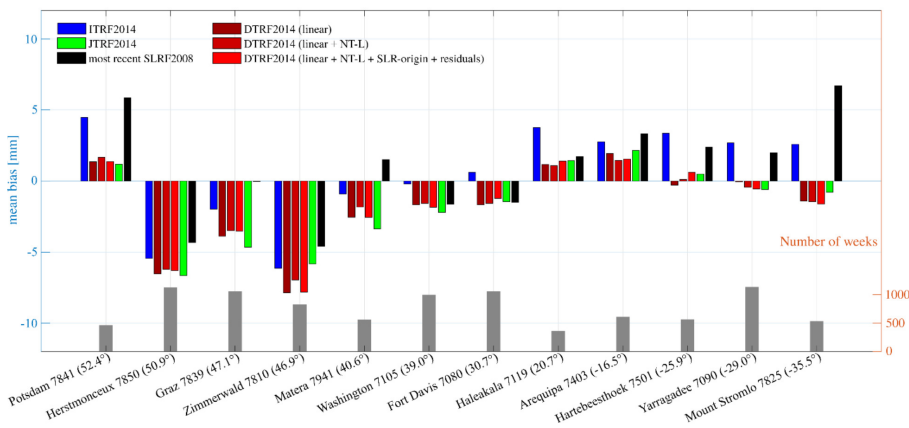


Fig. 1.5: Estimated mean station-specific weekly range biases for different ITRS realizations in the interpolation time period for LAGEOS-1. In addition, the number of processed weeks is shown for each station.

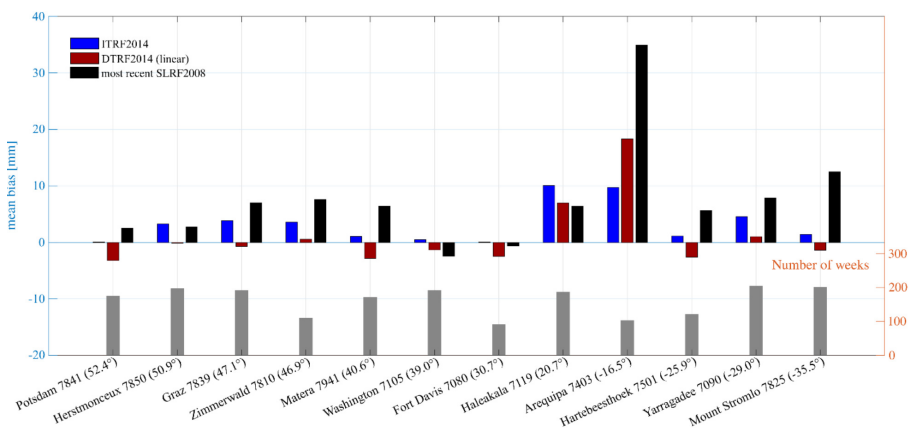


Fig. 1.6: Estimated mean station-specific weekly range biases for different ITRS realizations in the extrapolation time period for LAGEOS-1. In addition, the number of processed weeks is shown for each station.

In addition to these comparisons of range bias estimations, the ITRF2014 and DTRF2014 have been compared with the SLRF2008 by computing orbits of nine spherical satellites and testing the orbital fit. Table 1.3 shows the results for actually tracked spherical satellites for the time period 2015.0 until 2017.1. The rms fits were computed for all SLR stations and for the core stations, respectively. For all satellites used in this study, the DTRF2014 and ITRF2014 provide smaller rms fits than the SLRF2008.

Table 1.3: Comparison of mean orbital fit [in mm] to the actually tracked spherical satellites in the period 2015.0 until 2017.1 using different realizations of the terrestrial reference frame.

	DTRF2014		ITRF2014		SLRF2008	
	all stat	core stat	all stat	core stat	all stat	core stat
LAGEOS-1	14.1	7.9	14.8	8.5	23.1	11.8
LAGEOS-2	15.1	8.8	16.2	9.7	23.5	12.3
Etalon1	24.4	17.6	24.9	16.9	29.2	18.3
Etalon2	28.2	20.1	28.6	20.4	29.2	24.2
LARES	19.3	13.7	19.3	13.4	22.1	14.6
Larets	22.2	15.1	22.2	14.3	23.9	15.2
Starlette	19.1	13.9	19.2	13.1	21.7	14.4
Stella	20.6	14.2	20.6	14.4	22.9	16.3
Ajisai	21.5	14.3	21.8	14.2	24.4	16.5

SLR multi-satellite solution

Within the DGFI-TUM reprocessing campaign in 2016, SLR observations to 11 satellites have been reprocessed using most recent geophysical background models. The observations cover a time interval of 41 years between 1976 and 2017 (see Fig. 1.7, Bloßfeld et al. 2016a). The reprocessed data are used to determine station coordinates, EOP and gravity field parameters, such as the low degree Stokes coefficients in the framework of several projects at DGFI-TUM. The reprocessed data set enables long-term studies of global change phenomena. These investigations were performed in project PN6 “Consistent dynamic satellite reference frames and terrestrial geodetic datum parameters” within the DFG Research Unit (FOR1503) “Space-time reference systems for monitoring global change and for precise navigation in space”.

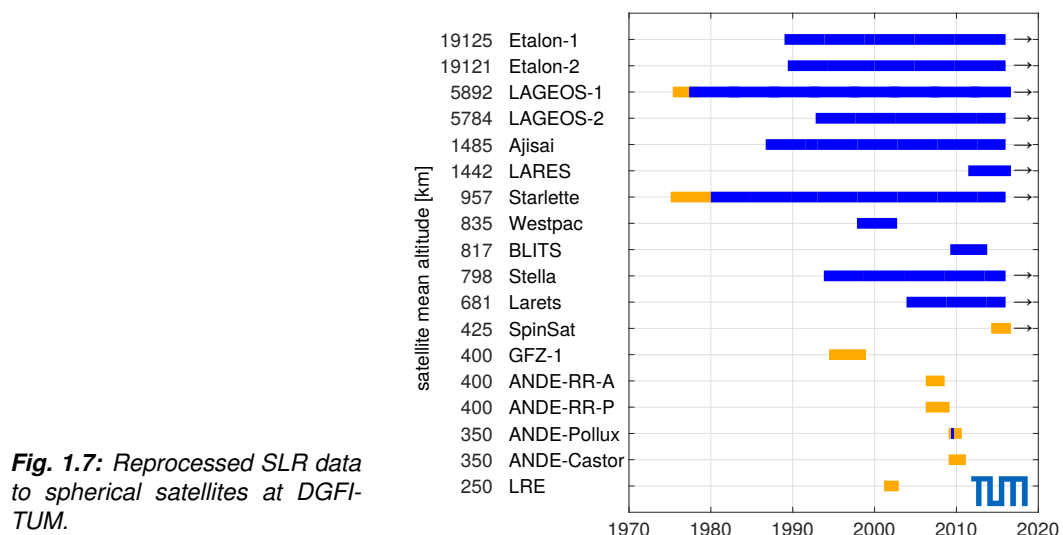


Fig. 1.7: Reprocessed SLR data to spherical satellites at DGFI-TUM.

Refined modeling of thermospheric drag

For the POD of non-spherical LEOs, the most significant perturbing non-gravitational acceleration is the thermospheric drag. The modelling of this perturbation strongly relies on the used macro-model of the satellite, the gas-surface interaction model, the composition of the thermosphere, and the relative velocity of the satellite w.r.t. the surrounding thermosphere. The DGFI-TUM software DOGS-OC was extended to accurately account for all these different effects. For more details, see Section 3.1 (Project INSIGHT).

1.4 Determination of Reference Frames

DTRF2014 realization

The DTRF2014 is a realization of the International Terrestrial Reference System (ITRS) computed by DGFI-TUM. The DTRF2014 consists of station positions and velocities of 1712 globally distributed geodetic observing stations of the observation techniques VLBI, SLR, GNSS and DORIS. Additionally, for the first time, non-tidal atmospheric and hydrological loading is considered in the solution. The DTRF2014 was released in August 2016 and incorporates observation data of the four space geodetic techniques up to the end of 2014 (Bloßfeld et al. 2016b; Seitz et al. 2016).

The DTRF2014 is an independent ITRS realization. It is computed on the basis of the same input data as the realizations JTRF2014 (JPL, Pasadena) and ITRF2014 (IGN, Paris). The three ITRS realizations differ conceptually. While DTRF2014 and ITRF2014 are based on station positions at a reference epoch and velocities, the JTRF2014 is based on time series of station positions. DTRF2014 and ITRF2014 result from different combination strategies: the ITRF2014 is based on the combination of solutions, the DTRF2014 is computed by the combination of normal equations.

The DTRF2014 comprises 3D coordinates and velocities of 1347 GNSS, 113 VLBI, 99 SLR and 153 DORIS stations. The reference epoch is 1.1.2005, 0h UTC. The Earth Orientation Parameters (EOP) - that provide the transformation between the celestial and terrestrial reference frame - were simultaneously estimated with the station coordinates. The EOP time series cover the period from 1979.7 to 2015.0. The horizontal station velocities of the DTRF2014 solution are shown in Fig. 1.8.

The DTRF2014 solution is available in one comprehensive SINEX file and four technique-specific SINEX files, as shown below:

- DTRF2014.snx: Estimated station positions and velocities of the space geodetic techniques GNSS, VLBI, SLR and DORIS and the full variance-covariance matrix (12 GB).
- DTRF2014_GNSS.snx: Estimated station positions and velocities of the GNSS network and the related full variance-covariance matrix.

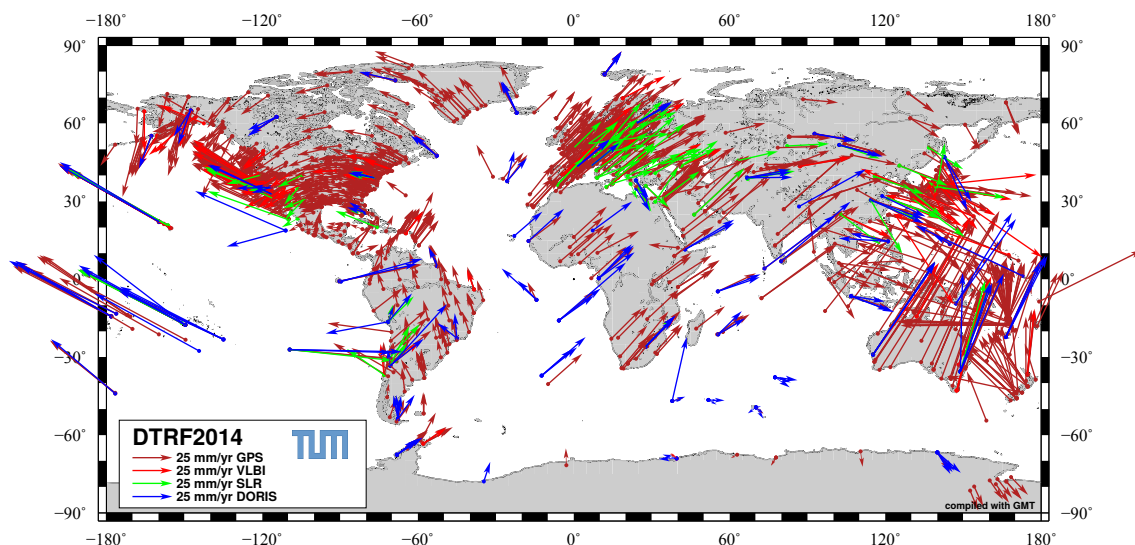


Fig. 1.8: Horizontal station velocities of the DTRF2014 solution.

- DTRF2014_VLBI.snz: Estimated station positions and velocities of the VLBI network and the related full variance-covariance matrix.
- DTRF2014_SLR.snz: Estimated station positions and velocities of the SLR network and the related full variance-covariance matrix.
- DTRF2014_DORIS.snz: Estimated station positions and velocities of the DORIS network and the related full variance-covariance matrix.

In addition, the DTRF2014 solution comprises the following time series files, necessary for the computation of the quasi-instantaneous station positions:

- DTRF2014_SLRorigin.txt: Translation time series of the origin derived from similarity transformations of SLR-only 15-day/weekly network solutions w.r.t. the DTRF2014.
- Loading time series: Weekly averaged atmospheric and hydrological non-tidal loading corrections applied in DTRF2014 computation for the correction of the respective signals. The data are provided by Tonie van Dam (personal communication) and are based on the atmosphere model NCEP and the hydrology model GLDAS.
- Station position residuals: Transformation residual time series obtained from similarity transformations of the technique-specific epoch-wise solutions w.r.t. the DTRF2014.

The DTRF2014 data can be accessed via the website of DGFI-TUM at:

- <http://www.dgfi.tum.de/en/science-data-products/dtrf2014/>

The following citation should be used for DTRF2014 data products:

- Seitz, Manuela; Bloßfeld, Mathis; Angermann, Detlef; Schmid, Ralf; Gerstl, Michael; Seitz, Florian (2016): The new DGFI-TUM realization of the ITRS: DTRF2014 (data). doi:10.1594/PANGAEA.864046.

Regional terrestrial reference frame in Latin America (SIRGAS)

The primary objective of SIRGAS (Sistema de Referencia Geocéntrico para las Américas) is the determination and maintenance of a reliable reference frame in Latin America and the Caribbean as a densification of the ITRF and as a regional realization of the ITRS (Sánchez et al. 2016). DGFI-TUM's research in the context of SIRGAS is focused on:

- Weekly processing of the SIRGAS Reference Frame (Fig. 1.9) in cooperation with the SIRGAS Analysis Centres installed in Latin America, namely, CEPGE Ecuador, CNPDG-UNA Costa Rica, CPAGS-LUZ Venezuela, IBGE Brazil, IGAC Colombia, IGN Argentina, IGM Chile, INEGI Mexico, and SGM Uruguay. These activities are developed in the frame of the IGS RNAAC SIR (IGS Regional Network Associate Analysis Centre for SIRGAS) and include the generation of weekly loosely constrained solutions and station positions aligned to the ITRF for all the SIRGAS reference stations.
- Computation of multi-year solutions to estimate the kinematics of the reference frame (Fig. 1.10) and to model the station velocity field as a basis for the estimation of regional surface deformations (Fig. 1.1);
- Estimation of co-seismic deformation models derived from discrete (weekly) station positions to incorporate seismic discontinuities in the computation of the reference frame and to support the precise transformation of coordinates referring to pre-seismic and post-seismic reference frame realizations;
- Modelling of seasonal movements at the combination level of the weekly solutions (Fig. 1.2).

DGFI-TUM makes the SIRGAS science data products available via www.sirgas.org and [ftp.sirgas.org](ftp://ftp.sirgas.org).

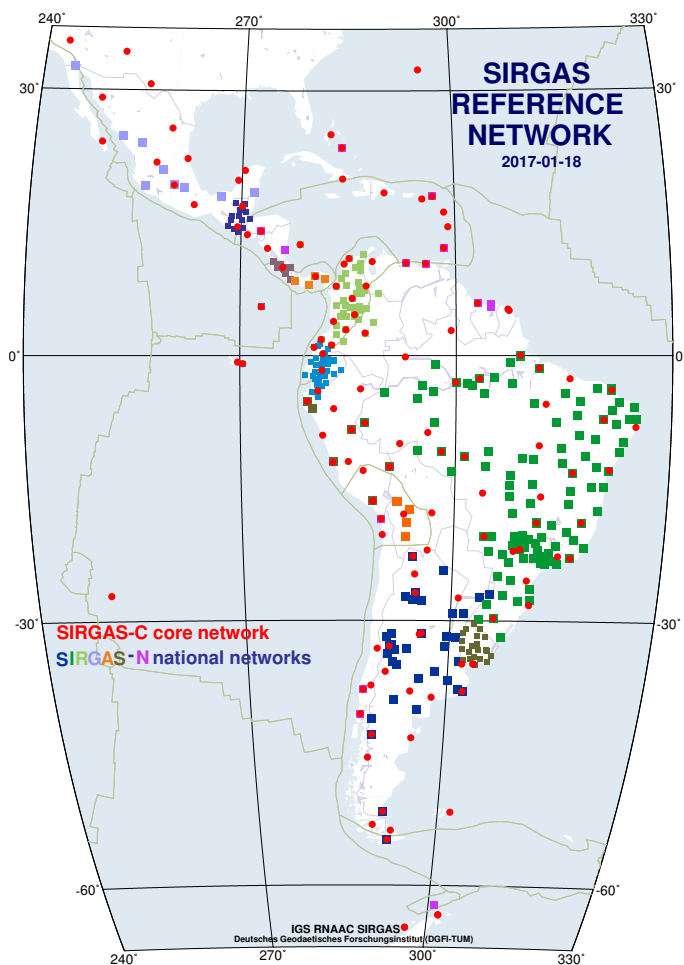


Fig. 1.9: SIRGAS reference network (as of January 2017). The SIRGAS core network (SIRGAS-C) provides the primary link to the global ITRF, while the national reference networks (SIRGAS-N) improve the geographical density of the reference stations and ensure the accessibility to the global reference frame at national and local levels.

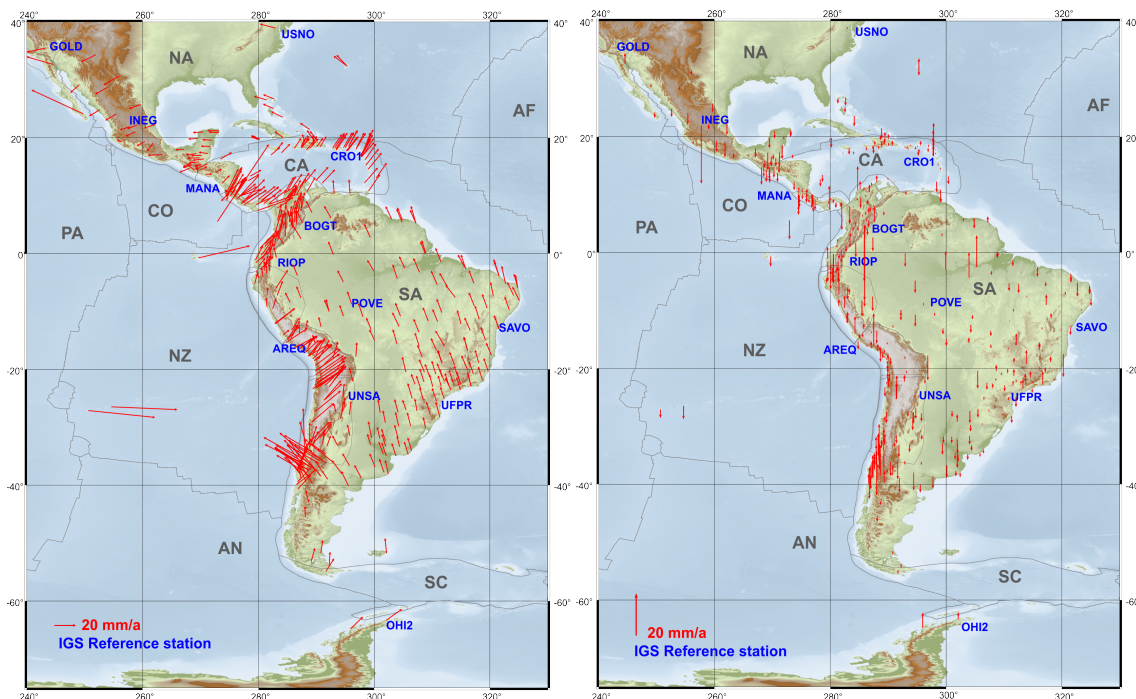


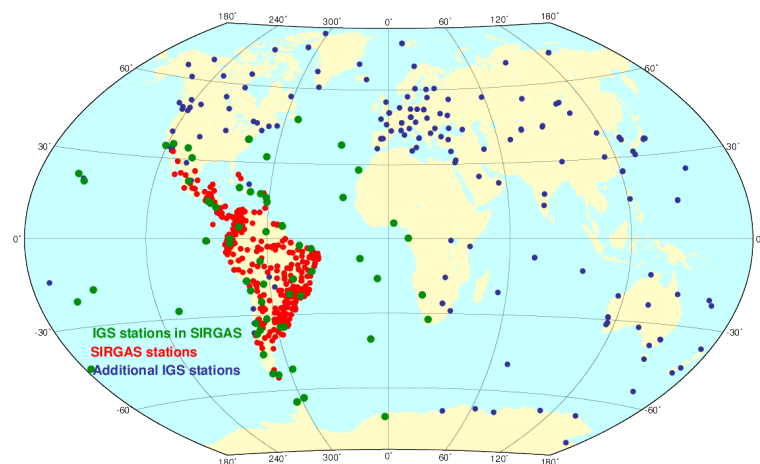
Fig. 1.10: Kinematics of the SIRGAS reference frame. It is based on a multi-year solution referring to the Igb08 frame, epoch 2013.0 and including 456 stations. Averaged RMS precision is ± 1.0 mm/a in the horizontal component (left) and 1,2 mm/a in the vertical component (right).

DFG Project DIGERATI

The objective of the DFG-funded project DIGERATI (Direct Geocentric Realisation of the American Reference Frame by Combination of Geodetic Observation Techniques) is the realisation of regional Epoch Reference Frames (ERF) for South and Central America by a combination of the three space techniques GNSS, SLR and VLBI at the normal equation level. Towards this aim, a major focus is on the development of a suitable combination strategy for a geocentric datum realisation of regional networks proposed within DIGERATI.

In this case, the GNSS network has to be extended beyond the regional network and must include SLR/GNSS and VLBI/GNSS co-located stations. A main objective is to identify the minimal GNSS network configuration, which is needed in order to transfer the datum from SLR/VLBI optimally to the regional network. As SLR is the most stable observation technique for the determination of the geocenter, globally well-distributed co-locations between SLR and the other techniques are essential for the realisation of the ERF origin. The existing regional SIRGAS network of nearly 400 stations was extended by globally distributed co-location sites and all available IGS core stations (see Fig. 1.11).

Fig. 1.11: Global GNSS network processed within the DIGERATI project. Red dots represent the regional SIRGAS stations, green dots represent the IGS stations included currently in the routine processing of the SIRGAS reference frame, blue dots represent the additional IGS stations included to realise a global network.



Based on this global network with about 700 stations the following empirical experiments were conducted:

- Processing of GPS and GLONASS observations including satellite orbit and EOP determination to allow a further combination of satellite orbits derived from different techniques, e.g. SLR and GNSS.
- Processing of GPS and GLONASS observations fixing GNSS orbits and EOPs to the IGS products (like in the current computation of the SIRGAS reference frame) to evaluate the sensibility of the SIRGAS coordinates to the simultaneous computation of orbits and EOPs.
- Processing of GPS observations including orbit and EOP determination to evaluate the sensibility of the results to the GLONASS orbit determination.

The results of the routine SIRGAS processing have been compared with those obtained from the global network processing. As an example, Fig. 1.12 shows the differences between the SIRGAS weekly positions and those obtained from the global network using GPS and GLONASS observations with orbit and EOP determination for the first week of June 2014. It is necessary to extend the computations to the wintertime (e.g. December) to identify if the observed discrepancies are caused by seasonal effects.

The benefits of a potential future SLR station network with a more homogeneous global station distribution and technically improved stations have been investigated using the simulation

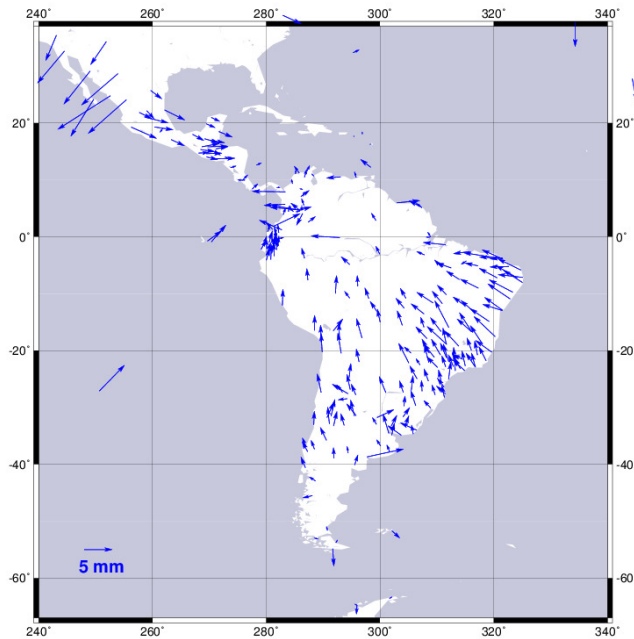


Fig. 1.12: Horizontal differences between the SIRGAS weekly positions and those obtained within the global network using GPS and GLONASS observations with orbit and EOPs determination. Differences in latitude (N): Mean value = 0.0029 ± 0.0018 m, Min = -0.0064 m, Max = 0.0073 m. Differences in longitude (E): Mean value = 0.0007 ± 0.0014 m, Min = -0.0111 m, Max = 0.0092 m.

modus of DOGS-OC, assuming the present station network to be extended by eight additional stations (see Fig. 1.13) that are already under construction or being considered for the future.

From the outcomes of the simulation study, we can conclude that an improved SLR network geometry as well as a technical improvement of the SLR stations, i.e., higher station performances resulting in a higher amount of measurements, are of equal importance. The effect of a potential future station network is a reduction of the weighted root mean square (WRMS) of the translation time series of an SLR-derived weekly ERF by up to 41 % and a reduction of the WRMS of the estimated Earth Orientation Parameters by up to 15 %.

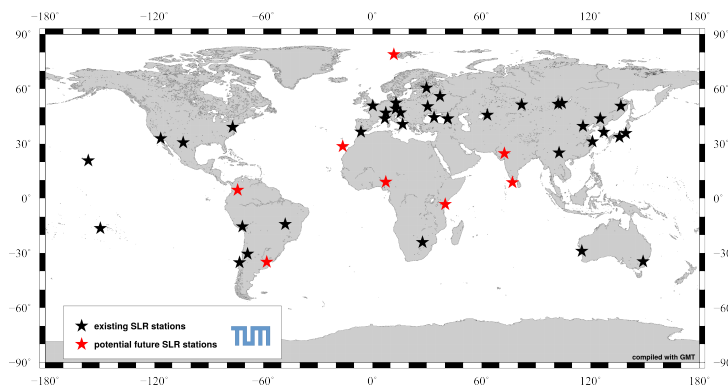


Fig. 1.13: Existing and potential future SLR stations.

Consistent realization of terrestrial and celestial reference systems

The work in this field has been performed in the framework of the project PN5 “Consistent celestial and terrestrial reference frames by improved modelling and combination” within the DFG Research Unit (FOR1503) on “Space-time reference systems for monitoring global change and for precise navigation in space”. The project follows IUGG Resolution 3 (2011) stressing “that the IUGG urged that highest consistency between the ICRF, the ITRF, and the EOP as observed and realized by the IAG and its components such as the IERS should be a primary goal in all future realizations of the ICRS”.

For a consistent realization of CRF and TRF, we prepared VLBI, GNSS, and SLR solutions with

Table 1.4: Multi-year (2005.0 - 2016.0) VLBI, GNSS, and SLR solutions

	VLBI	GNSS	SLR
Institution	DGFI-TUM	CODE (Steigenberger et al., 2014)	DGFI-TUM
Software	OCCAM	Bernese	DOGS-OC
Resolution	session-wise	daily	weekly
Datum definition			
Station coord.	NNR/NNT	NNR/NNT/NNS	NNR
Source coord.	NNR	—	—
Coord. jumps	according to DTRF2014 processing		

different temporal resolutions for 11 years (2005.0–2016.0; see Table 1.4). We accumulated the time series and generated technique-specific multi-year solutions with DOGS-CS. For VLBI, we estimated source coordinates, station coordinates and EOP simultaneously. In total, the multi-year VLBI-only solution contains 69 stations and 3518 sources including 284 defining and 39 special handling sources (Fig. 1.14). The latter are not accumulated over time. Fig. 1.15 shows a declination bias of the DGFI-TUM VLBI-only solution with respect to ICRF2 for southern defining sources that could also be detected by other IVS ACs. It might be caused by the observations of the new Australian VLBI network since 2010.

DGFI-TUM is represented in the IAU Working Group “Third Realisation of International Celestial Reference Frame” (ICRF3). The goal is to perform the combination of VLBI, GNSS and SLR as contribution to the ICRF3 solution. The combination strategy mainly follows the procedure used for the consistent realization of CRF and TRF.

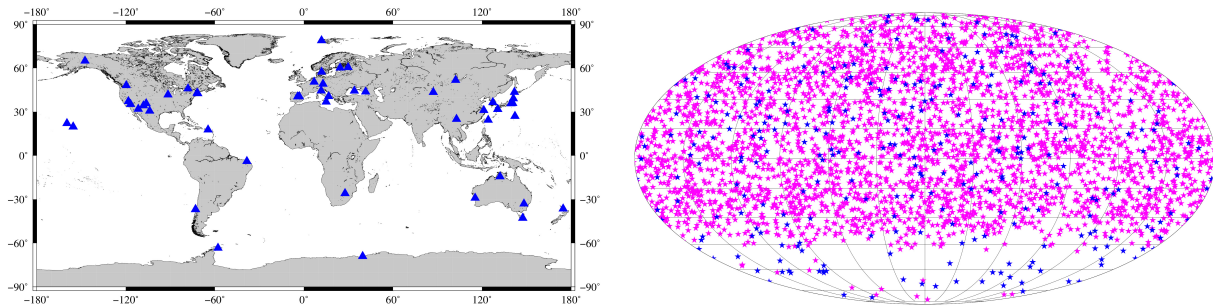


Fig. 1.14: VLBI station (left) and radio source (right) positions from the multi-year VLBI-only solution. There are 284 defining (blue) and other sources (magenta).

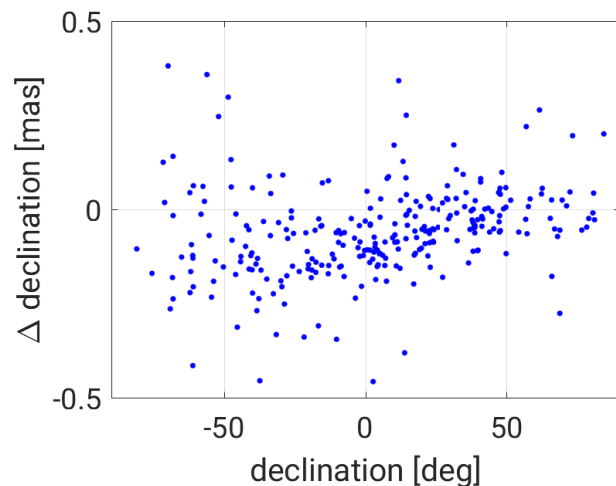


Fig. 1.15: Declination differences between the DGFI-TUM VLBI-only solution and the ICRF2 for defining sources.

DFG Project CIEROT

In September 2016, the DFG-funded project CIEROT (Combination of geodetic space observations for estimating cryospheric mass changes and their impact on Earth rotation) started at DGFI-TUM. This project focuses on the determination of the effect of mass changes within the cryosphere on Earth rotation from a combination of geometric and gravimetric space observations (see Figure 1.16).

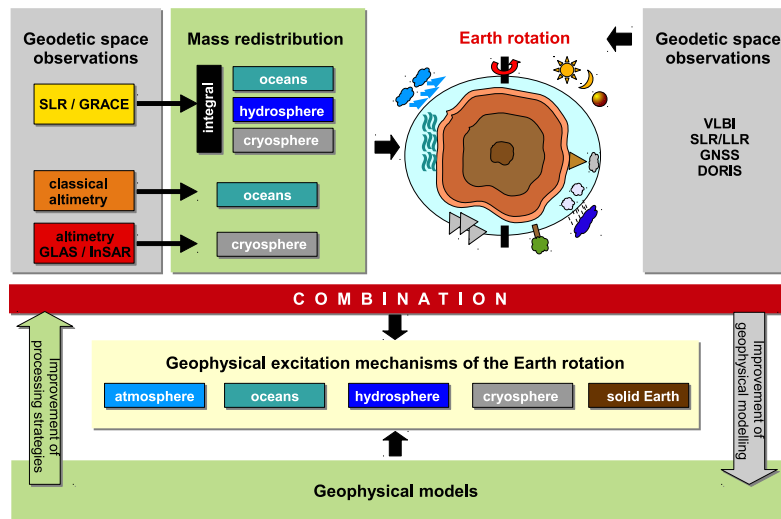


Fig. 1.16: Flow chart of the project CIEROT.

Redistribution and motion of masses in the Earth System cause Earth rotation variations. While the integral excitation mechanism is observed by geometric space techniques with high accuracy, the separation into the individual contributions from the subsystems of the Earth remains a challenge. Especially the estimation of the cryospheric mass effect has large uncertainties due to the absence of precise geodetic information on global scale and reliable cryosphere models.

Since 2002, gravity field changes of the Earth have been observed by the satellite mission GRACE (Gravity Recovery and Climate Experiment). The separation of the measurements into the contributions of the oceans, continental hydrosphere and cryosphere suffers from uncertainties due to (1) the de-striping and filtering of the GRACE data, (2) the separation of the individual contributions (leakage effect), (3) the reduction of glacial isostatic adjustment and (4) an appropriate replacement of the Stokes coefficients C_{10} , C_{11} , S_{11} and C_{20} . The latter two aspects affect, in particular, the estimation of ice mass changes. First analysis shows that estimations of the Antarctic mass trend (2006-2013) scatter of about 28 Gt/year due to the application of different solutions for the degree-1 Stokes coefficients, while the scatter due to the usage of different solutions for the Stokes coefficient C_{20} is about 10 Gt/year.

Since 2003 and 2010, respectively, ice height changes can be observed by the altimeter satellites ICESat and CryoSat-2 with high accuracy. The transformation of these measurements into ice mass changes requires knowledge of the ice dynamics and its density. Within this project, for the first time, geometric and gravimetric space observations will be combined in order to estimate the cryospheric mass effect on Earth rotation. By the combination of different geodetic space observations, weaknesses of individual observations can be compensated, and technique-specific strengths can be optimally accounted for. The findings will also provide information about the influence of increased ice melting and the corresponding sea level change on Earth rotation. Vice versa, the changes in Earth rotation will be analysed with respect to their impact on the mean annual temperature of the Earth. The resulting changes of mass and angular momentum within the cryosphere will also contribute to improve cryosphere models.

Vertical reference systems

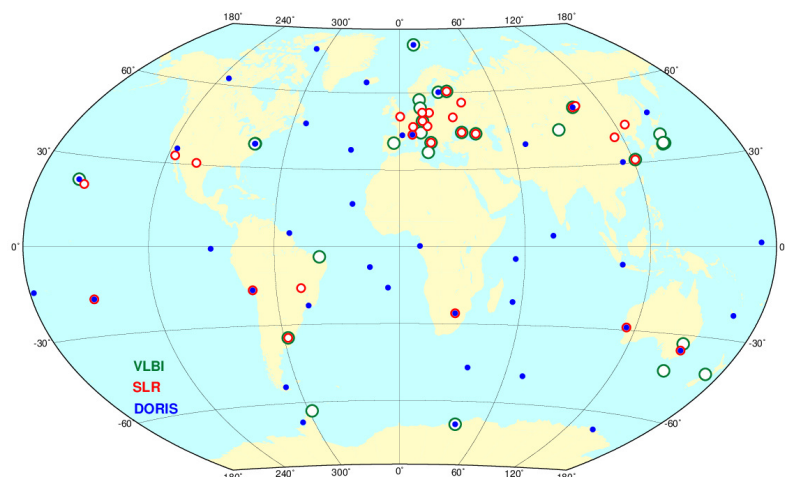
The IAG released in July 2015 a resolution for the definition and realisation of an International Height Reference System (IHR). The IHR is defined in terms of potential parameters: the vertical coordinates are geopotential numbers ($W(P) = C(P) = W_0 - W(P)$) referring to an equipotential surface of the Earth's gravity field realised by the conventional value $W_0 = 62\,636\,853.4 \text{ m}^2\text{s}^{-2}$. The spatial reference of the position P for the potential $W(P) = W(X)$ is given by coordinates X of the ITRF. This IAG resolution also states that parameters, observations, and data shall be related to the mean tidal system/mean crust (Sánchez et al. 2016).

At present, the main challenge is the realization of the IHR, i.e., the establishment of the International Height Reference Frame (IHRF). It is expected that the IHRF follows the same structure as the ITRF: a global network with regional and national densifications, whose geopotential numbers referring to the global IHR are known. According to the IAG objectives, the target accuracy of these global geopotential numbers is $1 \times 10^{-2} \text{ m}^2\text{s}^{-2}$. In practice, the precise realization of the IHR is limited by different aspects; for instance, there are no unified standards for the determination of the potential values $W(P)$, the gravity field modelling and the estimation of the position vectors X follow different conventions, the geodetic infrastructure is not homogeneously distributed globally, etc. This may restrict the aspired accuracy of $1 \times 10^{-2} \text{ m}^2\text{s}^{-2}$ to some orders lower (from $10 \times 10^{-2} \text{ m}^2\text{s}^{-2}$ to $100 \times 10^{-2} \text{ m}^2\text{s}^{-2}$). Consequently, the next step is to outline the minimum set of fundamentals needed for a reliable and sustainable realisation of the IHR. DGFI-TUM contributes to the implementation of the IHRF by:

- Identifying and defining the standards and conventions required to establish an IHRF consistent with the IHR definition. A main issue is the high-precise modelling of the time-dependent changes of the vertical coordinate (which reflects time variations of $X(P)$ and $W(P)$).
- Formulating the minimum requirements for the IHRF reference stations.
- Developing strategies for the collocation of IHRF reference stations with existing geometrical reference stations at different densification levels.
- Investigating processing strategies for the determination of precise potential values $W(P)$ and approaches for the vertical datum unification into the global IHR/IHRF.

These activities are developed under a strong international cooperation coordinated by DGFI-TUM through the working group "Strategy for the realisation of the International Height Reference System (IHR)". This is a joint working group of GGOS, IAG Commission 2 (Gravity field), IAG Commission 1 (Reference Frames), IAG Inter-commission Committee on Theory (ICCT), and the International Gravity Field Service (IGFS). As an example of the first achievements, Fig. 1.17 shows a preliminary selection of the IHRF core stations. Efforts concentrate at present in the determination of precise potential values for those stations.

Fig. 1.17: Selection of possible IHRF core stations (status Dec. 2016): Additional regional stations have to be considered to improve the geographical distribution of the sites. The final selection depends on the availability of gravity data for the computation of the potential values.



Related publications

- Bloßfeld M., Stefka V., Müller H., Gerstl M.: Satellite laser ranging – a tool to realize GGOS ? In: Rizos C., Willis P. (Eds.) IAG 150 Years, IAG Symposia 143, 540–547, 2016a, doi:[10.1007/1345_2015_202](https://doi.org/10.1007/1345_2015_202)
- Bloßfeld M., Seitz M., Angermann D., Moreaux G.: Quality assessment of IDS contribution to ITRF2014 performed by DGFI-TUM. *Advances in Space Research* 58(12), 2505–2519, 2016b, doi:[10.1016/j.asr.2015.12.016](https://doi.org/10.1016/j.asr.2015.12.016)
- Klopotek G., Artz T., Bellanger A., Bourda G., Gerstl M., Gordon D., Haas R., Halsig S., Hjelle G.A., Hobiger T., Hugentobler U., Iddink A., Kirkvik A.S., Lambert S., Plank L., Schmid R., Shu F., Titov O., Tong F., Wang G., Xu M., Zheng W.: Results from the VLBI Analysis Software Comparison Campaign 2015. In: Behrend D., Baver K.D., Armstrong K.L. (Eds.) *New Horizons with VGOS, International VLBI Service for Geodesy and Astrometry 2016 General Meeting Proceedings*, NASA/CP-2016-219016, 203–207, 2016
- Sánchez L.: SIRGAS Regional Network Associate Analysis Center Technical Report 2015. In: Jean Y., Dach R. (Eds.) *International GNSS Service Technical Report 2015*, 111–121, 2016, doi:[10.7892/boris.80307](https://doi.org/10.7892/boris.80307)
- Sánchez L., Čunderlík R., Dayoub N., Mikula K., Minarechová Z., Šíma Z., Vátrt V., Vojtíšková M.: A conventional value for the geoid reference potential W_0 . *Journal of Geodesy* 90(9), 815–835, 2016, doi:[10.1007/s00190-016-0913-x](https://doi.org/10.1007/s00190-016-0913-x)
- Sánchez L., Drewes H.: Crustal deformation and surface kinematics after the 2010 earthquakes in Latin America. *Journal of Geodynamics* 102, 1–23, 2016, doi:[10.1016/j.jog.2016.06.005](https://doi.org/10.1016/j.jog.2016.06.005)
- Sánchez L., Drewes H.: Crustal deformation and surface kinematics after the 2010 earthquakes in Latin America, links to crustal deformation model VEMOS2015 files. *PANGAEA*, 2016, doi:[10.1594/PANGAEA.862536](https://doi.org/10.1594/PANGAEA.862536) (Open Access)
- Schöne T., Bingley R., Deng Z., Gravelle M., Griffiths J., Guichard M., Habrich H., Hansen D., Hunegnaw A., Jia M., King M., Merrifield M., Mitchum G., Neilan R., Noll C., Prouteau E., Sánchez L., Santamaría-Gómez A., Teferle N., Thaller D., Tregoning P., Williams S., Wöppelmann G.: Tide Gauge Benchmark Monitoring Working Group Technical Report 2015. In: Jean Y., Dach R. (Eds.) *International GNSS Service Technical Report 2015*, 195–196, 2016, doi:[10.7892/boris.80307](https://doi.org/10.7892/boris.80307)
- Schwatke C.: EUROLAS Data Center (EDC) – Status Report 2014-2016. *Proceedings of the 20th International Workshop on Laser Ranging*, Potsdam, Germany, 2016
- Schwatke C.: EUROLAS Data Center (EDC) – Recent developments of the EDC. *Proceedings of the 20th International Workshop on Laser Ranging*, Potsdam, Germany, 2016
- Seitz M., Bloßfeld M., Angermann D., Schmid R., Gerstl M., Seitz F.: The new DGFI-TUM realization of the ITRS: DTRF2014 (data). *Deutsches Geodätisches Forschungsinstitut*, Munich, 2016, doi:[10.1594/PANGAEA.864046](https://doi.org/10.1594/PANGAEA.864046) (Open Access)

2 Research Area Satellite Altimetry

The requirements for a coordinated satellite altimetry program were firstly formulated at the 1969 Williamstown Conference on Solid Earth and Ocean Physics. Since these days, satellite altimetry has developed to an operational remote sensing technique with important applications in geodesy and many other Earth sciences. Starting with Seasat in 1978, the altimeter mission history includes a considerable number of missions with different orbit configuration, sampling characteristics, and measurement principles. In 2016, six contemporaneous satellites provide sea surface heights and related data sets with accuracies of a few centimeters. The precise, absolute, and nearly global determination of the ocean surface is an essential source of any research on ocean dynamics. Moreover, satellite altimetry allows for monitoring water level variations of inland water bodies and height variations of ice sheets and glaciers. This observation technique is therefore not only important for oceanography, but also for hydrology and cryosphere research as well as for geodetic applications such as marine gravity field determination and the unification of height systems.

DGFI-TUM maintains complete data holdings of all altimeter missions since 1991, including radar as well as laser observations. The institute operates an open database for satellite altimeter observations and derived high-level products (OpenADB). All altimeter missions are carefully harmonized and cross-calibrated on a regular basis in order to allow for long-term multi-mission applications with improved temporal and spatial resolution (Section 2.1). The multi-mission altimetry data set is used for various ocean and coastal applications (Section 2.2) and also for inland water level monitoring of lakes, rivers, reservoirs, and wetlands (Section 2.3).

2.1 Multi-Mission Altimetry

Open Altimeter Database

In order to ensure a long-term global dataset with optimal spatial and temporal resolution the combination of different altimeter missions is a necessary prerequisite. This requires a consistent dataset based on identical reference frames and corrected by harmonized geophysical correction models. Moreover, for most accurate sea level products, the application of the latest and best correction models is necessary. In 2016, the OpenADB database was supplemented by a variety of different new models (e.g., GOT4.10 ocean tide model and DTU15 mean sea surface) and new orbit products (e.g., based on GDR-E orbit standards). Moreover, reprocessed data of Cryosat-2 (Baseline C) and Jason-1 (GDR-E) were integrated in the database, as well as data of the new missions Jason-3 and Sentinel-3A. Based on all these improvements, a new version of multi-mission crossover analysis was performed (MMXO16) to compute updated time series of radial error corrections as well as improved along-track sea surface heights and sea surface anomalies.

Calibration of new altimetry missions

With the launch of Jason-3 in January and Sentinel-3A in February, the number of active altimetry missions has increased to six in 2016. DGFI-TUM started to analyse the new data sets as soon as they were provided to the calibration/validation community. In the first step, the

data sets were reformatted and integrated in DGFI-TUM's Multi-Version-Altimetry (MVA) data structure. In order to perform a data validation and to include the new missions in the DGFI-TUM's multi-mission data set, in a second step, a global multi-mission crossover analysis was performed. This reveals very good performance for both new missions.

Jason-3

Jason-3 was launched mid of January 2016. Only about one month later, the first usable dataset was available. For the first 6 months, the mission used exactly the same orbit as its precursor Jason-2, only some seconds away. In October Jason-2 was shifted to an interleaved orbit.

Jason-3 shows a range bias of about -3 cm with respect to TOPEX and to Jason-2. No significant drift behavior is detectable for the first 17 cycles (about half a year). The scatter of the radial errors yields 1.3 cm for Jason-3 IGDR (Intermediate Geophysical Data Record; latency of a few days) and 1.1 cm for Jason-3 GDR (post-processed data). The mean values for each cycle are illustrated in Fig. 2.1. The cycle averages show very good performance similar to other existing missions and no systematic effects. Moreover, Jason-3 shows minor geographically correlated mean SSH errors, which are only slightly larger than for Jason-2.

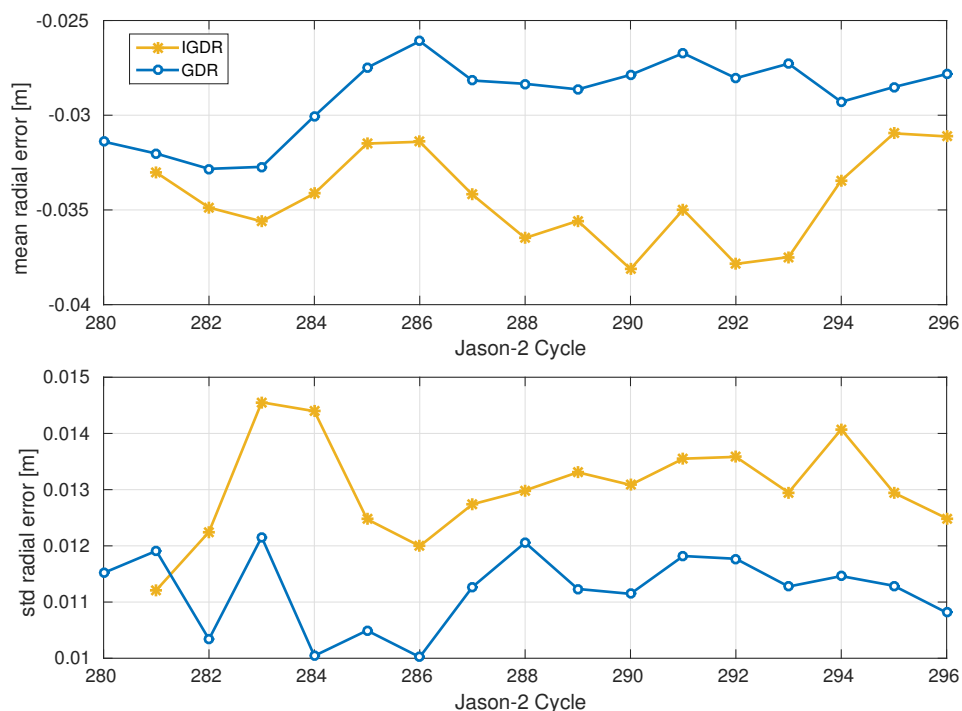


Fig. 2.1: Radial errors for Jason-3 with respect to TOPEX: 10-day means (top) and standard deviations (bottom) for post-processed (blue) and near real-time (yellow) products.

Sentinel-3A

Sentinel-3A is part of the European Copernicus program and is dedicated to operational oceanography. The mission was launched mid of February 2016 in a 27-day repeat orbit with an altitude of about 815 km. It is the first of a set of altimeter satellites to be launched within the next years (Sentinel-3B is planned for late 2017).

The multi-mission cross-calibration of the preliminary altimetry data set released to the Sentinel-3 validation team reveals a mean range bias of about -7 cm with respect to TOPEX for near real-time (NRT) data. The scatter of the radial errors is computed to be 2.2 cm. This is a bit larger than for the other missions, but it is still very promising for a NRT dataset. However, in contrast to the other missions, the current Sentinel-3A NRT data (three months from July to October 2016) reveal a significant North-South pattern with amplitudes up to 4 cm (see Figure 2.2).

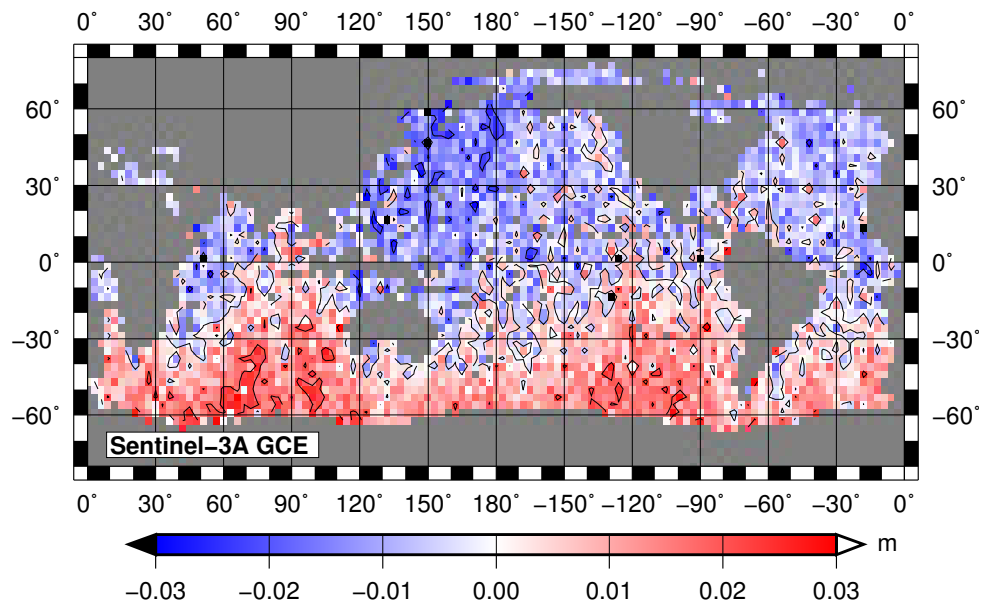


Fig. 2.2: Geographically correlated mean errors for Sentinel-3A (L2 Marine NRT data for three months).

2.2 Sea Surface

Empirical Ocean Tide Modelling

Since the launch of TOPEX/Poseidon satellite in 1992, ocean tide models reached remarkable results in deep ocean and shallow water tidal representation. However, lower performance of tide models is still found in coastal and Arctic regions where the availability and the quality of altimetric observations are highly influenced by the presence of land or ice. Coastal areas are also characterised by complex tidal regimes that depend on several factors, such as the bathymetry, the shape of the shelf, and the presence of additional minor tidal constituents. Difficulties in coastal tide description are encountered in many models, for which considerable discrepancies are found when compared. An example is given in Figure 2.3, where the solutions for the real part of M_2 tidal constituent are compared between DGFI-TUM's EOT11a model, TPX08, and FES2012, respectively. In both plots, the difference in the models becomes more significant as approaching the coast.

Up to present, the EOT model (whose last version is EOT11a) has shown good performance and robustness, however the tidal representation at high latitudes and coastal regions remains problematic. For this reason, DGFI-TUM has started a new study with the main purpose of updating the EOT tidal model with the latest altimetric data, focusing on areas where composite tidal regimes occur. The last improvements in altimetry, together with the recent enhancements of tide models, will allow a better description of coastal and Arctic tides. Moreover, the use of an extended time series up to present will lead to a major model robustness. For this study, the

most recent data of the OpenADB MVA database will be exploited, encompassing the missions TOPEX, Jason-1, Jason-2, ERS-2, Envisat, and Jason-3, reaching a time coverage of about 25 years. As a first approach, the model will describe the following constituents: M_2 , S_2 , N_2 , K_2 , $2N_2$, K_1 , O_1 , Q_1 , P_1 , S_1 , M_f , M_m , M_4 . Every tidal coefficient can be derived through the spherical harmonic analysis or the admittance technique. We will select those method that best describes the single tidal constituents. The estimation of each constituent is performed along-track, as this strategy dramatically improves the computational time. Further steps in the new EOT realisation will be a regional model analysis and validation with tide and bottom pressure gauges, as well as comparisons with empirical and hydrodynamic models.

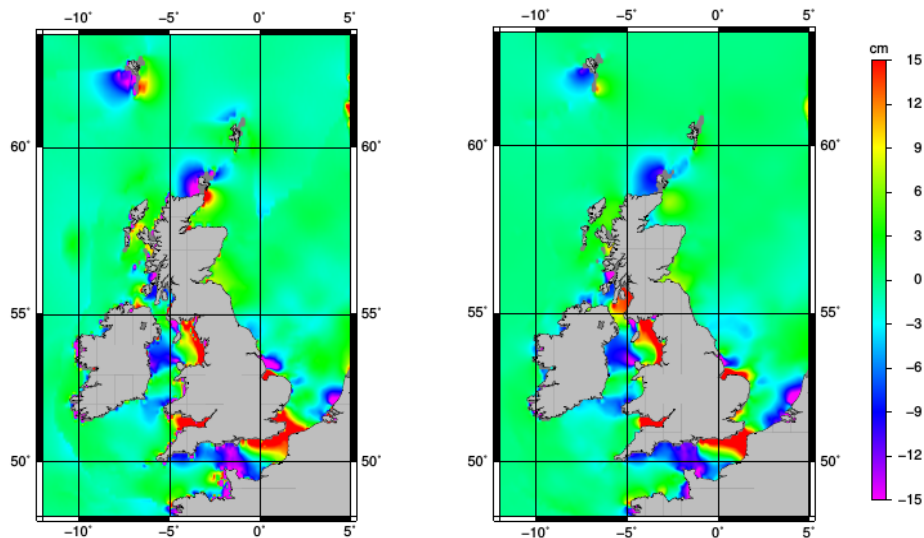


Fig. 2.3: Comparison of the real part of M_2 over Great Britain for EOT11a, FES2012, and TPX08: EOT11a versus TPX08 (left) and EOT11a versus FES2012 (right).

Further developments in Coastal Altimetry

In the last years, scientists from DGFI-TUM have developed the Adaptive Leading Edge Sub-waveform (ALES) retracker, an algorithm enabling the improvement of coastal altimetry datasets (Passaro et al., 2014¹). The ALES retracked coastal ranges are continuously improved and applied for various applications in collaboration with other scientists.

The first steps in the development of a dedicated Sea State Bias (SSB) correction have been validated. The SSB, linked with both the signal processing of the radar echo and the physics of the measurement, is one of the time-variable corrections that are applied to sea surface height estimates from satellite altimetry. With a mean of 5 cm and a time-variable standard deviation of 2 to 5 cm in the open ocean, it is currently one of the largest sources of uncertainty linked with the altimetric signal.

The potential of a dedicated SSB correction for coastal altimetry has been investigated in Gomez-Enri et al. (2016), in which the SSB recomputed for ALES Envisat tracks in the Strait of Gibraltar simply using the same empirical model of the standard product (therefore not optimized neither for the coast nor for the specific retracker) already yields to a better comparability with in-situ data from tide gauges. The sea level anomalies were then validated by means of

¹Passaro M., Cipollini P., Vignudelli S., Quartly G., Snaith H.: ALES: A multi-mission subwaveform retracker for coastal and open ocean altimetry. Remote Sensing of Environment 145, 173-189, 10.1016/j.rse.2014.02.008, 2014

a series of in-situ data from tide gauges along the Spanish coast (see Fig. 2.4), improving the along-track sea level anomaly (SLA) uncertainty by 25% (at 25-15 km from the coast).

The problem of more energetic signals in the coastal areas concerning seasonal time scales has been addressed by the use of the reprocessed ALES coastal along-track data for the Indonesian seas (Passaro et al., 2016, also using Cryosat-2 SAR altimetry data). The use of ALES data reveals the higher amplitude of annual cycles of the sea level in the presence of the Java Coastal Current south of the Java Island. It was possible to detect the semiannual Kelvin Wave travelling from the Indian Ocean into the internal seas of Indonesia.

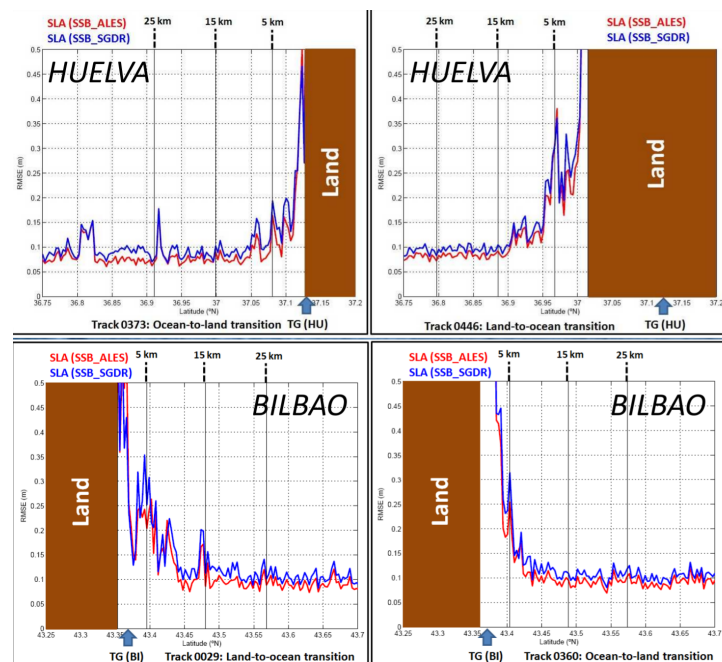


Fig. 2.4: Root Mean Square Error of Sea Level Anomaly (SLA) from ALES-reprocessed Envisat tracks w.r.t. four tide gauges located around the coast of Spain. In blue, the ALES high-rate SLA with SSB available in the standard product, in red the ALES high-rate SLA with SSB recomputed from ALES significant wave height and wind speed.

Arctic Ocean altimetry - open water detection and its validation

The Arctic ocean and its peripheral seas are among the regions on the Earth that are most affected by climate change. They are covered by a dynamic changing sea ice layer with significant influences on the Earth climate system. The Greenland Sea and the more northern located Fram Strait embody the main ice discharge pathways from the central Arctic ocean southwards. During the last decades, increasing sea surface temperatures as well as an amplified warm water inflow into the Arctic ocean provoke a decreasing of the sea ice extent and an accelerating mass loss of Greenland's marine-based outlet glaciers.

Since the ocean in the northernmost latitudes is partially covered by sea ice, the sea level estimation is limited to the leads, narrow cracks in the sea ice that can be several tens of kms long. Since these ocean patches are very smooth and do not have a developed wave field, the signal returned to the satellite is much stronger than the one reflected from the surrounding ice and can dominate the registered waveforms even if the lead is not located at nadir. Thus, the behaviour of the returned signal can be used to classify open water areas solely based on altimetry information.

DGFI-TUM develops different methods for the classification of measurements from different satellite missions based on pulse-limited altimeter waveforms and Delay-Doppler Stack data. Moreover, a validation methodology based on SAR image processing and automatic comparison to the altimetry along-track data is investigated in order to identify the performance of the water detection procedure.

Creation of a validation dataset: Open Water detection based on imaging SAR data

In order to create a validation possibility for the altimetry-based classification approaches an open water detection based on automatic SAR image processing has been developed by DGFI-TUM. Contemporary to the altimeter satellites, space-born SAR sensors provide regularly and spatially extended snapshots of rapid changing sea ice regions. In contrast to multispectral sensors, they are unaffected by clouds and illumination conditions, which enhance the opportunity to find spatio-temporally suited images for a robust and reliable comparison process. The strategy takes advantage of SAR scattering properties of different sea ice surface conditions. Very flat and smooth areas, for example small open water areas, feature very specular backscatter characteristics. They show up very dark in contrast to sea ice affected areas exhibiting a rougher surface and more diffuse reflections leading to brighter pixel values. In general, the brightness of the pixel is not only dependent on the surface conditions, but also on the transmitting frequency, the penetration depth and the incidence angle. In our approach, we use short-wave C-Band SAR data from Sentinel-1A, as well as Radarsat-2, and long-wave L-Band images from ALOS. To compensate the continual influence of the sea ice motion, the image coordinates are shifted by a mean sea ice velocity concerning the time gap between the acquisition dates of the altimetry and the SAR satellites. Figure 2.5 shows clockwise the image processing chain of a Sentinel-1 SAR image, i.e, the procedure for an automatic open water detection.

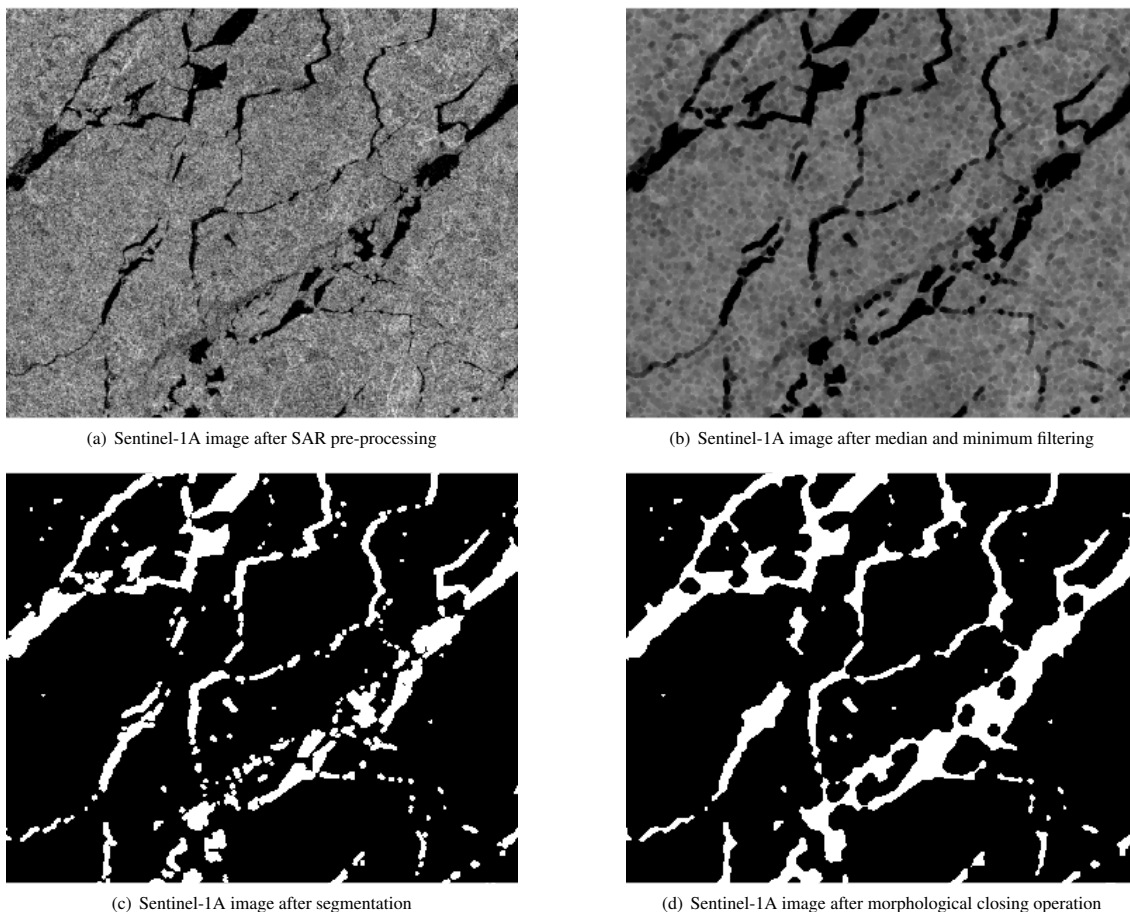


Fig. 2.5: Sentinel-1A image subset of about 24x24 km: (a) the original greyscaled SAR image after SAR pre-processing; (b) the same image after 5x5 pixel median and minimum filtering; (c) the binary image after segmentation by adaptive thresholding; (d) final image after closing operation giving open water in white and sea ice areas in black (after Passaro et al., submitted).

In order to emphasize the transition between ice and open water regions, the images have to be noise reduced by applying a median filter. In a next step, the greyscaled images undergo a minimum filtering to highlight dark pixel areas and to adjust to displacements caused by sea ice motion. To control the effect of minimum filtering, a structure or kernel matrix showing a variable neighborhood size and shape is used. Reliable results are reached by employing an octagon kernel with a radius of 3 pixels around the center pixel. After minimum filtering, the images have to be converted to binary map to indicate open water pixel by ones and ice pixels by zeros. Therefore, a segmentation based on an adaptive thresholding is employed to take into account illumination and contrast variations within the image. The last step processes a linking of fragmented and adjacent open water areas. Due to environmental and instrumental influences, for example wind, refreezing or an insufficient pixel resolution small open water regions brighten up and show a noisier scatter signature. As a consequence, leads and polynyas get divided after thresholding. To reconnect these areas, a mathematical morphological closing operation is used. It enlarges open water areas by mainly preserving their spatial extent and shape. Furthermore, it fills the gap between directly neighboring lead or polynya fragments. Similar to minimum filtering the closing operation is controlled by a kernel. In this case, the kernel size is set regarding to the pixel resolution of the used images. Detailed information on the method will be published in Passaro et al. (submitted). Analyzing the transition from Figure 2.5c to d the reconnecting of thin leads is clearly visible. More details on the approach will be published in Passaro et al. (submitted).

For the comparison between the SAR images and the altimetry open water detection results, the binary converted SAR pixels are interpolated to ice open water assigned altimetry track coordinates using nearest neighbor interpolation.

Unsupervised classification of pulse-limited altimeter waveforms

In the framework of the DFG-funded project NEG-OCEAN, DGFI-TUM develops an unsupervised classification algorithm to identify open water radar returns based solely on altimetry data themselves without the use of any well-known external training data or a-priori knowledge.

The shape of an altimetric radar return, called waveform, is strongly affected by the reflecting surface. Flat and smooth surfaces, such as calm open water regions, produce very narrow and single peaked waveforms, whereas more rough surfaces result in a diffuse and noisier waveform shape. We use different waveform features (e.g., the pulse width and the maximum power) to classify the altimetry observations.

In general, the developed unsupervised open water classification is based on two main steps containing an unsupervised waveform clustering section to set up a reference model followed by a classification part to label remaining waveform data. In order to evaluate the classification results, a comparison with imaging SAR data is conducted (see above).

At first, a reference model has to be created. For this purpose, a set of several waveforms, containing a majority of all possible scatter types has to be selected. To group the reference dataset automatically into a specific number of clusters representing various waveform types, a so-called partition clustering algorithm is performed based on six waveform features. For this task, K-medoids cluster algorithm is implemented which categorizes unsupervised the waveforms into a pre-defined number of K classes. Figure 2.6 shows exemplary the clustering for 30 classes based on derived waveform features of about 307000 Envisat waveforms. Afterwards, the obtained waveform model is used to classify and label all remaining waveforms. This is done by K-nearest neighbor, belonging to memory-based classifier methods.

In further steps, the clusters are assigned to different surface conditions in order to condense them to ocean, ice, and lead/polynya returns. This is done by analyzing the mean feature

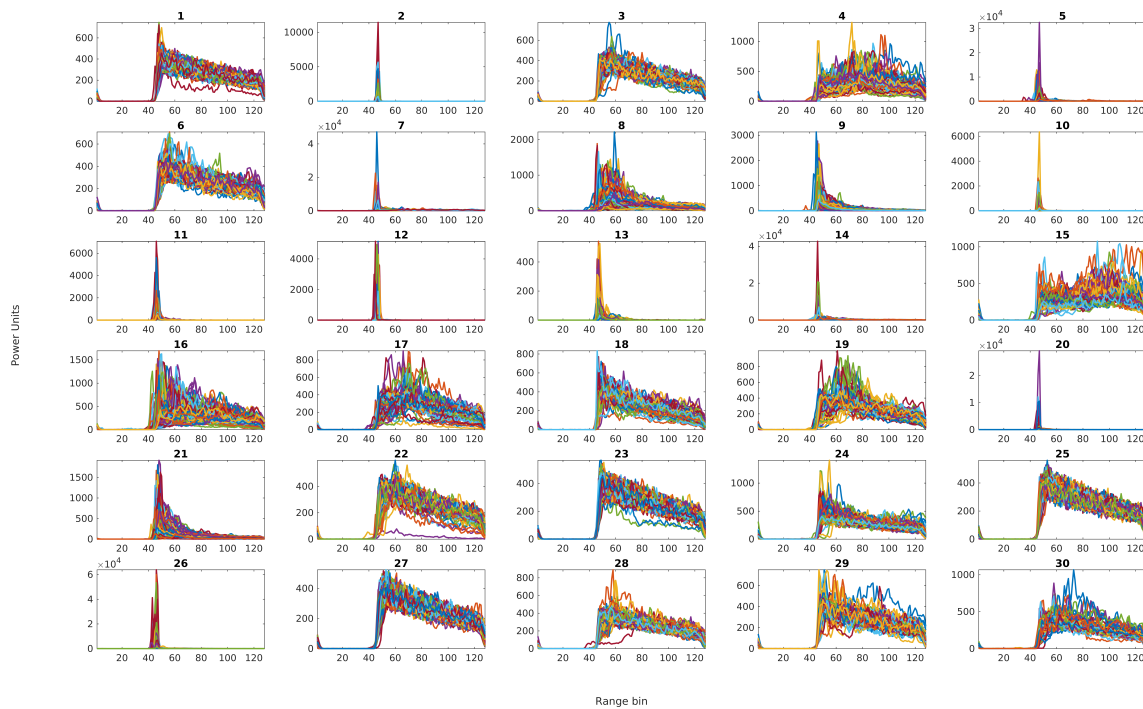


Fig. 2.6: Envisat waveform clusters after K-medoids clustering showing segmented waveforms (every twenty fifth per cluster)

values of each cluster and comparing exemplary chosen waveforms with imaging SAR data. For example, clusters displaying very narrow and clear single-peaked waveforms are labeled to the lead/polynya clusters (e.g., cluster numbers 2, 10, 11, 12, 20 and 26). Waveforms exhibiting a typical ocean-like shape, characterized among others by a weak trailing edge decline or decreased maximum power value, are allocated to ocean waveforms (e.g., clusters 1, 3, 6, 25, etc.). Remaining clusters represent ice returns. If there is no clearly interpretable signature they are set to undefined waveforms (e.g., clusters 5 and 15).

After the classification process, the results are evaluated by comparing them to binary converted SAR images (see above). Beside a visual comparison one further goal is to get quantitative information about the classification performance and efficiency. Therefore, the altimetry classification results are condensed to represent only open water and ice classes and interpolated to the corresponding binary converted pixel coordinates. The comparison results are summed up in a contingency table (see Table 2.1) providing statistical information about classification performance rate.

Figure 2.7 shows an Envisat-ALOS comparison before (left) and after (right) image processing. Cyan coloured altimetry observations identify open water classifications. Furthermore, white areas in the binary coded SAR images indicate open water areas. The snapshot takes place in May 2008 and is not corrected by ice-motion displacements due to an unsure ice drift di-

Table 2.1: 2D contingency table based on Envisat - ALOS comparison. The table shows the number of measurements classified as water/ice from altimetry with the corresponding classification from SAR.

	Altimetry (water)	Altimetry (ice)	Σ
SAR (water)	31	4	35
SAR (ice)	17	89	106
Σ	48	93	141

rection. Table 2.1 displays the corresponding rates of open water and ice detections of both datasets. Summing the diagonals and dividing by the total number of observations gives the true classification rate. In the current example, 85.1% of the comparison points are correctly classified. Furthermore, 88.6% of the SAR open water regions are also identified by altimetry. Moreover, analyzing Figure 2.7a the classification approach is able to detect openings in the ice with different spatial extent. However, comparing Figure 2.7b the SAR image processing is not always able to resolve very narrow lead fragments due to a limited pixel resolution or an insufficient thresholding. Therefore, the quantitative classification results have to be carefully evaluated by taken instrumental, processing and seasonal region dependent uncertainties into account.

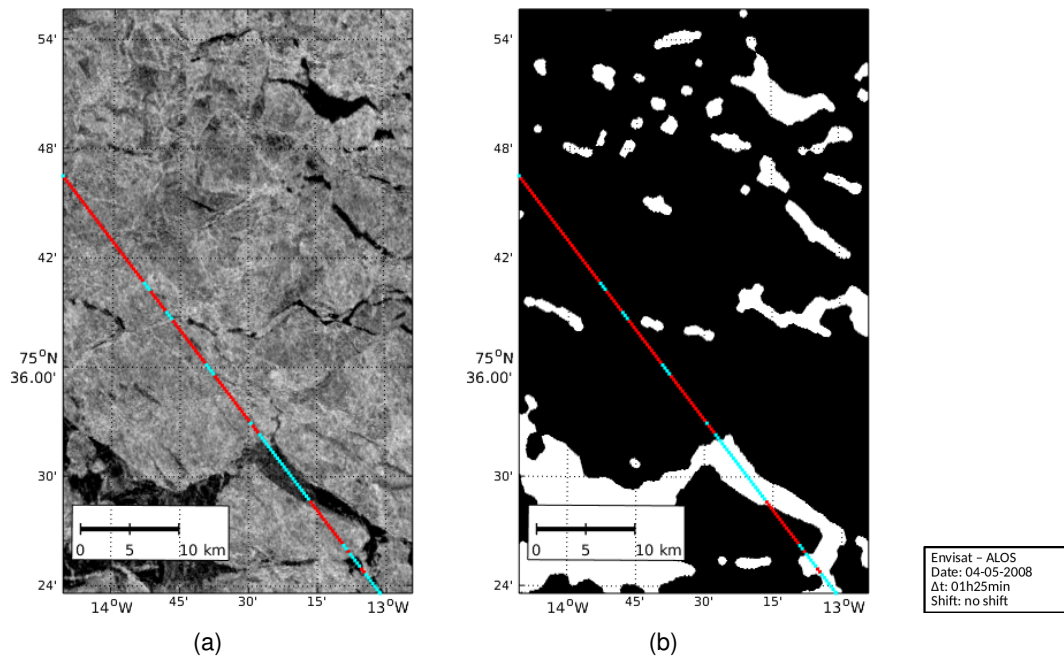


Fig. 2.7: Example of open water detection from Envisat and ALOS before (left) and after SAR image processing (right). Metadata information are given in the box. Red: altimeter ice detection, cyan: altimeter water detection.

Cryosat-2 SAR lead detection

In 2016, an innovative method to capture the fractures in the sea-ice-covered ocean surface based on Cryosat-2 (CS-2) Delay-Doppler measurements and its comparison with SAR images provided by Sentinel-1A was explored. CS-2 offers ways for improving the sea level records in sea-ice regions. Thanks to the Delay-Doppler processing of its echoes, it stores the signal registered by the satellite looking at the same resolution cell on the ground from different look angles. Nevertheless, most of the leads are less than a km wide, while CS-2 has a sampling interval of roughly 300 m (using the 20-Hz rate): in most of the cases, only one range measurement per lead will correspond to the distance at nadir. Being able to correctly identify the nadir echoes of these narrow means providing more sea level measurements, while avoiding errors due to off-nadir effects.

Using processing techniques inherited from the SAR processing, such as range compression and range migration correction, all the returns corresponding to the resolution cell (a 20-Hz sampling of the illuminated surface, i.e., one measurement every 300 m roughly) are aligned in a stack diagram. By summing up the returns in the across-track (range) dimension, the so-called stack waveform, or Range Integrated Power (RIP) waveform, can be generated. It

contains information concerning the backscattering properties of the illuminated surface, but it also reveals details of the distribution of the scatterers as the satellite spans different look angles passing over the nadir position. When the satellite moves over a very smooth surface, such as a small lake or a leads, the signal will be specularly reflected back and the RIP will be peaky. On the opposite, when flying over areas containing scatterers with different orientation, such as for wavy seas or ice, the backscattered power will be more normally distributed.

In order to characterise the RIP shape, the Stack Standard Deviation (SSD) and the Stack Kurtosis (SK) are already given in the official product. These two indices, although useful to classify the kind of waveform, are not sufficient to isolate the nadir return of a group of waveforms influenced by a lead backscatter. In order to compare the power at the zero look angle with the backscatter registered in the other looks, we defined a new parameter called Stack Peakiness (SP) from the RIP normalised by its maximum value in the following way:

$$SP = \frac{1}{\overline{P_{l,r}}} \quad \text{with} \quad \overline{P_{l,r}} = \frac{1}{N} \sum_{i=1}^N P(i)_{l,r} \quad (2.1)$$

where N is the number of looks excluding the nadir look and $P(i)_{l,r}$ is the power from the look angle i , excluding the nadir look (i.e., at its right or left). SP is therefore able to compare the power reflected from the same resolution cell at different view angles. The expected behaviour of SP in the case of a narrow lead crossing the CS-2 track is sketched in Figure 2.8.

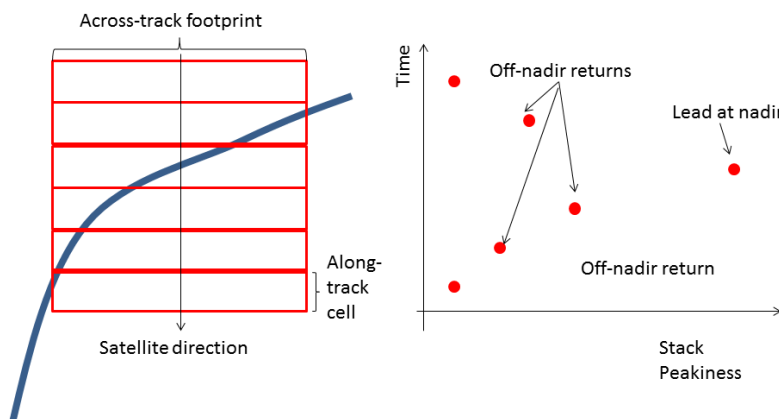


Fig. 2.8: Modelled lead (blue line) crossing over a CS-2 track (left) and expected SP behaviour (right).

When a lead enters the across-track pulse-limited footprint, the SP will be higher than a purely diffusive backscatter event, since the lead will scatter more energy back to the satellite. Nevertheless, the lead will still be slightly off-nadir in the across-track direction: a part of the incoming power will be specularly reflected away. Off-nadir leads are usually characterised by lower levels of backscatter power compared to leads at nadir. Consequently, a lead located off-nadir in the across-track direction will scatter less power back to the satellite, if compared with the same lead illuminated at nadir. The maximum SP, i.e., the time when the power at the zero look angle is strongest in comparison with the backscatter received at the other look angles, is therefore expected to correspond to the position in which the lead is at nadir.

In order to validate the classification, we designed a SAR image processing dedicated to provide information on open water areas in sea-ice regions (see above). A visual comparison between SP-classified CS-2 tracks and SAR images acquired in the Arctic Sea was performed using the latest published lead classification as a reference, which is based on a number of already existing CS-2 parameters, including SSD and SK (Ricker et al., 2014²).

²Ricker R., Hendricks S., Helm V., Skourup H., Davidson, M.: Sensitivity of CryoSat-2 Arctic sea-ice freeboard and thickness on radar-waveform interpretation. The Cryosphere, 8, 1607–1622, 2014

Several examples, like the one seen in Figure 2.9, could be acquired, in which the SP classification is able to isolate the nadir return while Ricker et al. is influenced by off-nadir returns.

Using the SAR images methodology described above, a quantitative validation was performed comparing the Fraction of False Detections (FFD), i.e. the fraction of points along the CS-2 track that are identified as leads by the altimeter-based method, but identified as ice on the SAR image, with the Fraction of Correctly Classified Leads (FCCL), i.e. the fraction of leads on the SAR image (along the CS-2 track) that are also seen by the CS-2 classification. In this case, the two compared methods scored the same ($FCCL/FFD=1.4$). On one side, this means that SP is able to considerably simplify the current state-of-the-art, by using a single index; on the other side, the strong filtering needed to classify the Sentinel-1 images implies a widening of the lead surface and therefore partially masks out the advantages of the SP classification.

As outcomes of this study, the SP index has been proposed to the European Space Agency (ESA) as an additional official stack parameter. Method and results will be published soon (Passaro et al., submitted).

Arctic Ocean altimetry: the Sea Level Climate Change Initiative

Sea level retrieval in high latitudes is normally hampered by the presence of sea ice. In this case, sea level needs to be computed on leads. ESA has fostered in recent years significant efforts to improve sea level at high latitudes. In this context, DGFI-TUM is part of the consortium of the Sea Level Climate Change Initiative (SL_cci), whose final aim is to provide significant data in the Arctic of importance to climate research.

The characteristics of the radar signal reflected from the leads are different from the typical behaviour in the open ocean. While the latter is characterised by a growing leading edge whose width depends on the sea state and a slowly decaying trailing edge, the former has a typical impulse-like shape that is often poorly sampled by the altimeter (the so-called peaky waveforms). Due to these differences, scientists have so far used different fitting algorithms to estimate the sea level from these signals, leading to considerable uncertainties and biases.

DGFI-TUM duties in this project are concentrated on the extension of the Adaptive Leading Edge Subwaveform (ALES) retracker, a waveform-fitting algorithm that has been successfully applied to improve the altimetry data quality and quantity in the coastal ocean (Passaro et al., 2016). The approach is, in fact, similar to the coastal ocean problem: to adapt a versatile algorithm to different kinds of signal shapes. The missions on which the retracking procedure is applied are Envisat and ERS-2, in its REAPER reprocessing release. While the ALES algorithm for Envisat already exists, the main innovations and objectives in the framework of this project are the tuning the ALES algorithm for ERS-2 REAPER and the adaptation of the ALES algorithm for lead-like waveforms. The outcome of this experimental extension has been called ALES+.

The key concept of ALES is preserved in ALES+: the isolation of a part of the signal to be retracked in order to exclude perturbations by areas of the footprint with different backscatter conditions, such as patches of calm waters, land or ice, while guaranteeing a comparable

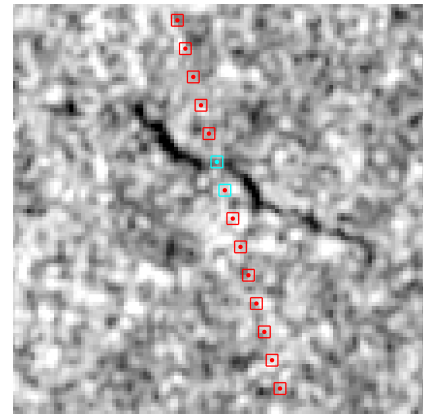


Fig. 2.9: 4.25 by 4.25 km zoom on a lead seen by Sentinel-1 image from 05/09/2015 at 12:46, with Cryosat-2 crossing the area at 16:36. SP (dots) in comparison with classification results of Ricker (squares). Lead detections are highlighted in cyan.

accuracy in typical open ocean conditions. The main innovations concern the oversampling of the signal and the introduction of a preliminary step to estimate the slope of the decaying trailing edge in the case of peaky waveforms. By using this constraint in the subsequent retracking, ALES+ is able to fit the leading edges of any waveform, regardless of the shape of the trailing edge.

An example of the effectiveness of the method is given in Fig. 2.10, in which the fitting error, i.e. a measure of the “goodness of fit”, is shown for peaky waveforms in the test region of the Svalbard, characterised by sea ice in the north of the islands. A value below 0.15 normalised power units is considered as a good fit.

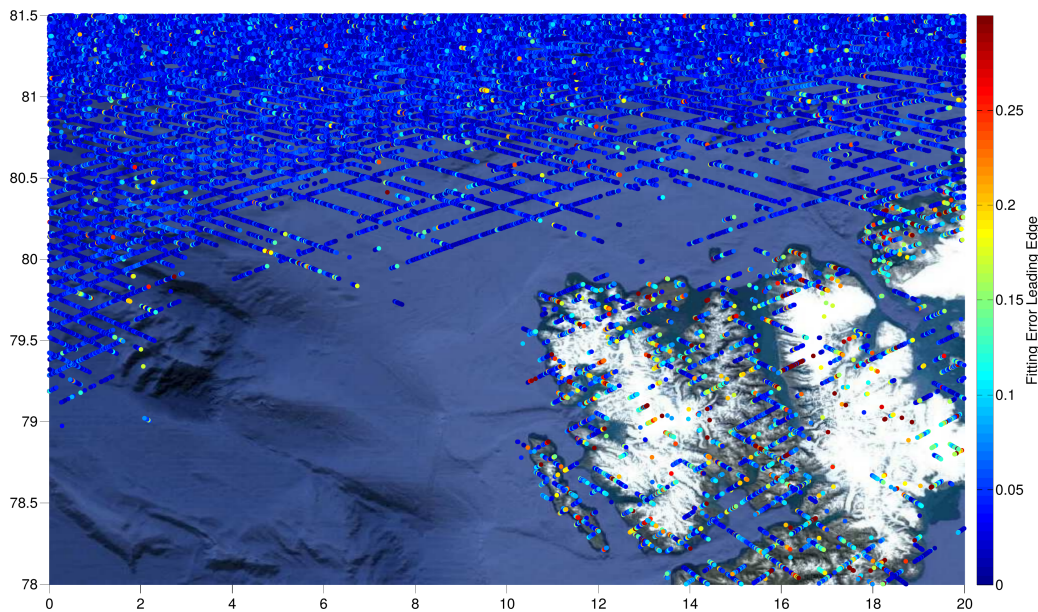


Fig. 2.10: Fitting error on the leading edge for ALES+ retracked Envisat cycle 10 in the Svalbard test region (peaky waveforms only).

Pulse-limited Altimeter Waveform Simulator

With the frame of a master thesis project, a software for simulating radar altimeter waveforms was developed. The created pulse-limited altimeter simulator produces realistic return signals over ocean, ice and snow based on given input parameters, such as altimeter specifications, satellite orbit information and the surface properties and its backscattering characteristics. The simulator allows for an improved understanding of how the presence of ice and snow in sea-ice regions influences the shape of an altimeter waveform, which is crucial for acquiring accurate sea surface height measurements.

The simulated results for homogenous ocean regions matched well to real altimetry data, and acquired the unique waveform shape specific to different satellite altimetry missions. The ocean-ice/snow simulations provided valuable results for characterizing waveforms over sea ice regions. When tested for specific ocean-ice/snow events (e.g. surface boundaries, leads, polynyas, sea ice), the simulator delivered waveforms consistent with real altimetry data.

2.3 Inland Altimetry

Computation of inland water levels in near real-time

Since 2013, the DGFI-TUM is developing the "Database for Hydrological Time Series of Inland Waters" (DAHITI). Currently, water level time series of more than 400 globally distributed inland water bodies are distributed to the public. The applied method for the estimation of water level time series is based on an extended outlier detection and a Kalman approach filter which is described in detail in Schwatke et al. (2015)³.

Up to now, only Sensor Geophysical Data Records (S-GDR) with a latency of about 60 days have been used and the time series were manually updated depending on data availability. In 2016, the data holding has been extended by using also Sensor Intermediate Geophysical Data Records (S-IGDR) with a latency of about 1–2 days. Based on these data sets, a large number of stations is now processed in near real-time (NRT) and updated shortly after the satellite's overflight.

Since all applied geophysical corrections (such as solid Earth tides and wet troposphere correction) are taken from external sources, the data sets only differ in the satellite orbits. For GDR products, final orbits from precise orbit determination (POD) are available, whereas the IGDR products contain preliminary MOE orbits (Medium Orbit Ephemeris). However, this results in height differences less than one centimeter. In contrast to the post-processed time series, no radial errors from multi-mission crossover analysis (Bosch et al., 2014)⁴ are available. Instead, global mean range biases are applied to account for inter-mission offsets. Comparisons show that the near real-time water levels only differ by a few centimeters from the post-processed final heights, meaning that the accuracy of the time series are almost not degraded.

Figure 2.11 shows the near real-time water level time series of Balbina Reservoir in Brazil (2008-07-14 to 2017-01-31), which is crossed by two Jason-2/Jason-3 tracks and computed on 2017-02-02 (two days after the latest overflight). In the first period, the time series is based on S-GDR data (blue). Since 2016-09-28, near real-time S-IGDR data have been used. The resulting water level time series shows no discontinuity when switching from S-GDR to S-IGDR data. This example documents the successful usage of S-IGDR data for the estimation of near real-time water level time series.

Exploitation of CryoSat-2 SAR data over lakes

At DGFI-TUM, an innovative processing strategy has been developed in order to estimate reliable water level time series for lakes from CryoSat-2 SAR observations (Göttl et al., 2016a). The selection of valid water returns is an essential step in inland altimetry applications. For this purpose, an unsupervised classification method for CryoSat-2 SAR multi-looked waveforms has been developed based on the k-mean algorithm. With this approach, changes in the water surface extent or surrounding inundation areas can be taken into account. In a first step, all CryoSat-2 SAR waveforms acquired in the spherical rectangular area of the Lake Tonle Sap are grouped automatically into 30 clusters according to three parameters: amplitude and width

³Schwatke C., Dettmering D., Bosch W., Seitz F.: DAHITI – an innovative approach for estimating water level time series over inland waters using multi-mission satellite altimetry. *Hydrology and Earth System Sciences* 19(10): 4345–4364, 2015, doi:[10.5194/hess-19-4345-2015](https://doi.org/10.5194/hess-19-4345-2015)

⁴Bosch W., Dettmering D., Schwatke C.: Multi-mission cross-calibration of satellite altimeters: constructing a long-term data record for global and regional sea level change studies. *Remote Sensing* 6(3): 2255–2281, 2014, doi:[10.3390/rs6032255](https://doi.org/10.3390/rs6032255)

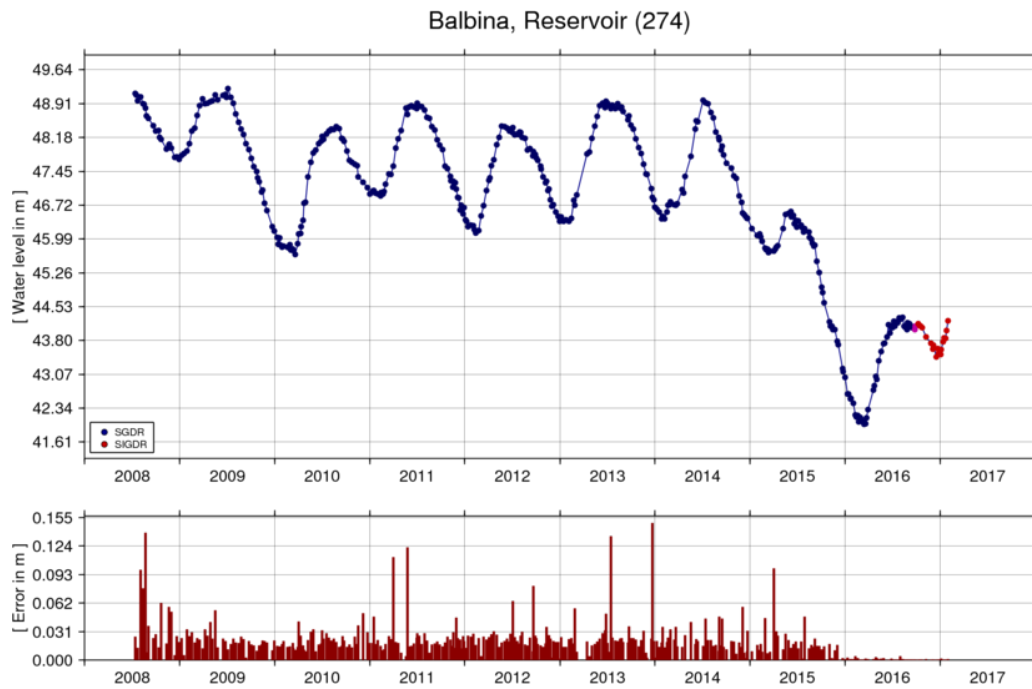


Fig. 2.11: DAHITI near real-time water level time series of Balbina Reservoir in Brazil, South America. The water level time series shows heights based on Jason-2 and Jason-3. The post-processed part of time series is plotted in blue (S-GDR), the near real-time part in red (S-IGDR). The bottom plot shows the uncertainties of the water level.

of the waveform as well as the bin position of the waveform centre of gravity. The large number of clusters is necessary in order to allow for a reliable clustering.

In a post-processing step, based on a visual inspection of the waveform shapes, the 30 clusters are grouped into three surface classes: water, land-water transition and land. While water-like waveforms conform to ocean-like waveforms, the waveforms at the land-water transition contain multiple peaks, and the land-like waveforms exhibit one strong single peak. Due to the fact that the Lake Tonle Sap exhibits nearly all features of landscape (i.e., lake, rivers, wetlands, and flat land except mountains), the clusters are transferable to other lakes. After the identification of waveforms belonging to the classes water or land-water transition, these waveforms are used for range estimation. We have developed a modified version of the Improved Threshold Retracker in order to obtain optimal results for the lake heights. This method is based on the identification of the optimal sub-waveform by employing height thresholds. Afterward, the median of the water heights of each track crossing the investigated lake is determined while outliers are rejected.

The validation of the derived CryoSat-2 SAR time series for the lakes Tonle Sap, Vättern, Okeechobee and Lough Neagh with in-situ gauging data yields RMS differences between 3 and 90 cm (see Table 2.2). Thus, the relative accuracy is better than 10% for all lakes. Compared to modeled CryoSat-2 water heights derived according to the approach used in the Alt-Water database our water level time series are slightly improved in terms of RMS accuracy but they contain more gaps due to the lack of reliable observations (see Figure 2.12 for the Lake Okeechobee). In comparison with classical radar altimeter missions (Envisat, Jason-2, SARAL/AltiKa), the SAR-based time series show smaller RMS differences for the smaller lakes but larger RMS differences for the large lakes covered by multiple repeat missions. The presented innovative processing strategy can be easily adopted to other satellite altimetry SAR data, such as from the new Sentinel-3 mission.

Table 2.2: RMS differences [cm] and squared correlation coefficients (R^2) of the water level time series derived from satellite altimetry with respect to in-situ gauging data for the time span [08.04.2010 - 31.12.2015]. Furthermore the size of the lakes [km^2], the number of CryoSat-2 tracks crossing the lakes as well as the number of points in the water level time series (No.) are given (identical with the number of used data points for the comparison with in-situ data).

lake	size	tracks	DGFI-TUM			DTU			DAHITI		
			RMS	R^2	No.	RMS	R^2	No.	RMS	R^2	No.
Tonle Sap	2600	107	90.1	0.90	107	96.1	0.87	137	72.4	0.93	233
Vättern	1912	76	3.9	0.79	71	4.6	0.75	71	4.0	0.73	29
Okeechobee	1900	54	3.8	0.99	52	7.3	0.98	73	4.9	0.97	33
Neagh	392	54	3.1	0.95	43	6.5	0.88	47	4.2	0.94	30

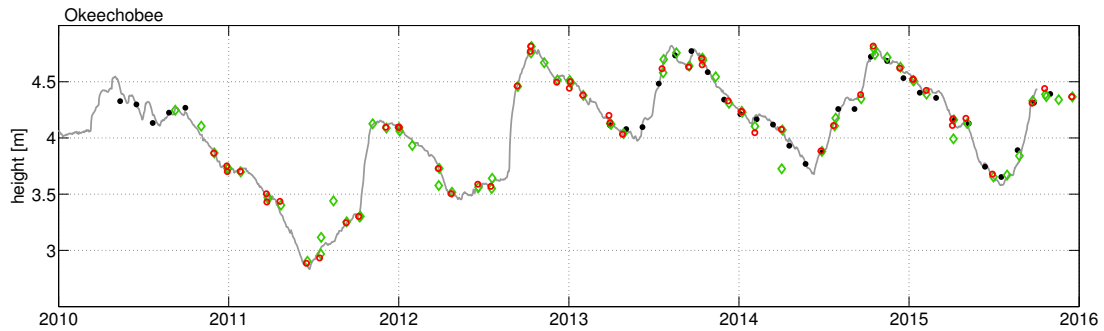


Fig. 2.12: Water level time series solutions for the Lake Okeechobee: DGFI-TUM (red), gauging stations (gray), DAHITI (black) and DTU (green).

High-resolution river water levels based on multi-mission altimetry data

Measuring water level changes of rivers with satellite altimetry got well established in the last years. With the altimetry missions Envisat, SARAL, and Jason-2 it is possible to estimate time series of water levels at specific locations where the satellite track crosses the river. The temporal resolution of the water level time series is always bound to the repeat time of the satellites that is 35 days for Envisat and SARAL and 10 days for the Jason-2 mission. Combining measurements from different passes and missions could improve this temporal resolution as it is already done for lakes in DGFI-TUM's Database for Hydrological Time Series of Inland Waters (DAHITI). This is possible for lakes due to their equipotential surface. However, river water levels are changing rapidly over space which hinders a similar approach. It is not easy to link observations from different locations together without detailed knowledge of the river topography as well as slope, flow velocity, and seasonal behaviour. We developed a new statistical approach to combine the multi-mission altimetry to a temporal high resolution time series without this detailed information.

The method is based on ordinary spatio-temporal kriging. The kriging method predicts a water level at any point along the river and any point in time based on all other observations. We used Envisat, Envisat-EM, SARAL, and Jason-2 data in combination, resulting in an irregular spatial-temporal sampling of the river system. The prediction of a water level is defined as the weighted sum of all the altimeter measurements $\mathcal{Z} := \{Z(\mathbf{s}_1, t_1), \dots, Z(\mathbf{s}_n, t_n)\}$:

$$p(\mathbf{s}_0, t_0) = \sum_{i=1}^n \lambda_i Z(\mathbf{s}_i, t_i). \quad (2.2)$$

The weights λ_i should sum up to 1 and are estimated based on a covariance model C that describes the relationship between the measurements and between the predicted water level

and the measurements.

$$\boldsymbol{\lambda} = (\lambda_1, \dots, \lambda_n) = \left(\mathbf{c} + \mathbf{1} \frac{(\mathbf{1} - \mathbf{1}^\top \boldsymbol{\Sigma}^{-1} \mathbf{c})}{\mathbf{1}^\top \boldsymbol{\Sigma}^{-1} \mathbf{1}} \right)^\top \boldsymbol{\Sigma}^{-1}, \quad (2.3)$$

where $\mathbf{1} = (1, \dots, 1)^\top$, $\mathbf{c} = (C((\mathbf{s}_0, t_0), (\mathbf{s}_1, t_1)), \dots, C((\mathbf{s}_0, t_0), (\mathbf{s}_n, t_n)))^\top$, $\boldsymbol{\Sigma} = (C((\mathbf{s}_i, t_i), (\mathbf{s}_j, t_j)))_{i,j=1\dots n}$.

As one can see from the formulas above the crucial point of the kriging method is the modelling of the covariances. The covariances have to mirror the spatial and temporal variations of the river as seen in the altimeter measurements. With the covariances, it is possible to link all measurements together across time and space. We developed two different spatio-temporal covariance models: one that assumes that the data are stationary both in space and time, and one that considers the space as non-stationary.

With this method, we were able to predict water level time series with a 5-day resolution at every point along the river. For validation purposes, we predicted the water level to the site of gauging stations. In Figure 2.13, the predicted time series for both covariance models in Luang Prabang are shown together with in-situ data. For all gauging stations, we found RMSE (root mean square errors) between 0.5 m and 1.0 m with coefficients of determination above 0.9.

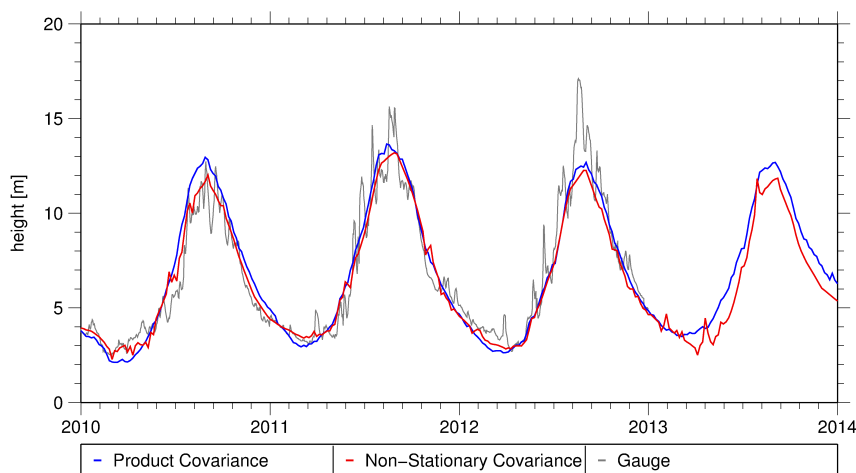


Fig. 2.13: Water level time series (subset of four years) at Luang Prabang: altimetry-based results (blue and red) and in-situ data (grey)

The method and all results for the Mekong area have been published in Boergens et al. (2016a). This paper also provides more details on the different covariance models appropriate for this river.

Water level and water volume changes in inundation areas

Wetlands store over 10% of the global surface water, which is five times the amount of water stored in rivers globally. For lakes and rivers, it is by now common to use satellite altimetry to access water level and water volume changes. However, altimetry over wetlands is more challenging due to the topography and the sporadic nature of water expanse. Wetlands consist of many small pools connected with small streams. These pools have different water levels as the wetlands overall has a slope in the terrain. Additionally, many of the pools are only seasonal and the inundate area changes significantly during the annual and inter-annual cycle.

In Dettmering et al. (2016a), water levels of the Pantanal wetlands are estimated based on Envisat data (2002–2010) as a case study for wetlands altimetry. Over wetlands, it is not possible to have well defined virtual stations like for rivers (crossing of river with satellite track). Therefore, the altimeter track is divided into 0.1 degree long bins on which a mean water level is estimated. It is assumed that in these 0.1° bins no significant height change occurs. Inside each

bin, all altimeter observations are classified into water and land measurements. Afterwards, only the water measurements are used to estimate a mean water level for each pass in the bin. All passes together of one bin form a water level time series - at least for those bins that are sporadically inundated. In Figure 2.14, an exemplary time series is shown for a bin with almost permanent inundation. For each bin, it is also possible to quantify flood frequencies and flood duration.

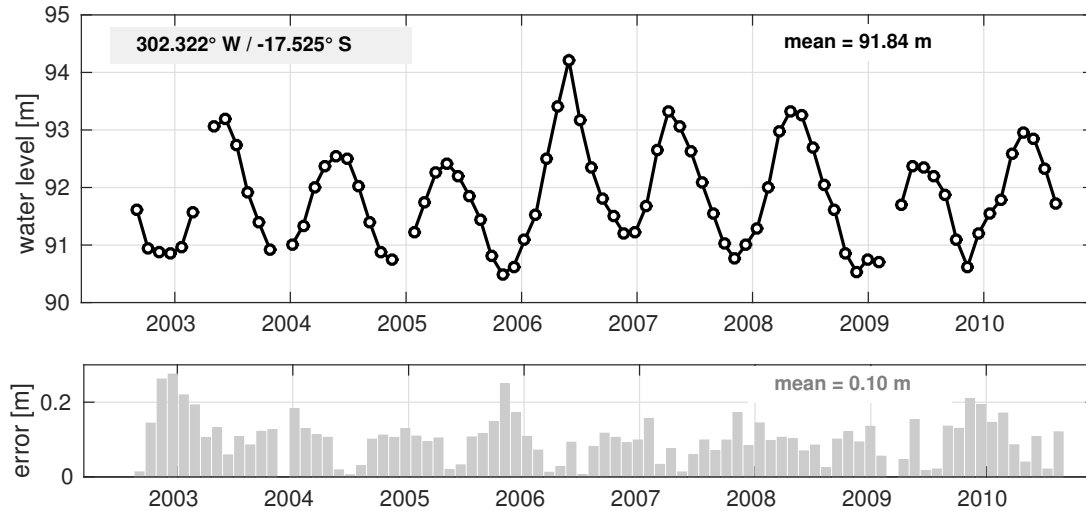


Fig. 2.14: Water level time series for one station in the Pantanal (top) and estimated uncertainties (bottom).

For the estimation of water volume changes, information about the inundated area is needed beside the water level changes. A time series of inundated area is provided by the GIEMS dataset⁵. In this dataset, for each month between 1993 and 2007 the inundated area of 784 km² large cells is given. For those cells that are crossed by an altimeter track, water volume change can be estimated. For each GIEMS cell, the water level time series of all covered 0.1 degree bins are combined to one time series of water level variation. It is assumed that this time series is representative for the change of water level in the whole GIEMS cell. For the years 2002 to 2007, where altimetry and GIEMS data overlap, it is possible to relate the inundated area to the water level. This relationship is shown in Figure 2.15. A hysteresis is well visible. A hysteresis occurs when the relationship of inundated area and water level depend on whether the water is rising or falling. For the overlapping years and under the consideration of the hysteresis, the relationship can be formalised and used to extrapolate it to the years after the end of the GIEMS dataset.

With all this in place, we are able to estimate the water volume change for each GIEMS cell for the whole altimetry time period of 2002–2010. The volume change between two points in time t_i and t_{i-1} is calculated with the pyramid formula:

$$\Delta V(t_i, t_{i-1}) = \frac{1}{3}(H_t - H_{t-1})(A_t + A_{t-1} + \sqrt{A_t A_{t-1}}) \quad (2.4)$$

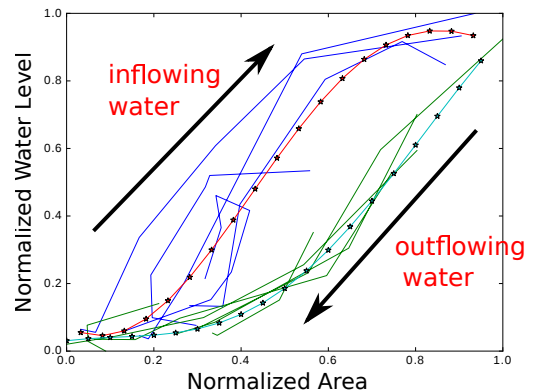


Fig. 2.15: Relationship between inundation area and water level with hysteresis in the Pantanal.

⁵<https://lerma.obspm.fr/spip.php?article91&lang=en>

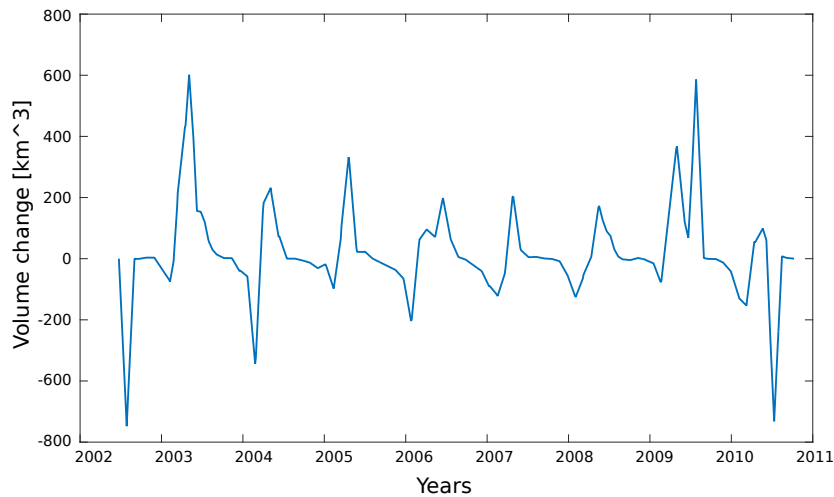


Fig. 2.16: Time series of water volume change in the Pantanal

where H is the water level height and A the area at the time points. The volume change time series for a GIEMS cell in the middle of the Pantanal is shown in Figure 2.16. After a swift flood the water volume is slowly declining and remains for most of the year on a more or less stable plateau. Only shortly before the onset of the new flood the water volume drops to a minimum.

Related publications

Boergens E., Buhl S., Dettmering D., Klüppelberg C., Seitz F.: Combination of multi-mission altimetry data along the Mekong River with spatio-temporal kriging. *Journal of Geodesy*, doi:[10.1007/s00190-016-0980-z](https://doi.org/10.1007/s00190-016-0980-z), 2016a

Boergens E., Buhl S., Dettmering D., Schwatke C., Seitz F.: The kriging method for combining multi-mission altimetry over the Mekong river. In: Ouwehand L. (Ed.) *Proceedings of the Living Planet Symposium 2016, Prague, Czech Republic, ESA SP-740*, 2016b

Boergens E., Dettmering D., Schwatke C., Seitz F.: Treating the hooking effect in satellite altimetry data: a case study along the Mekong River and its tributaries. *Remote Sensing* 8(2), 91, doi:[10.3390/rs8020091](https://doi.org/10.3390/rs8020091), 2016c

Dettmering D., Schwatke C., Boergens E., Seitz F.: Potential of ENVISAT radar altimetry for water level monitoring in the Pantanal wetland. *Remote Sensing* 8(7), 596, doi:[10.3390/rs8070596](https://doi.org/10.3390/rs8070596), 2016a

Dettmering D., Strehl F., Schwatke C., Seitz F.: Satellite altimetry and SAR remote sensing for monitoring inundation in the Pantanal wetland. In: Ouwehand L. (Ed.) *Proceedings of the Living Planet Symposium 2016, Prague, Czech Republic, ESA SP-740*, 2016b

Gómez-Enri J., Cipollini P., Passaro M., Vignudelli S., Tejedor B., Coca J.: Coastal altimetry products in the Strait of Gibraltar. *IEEE Transactions on Geoscience and Remote Sensing* 54(9), 5455–5466, doi:[10.1109/TGRS.2016.2565472](https://doi.org/10.1109/TGRS.2016.2565472), 2016

Göttl F., Dettmering D., Müller F. L., Schwatke C.: Lake level estimation based on CryoSat-2 SAR altimetry and multi-looked waveform classification. *Remote Sensing* 8(11), 885, doi:[10.3390/rs8110885](https://doi.org/10.3390/rs8110885), 2016a

Göttl F., Schwatke C., Dettmering D.: Combination of Envisat, CryoSat-2 and SARAL/AltiKa measurements for estimating water level variations of lakes. In: Ouwehand L. (Ed.) *Proceedings of the Living Planet Symposium 2016, Prague, Czech Republic, ESA SP-740*, 2016b

Müller F. L., Passaro M., Dettmering D., Bosch W.: Sea ice leads and polynya detection using multi-mission altimetry in the Greenland Sea. In: Ouwehand L. (Ed.) *Proceedings of the Living Planet Symposium 2016, Prague, Czech Republic, ESA SP-740*, 2016

- Passaro M., Dinardo S., Quartly G.D., Snaith H.M., Benveniste J., Cipollini P., Lucas B.: Cross-calibrating ALES Envisat and CryoSat-2 Delay-Doppler: a coastal altimetry study in the Indonesian Seas. *Advances in Space Research* 58(3), 289-303, doi:[10.1016/j.asr.2016.04.011](https://doi.org/10.1016/j.asr.2016.04.011), 2016
- Passaro M., Müller F. L., Dettmering D.: Lead Detection using Cryosat-2 Delay-Doppler Processing and Sentinel-1 SAR images. *Advances in Space Research*, submitted
- Rudenko S., Dettmering D., Esselborn S., Fagiolini E., Schöne T.: Impact of Atmospheric and Oceanic De-aliasing Level-1B (AOD1B) products on precise orbits of altimetry satellites and altimetry results. *Geophysical Journal International* 204(3), 1695-1702, doi:[10.1093/gji/ggv545](https://doi.org/10.1093/gji/ggv545), 2016
- Schlaffer S., Chini M., Dettmering D., Wagner W.: Mapping wetlands in Zambia using seasonal backscatter signatures derived from ENVISAT ASAR time series. *Remote Sensing* 8(5), 402, doi:[10.3390/rs8050402](https://doi.org/10.3390/rs8050402), 2016

3 Cross-Cutting Research Topics

The three overarching research topics Atmosphere, Regional Gravity Field, and Standards and Conventions are highly cross-related to the research areas Reference Systems and Satellite Altimetry for which they provide important contributions.

The atmosphere (Section 3.1) affects the measurements of all space geodetic observation techniques. On the one hand, atmospheric effects, i.e. signal delay and signal bending are major error sources that need to be considered. Thus the optimisation of respective correction models means an important research challenge. On the other hand, the measurements of the geodetic observation techniques that are influenced by the atmosphere in different ways provide valuable information on its state and dynamics. This information is of great interest for other disciplines such as meteorology, navigation and atmospheric sciences. In particular DGFI-TUM has built up strong expertise in modelling and prediction of global and regional physical structures of the Earth's ionosphere (4D electron content, space weather) from the joint analysis of space geodetic observations.

The precise knowledge of the Earth's gravity field (Section 3.2) is vital for various applications in geodesy, such as the realisation and unification of height systems and the determination of high-precision satellite orbits. The latter are a prerequisite for the computation of accurate reference frames or for reliable estimates of water heights from satellite altimetry. Furthermore, the geoid provides the reference surface for the ocean circulation. Temporal changes of the gravity field contain information about mass transports in the Earth system and are of great interest, for example, for the investigation of dynamic processes in the Earth's interior or within the hydrosphere. The DGFI-TUM primarily focuses on theoretical and practical aspects of regional gravity field determination. The goal is the creation of high-resolution and high-precision potential fields for delimited areas through a combination of various available data sets, e.g. satellite gravity field information, satellite altimetry, or terrestrial and airborne gravity data.

A fundamental prerequisite for any meaningful combination of different data sets is the definition and application of common standards and conventions (Section 3.3) in order to assure highest consistency of parameters and products. In the frame of the Global Geodetic Observing System (GGOS) the DGFI-TUM manages the GGOS Bureau of Products and Standards (BPS) that is jointly operated with partners of the FGS.

3.1 Atmosphere

The Earth's atmosphere can be structured into various layers depending on different physical parameters such as temperature or charge state. In the latter case we distinguish mainly between the neutral atmosphere up to roughly 50 km altitude and the ionosphere approximately between 50 km and 1000 km altitude.

The Earth's ionosphere plays a key role in monitoring space weather, because it responds to solar storms with an increase of the electron density. Space-geodetic observation techniques, such as terrestrial GNSS, satellite altimetry, space-borne GPS (radio occultation), DORIS and VLBI provide valuable global information about the state of the ionosphere. In this context the project OPTIMAP (Operational Tool for Ionospheric Mapping and Prediction), already introduced in the last years' annual reports, deals with the deployment of an operational service for the provision of ionosphere information including the effects of solar events in near real-time. Due to the coupling processes between the ionosphere and the themosphere space weather

is also affecting – indirectly – the thermospheric drag and, thus, it influences the movement, i.e. the orbit of a satellite. In this context the project INSIGHT (Interactions of Low-orbiting Satellites with the Surrounding Ionosphere and Thermosphere) aims on the improvement of thermospheric models by introducing SLR observations and ionosphere information.

In the reporting period, DGFI-TUM was working on four atmosphere projects. Besides the three projects OPTIMAP, ADAPIO and INSIGHT already introduced in the last year's annual report, the project AUDITOR (Advanced Multi-Constellation EGNSS Augmentation and Monitoring Network and its Application in Precision Agriculture) is running since January 2016. AUDITOR is a project within the Horizon 2020 programme of the European Commission. It is a joint initiative of an international consortium of small and medium enterprises (SME) and universities under the leadership of a Spanish company. The goal of the project is the implementation of a novel precise positioning technique – based on augmentation data – in a customized GNSS receiver. To reach this goal sophisticated ionosphere models have to be developed and implemented to increase the accuracy in real-time at the user side. The main ambition of the project is to reduce the convergence time of precise point positioning for multi-frequency receivers and to increase the accuracy for single-frequency receivers. The contributions of DGFI-TUM are focusing on the development of novel algorithms to provide enhanced ionospheric corrections. This includes the development of a data adaptive approach to produce high resolution maps of the vertical total electron content (VTEC) for specific regions in (near) real-time; for more details see López et al. (2016).

Since the work plans of DGFI's ionosphere projects includes (1) the combination of the different space-geodetic observation techniques, (2) the computation of high-resolution regional VTEC maps and (3) the application of Kalman filtering for near real-time applications, we present in the following three components related to the three aforementioned items, namely the pre-processing of DORIS data, the densification of ionosphere maps and the sequential estimation using Kalman filtering.

Pre-processing of DORIS data

The terrestrial GPS and GLONASS observations provide a high-resolution coverage of the continental regions. Additional techniques, such as DORIS, satellite altimetry and radio occultation measurements to Low-Earth-Orbiting (LEO) satellites cannot entirely eliminate the data gap problem, e.g. over the oceans, but can considerably bridge gaps. During 2016, the DGFI ionosphere modelling software was extended for the pre-processing of DORIS observations, in particular for the processing of the two additional satellites SARAL and HY-2A.

The novel data pre-processing module extracts ionospheric L_4 measurements from raw DORIS carrier-phase observables λ_ϕ by applying the carrier-phase ionospheric combination technique as shown in Fig. 3.1. The geometric correction ΔD is determined in the data pre-processing step whereas the combined Carrier Phase Bias CPB_4 is estimated by Kalman filtering. As examples the Fig. 3.2 depicts data extracted from HY-2A (top) and SARAL (bottom). The geographical locations of the ionospheric pierce points (IPPs) related to the measurements of the two satellites are illustrated in Fig. 3.2.

Densification of Ionosphere Maps – Two-Level-Model

Since 1998, the International GNSS Service (IGS) provides Global Ionosphere Maps (GIM) with a latency of a few hours or even days. Each GIM is a combination of the individual solutions of the different IGS Analysis Centers (CODE, UPC, JPL, ESOC) and, thus, only depending on the data of the global IGS network. Usually the GIMs represent the low-frequency part – a

spherical harmonic expansion would be truncated at degree and order 15 – and are therefore not convenient for regional applications such as precision agriculture. The reason for this procedure is the rather inhomogeneous distributed data over the globe including large data gaps, e.g. over the oceans. To increase the spectral information of the model the resolution level had to be adapted to the data. For this purpose a densification procedure was developed which

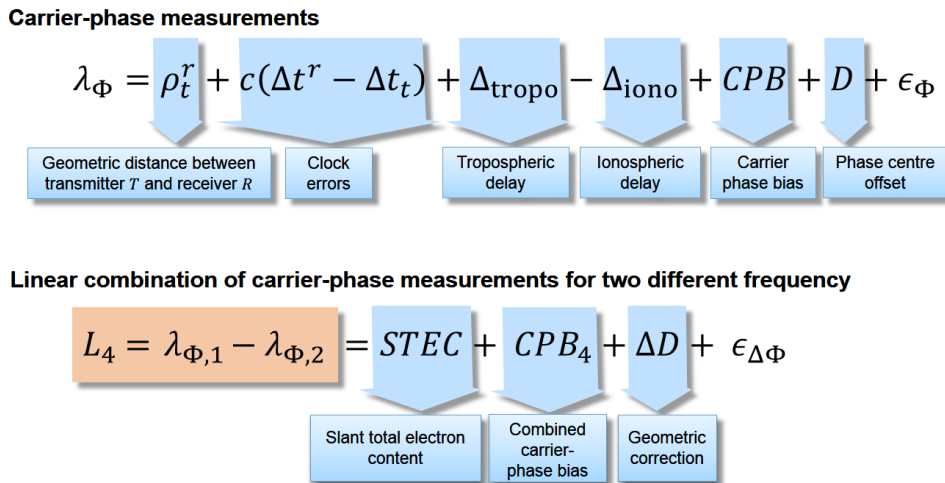


Fig. 3.1: Observation equation for the carrier-phase observable L_4 from the difference of the two DORIS carrier-phase measurements $\lambda_{\Phi,1}$ and $\lambda_{\Phi,2}$

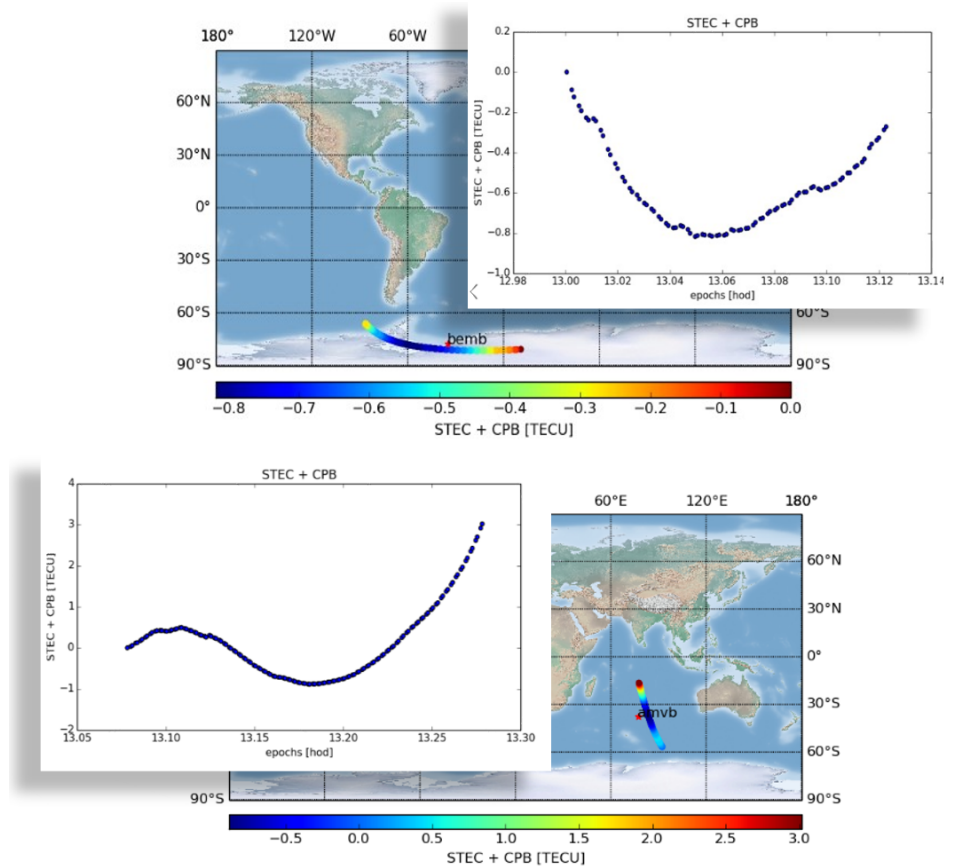


Fig. 3.2: Biased DORIS observations $STEC + CPB_4$ (shifted w.r.t. the first observation) at the ionospheric Pierce Points (IPPs) through a satellite pass: the top panel shows HY-2A satellite observations on August 23, 2016 between 13:4:41 and 13:16:41. The bottom panel shows SARAL observations from August 23, 2016 between 13:00:01 and 13:07:21.

is based on B-spline expansions but additionally allows for the combination of a low-resolution global and a high-resolution regional model part. Such a "Two-Level-Model" (TLM) consists of a global representation $VTEC_{\text{glob}}(\varphi, \lambda)$ on the first level and regional high-resolution ionosphere variations $\Delta VTEC_{\text{reg}}(\varphi, \lambda)$ on the second level according to

$$VTEC_{\text{reg}}(\varphi, \lambda) = \underbrace{VTEC_{\text{glob}}(\varphi, \lambda)}_{1^{\text{st-level}}} + \underbrace{\Delta VTEC_{\text{reg}}(\varphi, \lambda)}_{2^{\text{nd-level}}}. \quad (3.1)$$

As shown in Fig. 3.3 the TLM approach is based solely on B-spline modelling. While the global part is based on tensor products of polynomial B-splines $N_{J_1, k_1}(\varphi)$ and trigonometric B-splines $T_{J_2, k_2}(\lambda)$ to ensure the "wrapping around" effect on the globe Ω (see e.g. Erdogan et al. 2017), the regional model part uses tensor products of polynomial B-splines $N_{J_3, k_3}(\varphi)$ for the latitude representation and $N_{J_4, k_4}(\lambda)$ for the longitude representation within the densification area $\Delta\Omega$.

The set of global coefficients $d_{k_1, k_2}^{J_1, J_2}$ as well as the receiver and satellite biases DCB_r and DCB^s are estimated in a first adjustment step from globally distributed observations y_{glob} of space-geodetic observation techniques, namely GNSS, satellite altimetry, DORIS and radio occultation measurements to LEO satellites via Kalman filtering. In the second step the set of the coefficients $d_{k_3, k_4}^{J_3, J_4}$ of the regional B-spline model together with additional receiver biases DCB_r is estimated from the "observed" differences between additional measurements y_{reg} available within the regional densification area and the corresponding estimations $\widehat{VTEC}_{\text{glob}}$ of the global

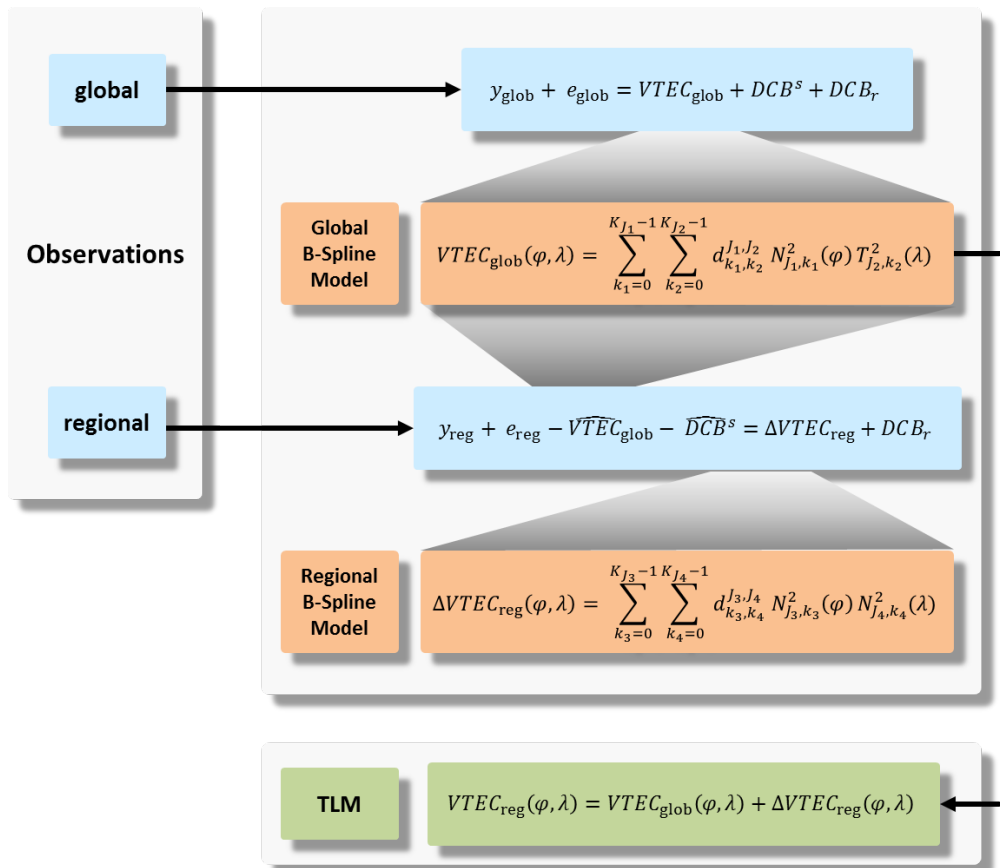


Fig. 3.3: Flowchart of the developed TLM combining a global B-spline model, estimated from global observations y_{glob} considering their measurement errors e_{glob} , and the regional densification B-spline model computed from the observations y_{reg} considering their errors e_{reg} and introducing the estimated global model values $\widehat{VTEC}_{\text{glob}}$. The sets of global coefficients $d_{k_1, k_2}^{J_1, J_2}$ and regional coefficients $d_{k_3, k_4}^{J_3, J_4}$ as well as the receiver biases DCB_r and the satellite biases DCB^s are the unknown parameters of the TLM and are estimated in the following step by means of Kalman filtering.

1st-level model as well as the estimated satellite biases \widehat{DCB}^s . It is worth to be mentioned that the global model is defined within a Sun-fixed geomagnetic coordinate system whereas the regional model is set up in an Earth-fixed geographical coordinate system. (Note, in Fig. 3.3 for simplification reasons we do not distinguish between these two definitions and use the same Greek letters φ and λ for latitude and longitude). Following the concept described before two open issues remain, namely,

1. how to divide the set \mathcal{D} of all available observations into a set \mathcal{D}_1 of global observations y_{glob} and a set \mathcal{D}_2 of observations y_{reg} related to the regional densification area $\Delta\Omega$ and
2. how to determine the resolution levels J_1 to J_4 of the two B-spline expansions?

It should be noted that the densification data set \mathcal{D}_2 may consist of several data sets $\mathcal{D}_{2,a}, \mathcal{D}_{2,b}, \dots$ related to non-overlapping densification areas $\Delta\Omega_A, \Delta\Omega_B, \dots$ such that $\mathcal{D}_2 = \mathcal{D}_{2,a} \oplus \mathcal{D}_{2,b} \oplus \dots$. Following Nyquist's theorem relations can be defined between the global resolution levels J_1 and J_2 , i.e. the numbers $K_{J_1} = 2^{J_1} + 2$ and $K_{J_2} = 3 \cdot 2^{J_2}$ of the B-spline functions $N_{J_1, k_1}^2(\varphi)$ and $T_{J_2, k_2}^2(\lambda)$ with respect to the geomagnetic latitude φ and longitude λ , respectively, the sampling intervals $\Delta\varphi$ and $\Delta\lambda$ of the observation sites as well as the maximum degree $n = n_{\text{max}}$ of an adapted spherical harmonic expansion of the global VTEC signal. Similar expressions can be formulated for the resolution levels J_3 and J_4 , i.e. the numbers $K_{J_3} = 2^{J_3} + 2$ and $K_{J_4} = 2^{J_4} + 2$ of the B-spline functions $N_{J_3, k_3}^2(\varphi)$ and $N_{J_4, k_4}^2(\lambda)$ with respect to the geographic latitude φ and longitude λ related to a densification area. Since the VTEC products of the IGS Analysis Centers CODE and ESOC are defined as spherical harmonic expansions up to maximum degree $n_{\text{max}} = 15$, we chose the values $J_1 = 4$ and $J_2 = 3$ for the global resolution levels. The corresponding values J_3 and J_4 for the regional model do not only depend on the sampling intervals and the signal structure but also on the size of the densification area. Based on these considerations we determined the set \mathcal{D}_1 of global observations by segmenting the Earth's surface into bins of a size related to the sampling intervals $\Delta\varphi$ and $\Delta\lambda$. In the example presented in Fig. 3.4 we defined bins with a size of $10^\circ \times 10^\circ$. For all bins in which more than two receiver stations of the global IGS network are located, we selected this receiver station which is the nearest to the centre of the bin. Then all observations of the chosen receiver stations, related to the corresponding IPPs, are collected in the global set \mathcal{D}_1 . The observations of the not chosen stations within the bins are potential candidates for the regional data set \mathcal{D}_2 . Figure 3.4 shows in the left panel all available stations in near real-time (NRT) – with one hour latency – from the global IGS network (red) and from the regional open network in Europe, EUREF (blue). The right panel depicts the selected stations of the IGS network with a more homogeneous distribution over the globe Ω . The observations related to the IPPs of the chosen receiver stations define the data set \mathcal{D}_1 .

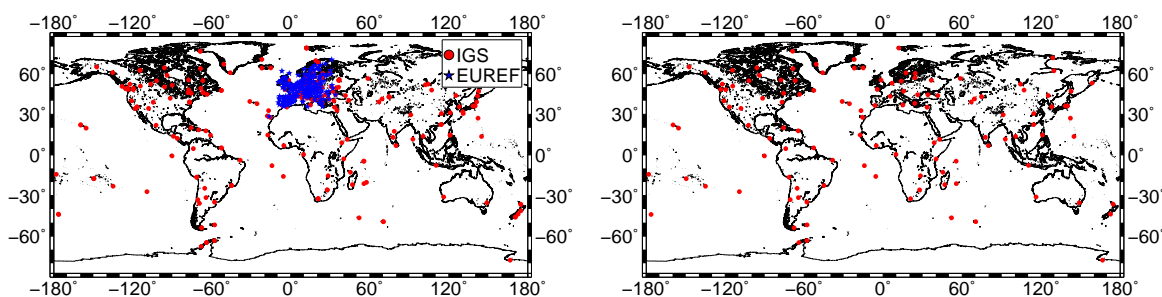


Fig. 3.4: Station positions of the IGS network in red and the EUREF network in blue (left panel); selected receiver stations after the data separation based on bin segmentation with bin size of $10^\circ \times 10^\circ$ (right panel): the measurements from the selected stations are collected in the set \mathcal{D}_1 and are inserted as observations y_{glob} into the global modelling as shown in Fig. 3.3.

Besides the receiver stations for the global model Fig. 3.5 depicts the receiver stations for a regional densification in Europe. The observations related to the IPPs of the latter stations are collected in the data set \mathcal{D}_2 . Since the relation $\mathcal{D}_1 \cap \mathcal{D}_2 = \emptyset$ holds, no observation can be a member of both data sets. Consequently, we assume that correlations between the two data sets of the TLM can be neglected.

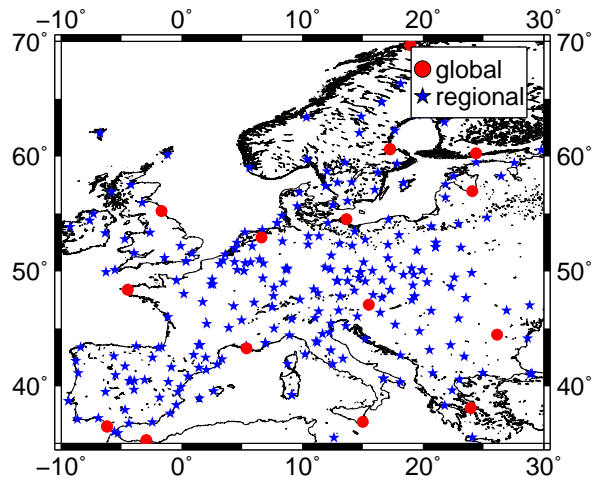


Fig. 3.5: Receiver positions from the IGS and the EUREF network for the global model (red dots) and for the regional model (blue stars) within the chosen densification area $\Delta\Omega$.

Sequential estimation of global vertical total electron content (VTEC)

A NRT processing framework using GNSS measurements to monitor the spatial and temporal variations of VTEC globally has been further developed at DGFI-TUM in the last year (Erdogan et al., 2017). The different steps of the procedure are shown in Fig. 3.6.

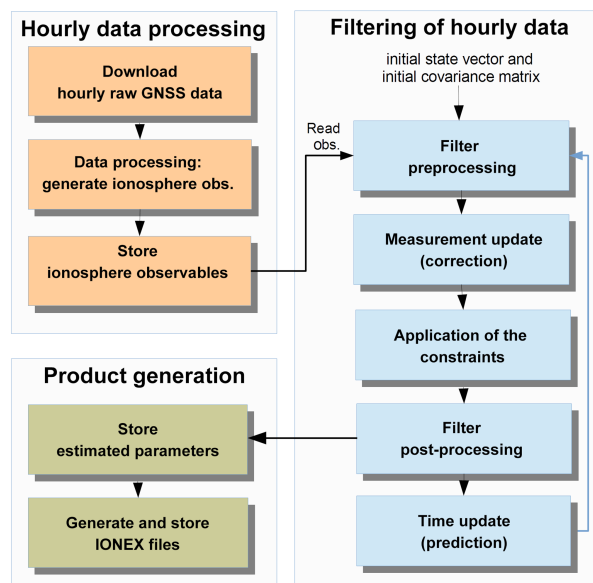


Fig. 3.6: Overall scheme of DGFI's procedure to estimate ionospheric parameters and to generate global near real-time VTEC maps; for details see Erdogan et al. (2017).

As already mentioned before DGFI's VTEC representation is based on a two-dimensional series expansion in terms of tensor products of polynomial and trigonometric B-spline functions up to the resolution levels $J_1 = 4$ and $J_2 = 3$. The unknown parameters, i.e. the B-spline coefficients $d_{k_1, k_2}^{J_1, J_2}$ and additional bias parameters introduced by the different measurement techniques, e.g., the DCBs in case of GNSS, are estimated by Kalman filtering (KF). KF allows the determination of the current state of a system by processing data immediately after acquisition. In the final step of the procedure, the estimated ionospheric parameters are stored and utilised to generate ionosphere products, e.g., IONEX-formatted files including the global VTEC maps.

To assess the quality of our VTEC products two different validation methods are considered, (1) the self-consistency analysis (SCA) and (2) the comparison with VTEC values obtained from the Jason-2 altimetry mission. For the SCA we use the final, i.e., the post-processed, products of the four IGS Analysis Centers CODE, JPL, ESOC and UPC, because they are widely accepted as well-established standards. Note, these final products are available with a latency of days or even weeks, whereas our results – using the pre-processing strategies – are evaluated and provided in NRT.

The performance of the SCA is based on the values

$$dSTEC(t_k) = dSTEC_{obs}(t_k) - dSTEC_{map}(t_k) \tag{3.2}$$

where $dSTEC_{obs}(t_k)$ is the difference of the GPS geometry-free linear combination L_4 observed at time (epoch) t_k with another geometry-free linear combination computed on the same continuous arc but at a reference epoch characterized by the highest elevation angle. The computed $dSTEC$ values from the VTEC maps denoted as $dSTEC_{map}(t_k)$ at the same epochs are obtained by multiplying the estimated VTEC values with an elevation-dependent mapping function, e.g., the modified single-layer mapping (MSLM) function. As an example the RMS values of daily $dSTEC(t_k)$ variations obtained during a time interval between August 11 and August 25, 2016 are presented in Fig. 3.8 for the selected observation sites shown in Fig. 3.7.

According to the SCA, the mean RMS value of DGFI’s solution “dfrg” amounts 1.81 TECU. The four IGS Analysis Centers, CODE, JPL, UPC and ESOC, as well as the IGS combination product exhibit comparable RMS errors between 1.70 and 2.00 TECU.

The second validation method for our VTEC products is based on satellite altimetry data. The Jason-2 satellite, which is equipped with a dual-frequency altimeter, allows directly extracting

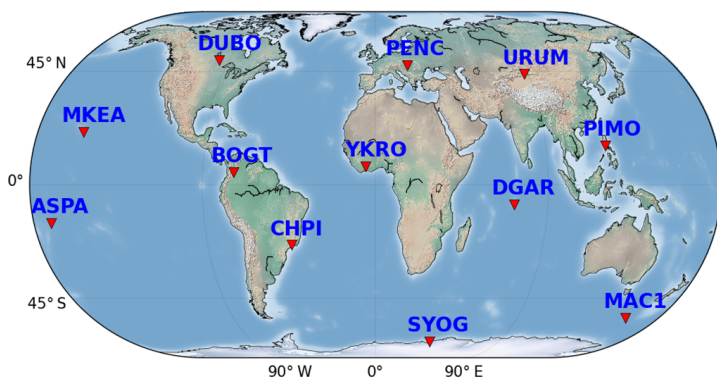


Fig. 3.7: The geographical locations and the identifiers of the receiver sites used in the SCA by analyzing the $dSTEC$ values.

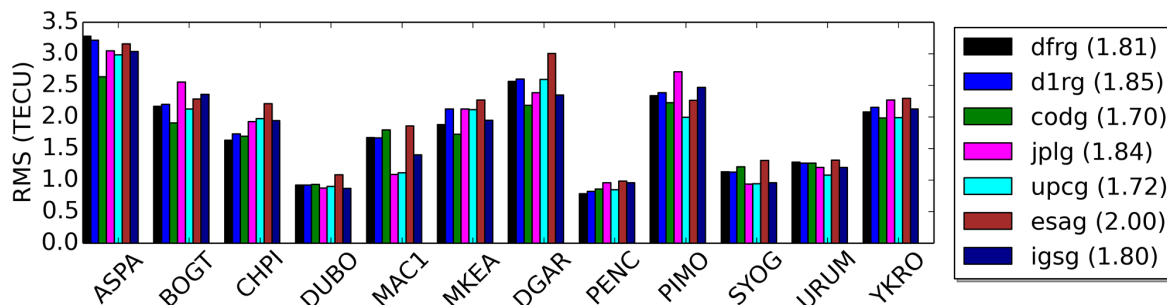


Fig. 3.8: Results of the statistical evaluations presenting the RMS values of the differences between the observed and the computed $dSTEC$ values according to Eq. (3.2), which cover the days between August 11 (DOY 224) and August 25 (DOY 238), 2016. The VTEC products are labeled by the following standard convention for the IONEX files as “igsg”, “codg”, “jplg”, “esag” and “upcg”, which are provided by the IGS and its Analysis Centers, namely CODE, JPL, ESOC and UPC. In this sense, the label “dfrg” refers to the estimated VTEC maps of DGFI-TUM with a temporal resolution of a KF step size of 5 min, whereas “d1rg” is generated from “dfrg” and comprises VTEC maps with a temporal resolution of 1 h; all data is given in TECU ($1 \text{ TECU} = 10^{16} \text{ el/m}^2$).

VTEC without applying any mapping function. In Fig. 3.9 the results of the comparison along the satellite tracks within oceanic regions are given in terms of RMS differences. The VTEC solutions “dfrg” and “d1rg” show larger values only at August 17 (DOY 230), 2016, but smaller deviations for the rest of the test period. The solutions have an average RMS error of 4.7 TECU, and are in close accordance with the solutions computed by the other IGS Analysis Centers ranging from 4.0 to 4.7 TECU.

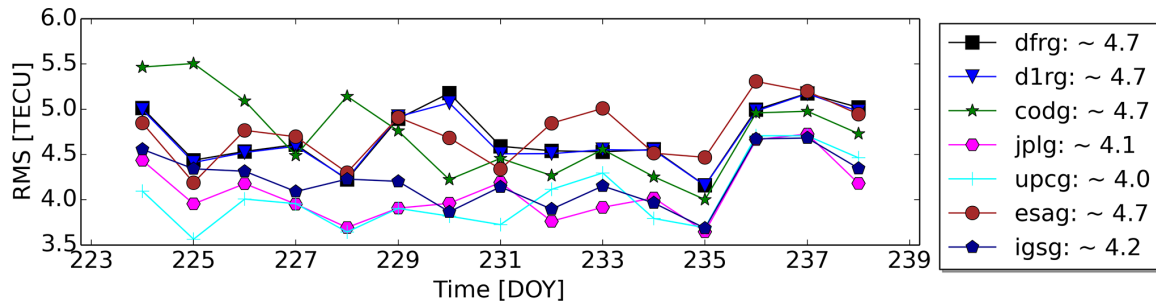


Fig. 3.9: Comparison of VTEC values acquired from the analysis centers and the DGFI-TUM solutions with Jason-2 altimetry VTEC data in terms of RMS values of deviations from DOY 224 to DOY 238, 2016.

The results of the two validation methods shown before are very promising and reveal a general conformity of DGFI’s VTEC product with the results of the IGS Analysis Centers. A study for conducting further tests based on much longer data sets collected under different solar conditions is still ongoing.

The classical KF, which is recursively running a prediction step (time update) and a correction step (measurement update), requires the a priori definition of the model uncertainties which are represented by process and measurement noise covariance matrices. However, the model uncertainties can vary in time or can show different characteristics for each measurement technique. To handle the measurement model uncertainty, an adaptive approach based on variance component estimation was already incorporated into KF. The adaptive approach is now extended to an autonomous handling of the prediction model uncertainties during run-time. The process noise covariance matrix of the KF prediction step is set with respect to the VTEC signal structure and varying in the spatial and temporal domain.

Concerning the huge amount of data provided by many GNSS receivers distributed worldwide, it is obvious that special modelling approaches for KF have to be taken into account to deal with the computational overload that is especially crucial for NRT applications. In this sense, advanced alternative representations of the KF equations were investigated and implemented in the software to speed up the recursion and to decrease the computational burden. Consequently, the processing of very large ionosphere data is ensured to be assimilated in a KF in time without violating the NRT requirements in terms of computational latency.

Thermospheric density estimation

Since for a satellite at low orbit altitude (less than 2000 km) the thermospheric drag causes the largest perturbing acceleration a_{drag} , DGFI-TUM is investigating the quality of existing thermospheric neutral density models for its precise orbit determination (POD) procedures (see also Chapter 1.3 of this report). Therefore, the DFG-funded project INSIGHT – already introduced in the last year’s annual report – focuses amongst others on the influence of the thermosphere on geodetic sensor systems installed on low-orbiting satellites (LEOs).

At DGFI-TUM, the neutral density ρ_m of the thermosphere is estimated from SLR observations of LEO satellites. In a case study, SLR observation to the ANDE-Pollux satellite (alti-

Table 3.1: RMS of the 6-hourly estimated scale factors for each thermospheric model (the wind model HWM14 is always included).

Thermospheric model	SLR orbit RMS [cm]	RMS (f_s) [-]	mean (f_s) [-]
NRLMSISE-00	0.4004	0.74	0.70
CIRA86	0.4119	0.75	0.69
DTM2013	0.2939	0.85	0.82
JB2008	0.2662	0.93	0.90

tude about 350 km) are used. To test the sensitivity of SLR measurements to density variations, four recent thermospheric density models have been used as background models.

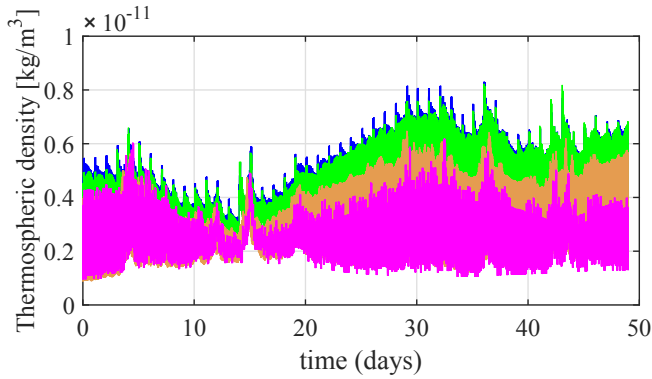


Fig. 3.10: Modeled thermospheric densities used as a priori values in DGFI-TUM POD, using the colours of Table 3.1.

From Fig. 3.10, it can be seen that the models show offsets w.r.t. each other. In order to compensate such offsets, DGFI-TUM uses a refined drag computation based on an additional scaling parameter f_s which is estimated during the POD process. To be more specific, the acceleration \mathbf{a}_{drag} is defined as

$$\mathbf{a}_{\text{drag}} = -\frac{1}{2} f_s \frac{A_{\text{ref}}}{m} C_D \rho_M v_{\text{rel}}^2 \mathbf{u}_D, \quad (3.3)$$

with the satellite-specific cross-section A_{ref} , the mass m of the satellite, the physically modelled satellite-specific drag coefficient C_D , the relative velocity v_{rel} of the satellite w.r.t. the thermosphere and the unit vector \mathbf{u}_D of the satellite motion w.r.t. the thermosphere. Fig. 3.11 shows the estimated scaling factors for the different thermospheric density models in the colouring of Table 3.1. It can be clearly seen that most of the estimated scaling factors are less than one which means that the a priori thermospheric density models are overestimating the neutral density to a certain extend (see also mean values in Table 3.1) or that the physical modelling of C_D results in a too great coefficient.

Fig. 3.12 shows the scaled neutral thermospheric densities ($f_s \cdot \rho_m$). All densities are scaled towards the JB2008 model which has the minimum estimated scale factor \hat{f}_s in this case study.

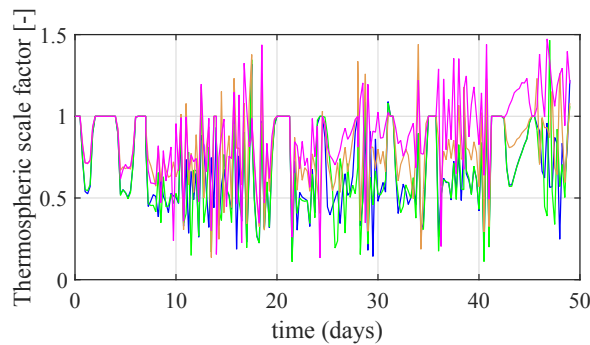


Fig. 3.11: Estimated scaling factors f_s .

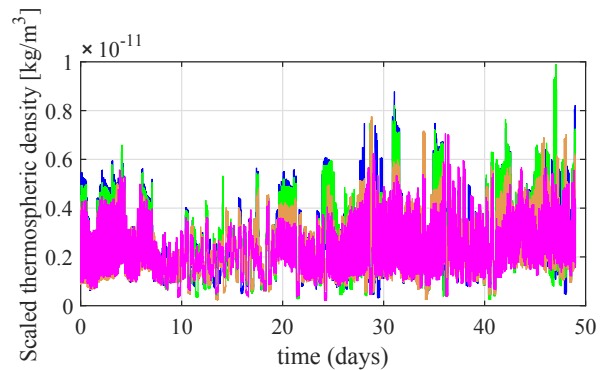


Fig. 3.12: Scaled thermospheric densities.

Related publications

Erdogan E., Schmidt M., Seitz F., Durmaz M.: Near real-time estimation of ionosphere vertical total electron content from GNSS satellites using B-splines in a Kalman filter. *Annales Geophysicae* 35(2), 263–277, 2017, doi:[10.5194/angeo-35-263-2017](https://doi.org/10.5194/angeo-35-263-2017)

Liang W., Limberger M., Schmidt M., Dettmering D., Hugentobler U.: Combination of ground- and space-based GPS data for the determination of a multi-scale regional 4-D ionosphere model. In: Rizos C., Willis P. (Eds.) *IAG 150 Years, IAG Symposia 143*, 751–758, 2016, doi:[10.1007/1345-2015-25](https://doi.org/10.1007/1345-2015-25)

Limberger M.: Ionosphere modeling from GPS radio occultations and complementary data based on B-splines. PhD thesis, German Geodetic Commission, C755, 2015

López E. et al.: Advanced multi-constellation EGNSS augmentation and monitoring network (AUDITOR). In: *Proceedings of the Global Wireless Summit (GWS 2016)*, 2016

3.2 Regional Gravity Field

Gravity glasses offer a view of the Earth's interior

How does the ice on the polar caps change? And which are the geological characteristics of the Earth's crust beneath? What is the structure of the boundary between the Earth's crust and mantle? Geophysicists will be able to answer these questions in the future using gravity field measurements from ESA's (European Space Agency) GOCE (Gravity Field and Steady-State Ocean Circulation Explorer) mission. In order to provide the fundamental basis, we prepared the measurement data mathematically in such a way that they can be used to resolve structures deep below the surface, see Bouman et al. (2016). Since the gravitational force differs from location to location, the masses in oceans, continents and deep in the Earth's interior are not distributed equally. These variations, which are invisible to the human eye, have been measured by highly sensitive acceleration sensors on board of GOCE. The satellite transmitted several hundred million data records to ground control between 2009 and 2013. This data has helped us to map the Earth's gravity field with great precision. And now – by putting on the gravity glasses – we can use the measurement values to see deep beneath the surface of our planet.

On the gravity field map in Fig. 3.13, for example, the wide, red stripe in the North Atlantic symbolizes increased gravity. This is consistent with the plate tectonic model: between Greenland and Scandinavia thick and heavy material rises up from the Earth's mantle along the mid-ocean ridge, cools down and creates fresh oceanic crust. With the gravity field measurements we can provide additional information to the plate tectonic model as we can draw conclusions regarding density and thickness of the different plates. Consequently, the Earth's crust becomes visible.

In general, the GOCE data proved difficult to interpret because the satellite's height and orientation fluctuated as it orbited the Earth. The location of the satellite could be pinpointed at any time using GPS. So, each measurement has to be correlated with the coordinates saved when evaluating the data. Preparing GOCE data for two years incorporates transforming the data in such a way as to enable geophysicists to use it without additional adjustments going forward.

Two grids – two eyes. The trick: The measurement values were not correlated with the actual trajectory of the satellite; instead, they were converted into two reference ellipsoids. These

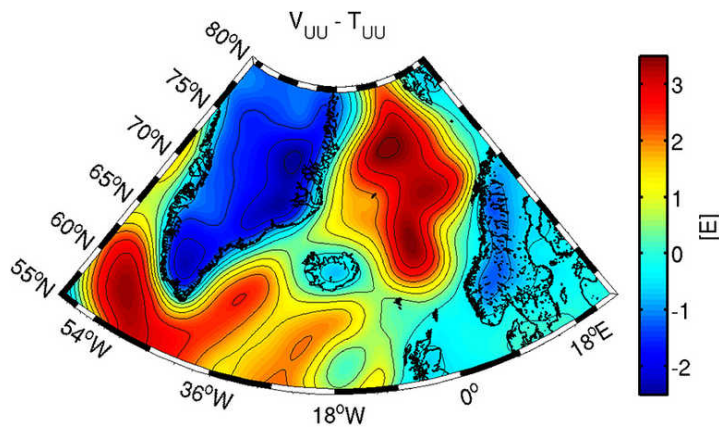


Fig. 3.13: Gravity gradients V_{UU} in vertical UU (up) direction for the North Atlantic region, reduced by topography T_{UU} ; for details see Bouman et al. (2016).

ellipsoids, which surround the Earth at heights of 225 and 255 km, have a fixed height and their geographical orientation is defined, too. Each ellipsoid consists of 1.6 million grid points that can be combined. In this way – as with stereoscopic vision with two eyes – the third dimension becomes visible. Combining this information further with a geophysical model, yields a three-dimensional image of the Earth. This method is very interesting for geophysicists. Previously, the models were predominantly based on seismic measurements. The new GOCE data allows to check and improve, for example, boundaries between the Earth's crust and mantle. Using the geodetic data from the GOCE mission will enable to examine the structure of the entire crust in more detail in the future. Further, dynamic movements will become visible, such as the melting of the polar ice sheets, which seismology could not see.

The GOCE+ GeoExplore project was supported by the ESA as part of the Support to Science Element (STSE). The related publication from Bouman et al. (2016) appeared in the research news of TUM on 14/03/2016, see Weiner and Reiffert (2016), and in "Frankfurter Neue Presse" on 26/03/2016 (see Fig. 3.14), see Mackowiak (2016).

Multi-resolution composition

The structure of the gravity field at the Earth's surface is detectable by several observation types, but high-resolution information can only be obtained from precise local measurement techniques, such as terrestrial gravimetry. In order to benefit from the advantages of all observation types in gravity field modelling, the principle of a multi-resolution representation (MRR) is applied within a regional modelling approach using radial spherical basis functions (SBF). Figure 3.15 schematically visualizes the general strategy. According to Lieb (2017), it incorporates

- spectrally splitting the frequency domain into long-, medium- and short-wavelength parts by levels j , each defined by an upper spherical harmonic (SH) degree $l_j = (2^j - 1)$ and a maximum spatial resolution $\rho_{\max,j} = 20000[\text{km}]/l_j$, cf. Fig. 3.15 (a),
- classifying the data sets (satellite gravimetry in blue, altimetry in green, air-/shipborne and terrestrial gravimetry in orange/yellow) according to their low, medium, or high (spectral/spatial) resolution cf. Fig. 3.15 (a),
- applying SBFs (here we use the Shannon kernel) as low- and band-pass filters by setting a specific, level- j -depending number of Legendre coefficients different from zero, cf. Fig. 3.15 (b),
- modelling the referring detail signals $G_j(x)$ at any location x from the observation groups which contribute relatively to each other most valuable information by setting up appropriate estimation models at each level $j = j' + 1, \dots, J$,

Samstag, 26. März 2016

FORSCHUNG UND TECHNIK

Blick durch die „Gravitationsbrille“

Aufbereitete Daten des Schwerfeld-Messsatelliten „Goce“ lassen Strukturen tief unter der Erdoberfläche sichtbar werden

Wie verändert sich das Eis der Polkappen? Welche geologischen Eigenschaften hat die Erdkruste? Das sind Beispielfragen der Geophysiker über die Prozesse, die den Bau unserer Erde prägen. Geodäten der TU München haben die Messdaten des Esa-Satelliten „Goce“ so aufbereitet, dass sie quasi als Gravitationsbrille einen Blick tief unter die Oberfläche unserer Heimatwelt erlauben.

VON BERNHARD MACKOWIAK

München. Angenommen, wir könnten von Natur aus unsere Umwelt nicht nur im sichtbaren Licht wahrnehmen, sondern auch Gravitationsfelder zehntausendfach überhöht erkennen oder ein fündiger Optiker hätte eine Spezialbrille entwickelt – welches Bild würde die Erde aus dem All dann bieten? Es wäre ein verblüffendes, ja fremdartiges. Unsere Erde ersähe nicht rund, sondern verbaut wie eine Kartoffel. Unser Heimatplanet ist keine Kugel von einheitlicher Masse, sondern seine Massen sind in den Ozeanen, Kontinenten und tief im Innern ungleich verteilt. Das bleibt nicht ohne Folgen für die Gravitationskraft, die alles auf diesen Planeten im Wertsinn „bodenständig“ sein lässt. Das Phänomen der unterschiedlichen Massenkonzentration lässt die Schwere daher von Ort zu Ort verschieden sein.

Im Alltagsleben sind diese Schwereabweichungen nicht zu bemerken, und für das menschliche Auge unsichtbar. Dafür bedarf es schon des besonderen Überblicks aus dem All mit Hilfe speziell ausgerüsteter Satelliten, wie des 2009 von der Esa gestarteten „Gravity field and steady-state Ocean Circulation Explorer“, kurz „Goce“.

„Vor Jahre unrorundete die fünf Meter lange und 1,1 Tonnen schwere künstliche Mond unserer blauen Planeten in gut 250 Kilometer Höhe, um das irdische Schwerfeld noch genauer zu vermessen, als es die 2002 gestartete Nasa-DLR-Dop-

pelatelliten-Mission „Grace“ (Gravity Recovery And Climate Experiment) vermessen.

Wichtigste Ziel der „Grace“-Mission ist, die zeitlichen Veränderungen des Schwerfeldes zu messen; „Goce“ dagegen lieferte bis zu seinem Vergehen im November 2013 eine deutlich höhere räumliche Auflösung des statischen Schwerfeldes. „Goce“ Kerninstrument war ein sogenanntes Schwereradiometer. Es bestand aus sechs extrem feinen Beschleunigungsmessern, die paarweise in drei senkrecht zueinander liegenden Ebenen angeordnet waren. Der Abstand der beiden Sensoren eines Paares betrug jeweils 0,5 Meter. „Die Sensoren messen die Beschleunigung aufgrund der Gravitation mit einer Genauigkeit von 10⁻¹²“, beschreibt Johannes Bouman das Verfahren.

„Das bedeutet, dass man die Schwerebeschleunigung bis zu einer Genauigkeit von 12 Nachkommastellen auflösen kann. Allerdings kann man nicht die Schwerebeschleunigung in absolutem Sinn messen (das wäre die Zahl 9,81... m/s² die man in der Schule lernt), sondern den sehr kleinen Unterschied der Schwerebeschleunigung zwischen den beiden Sensoren eines Paares, also über 0,5 Meter Distanz. Diese Abweichung wird dadurch verursacht, dass sich beide Sensoren des Paares unterschiedlich weit (nämlich 0,5 Meter) von der Erde entfernt befinden.“

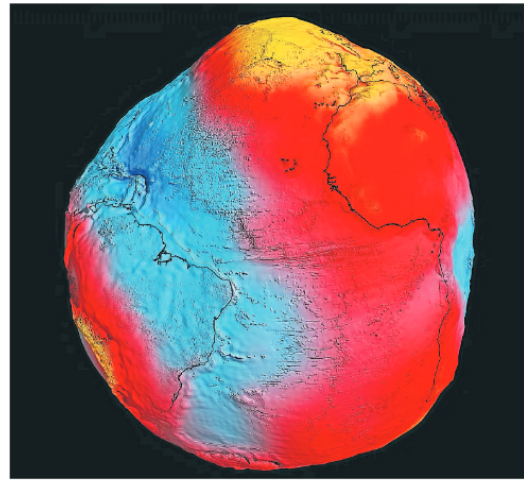
Diese hochgenauen Messungen schlugen sich in mehreren hundert Millionen Datensätzen nieder, die der Satellit während seiner Mission zur Bodenstation gefunkt hat. „Dank dieser Daten ist es gelungen, das Gravitationsfeld der Erde nicht nur mit bisher unerreichter Genauigkeit zu kartieren, sondern wir können die Messwerte nutzen, um – quasi durch die Gravitationsbrille – tief unter die Oberfläche unserer Planeten zu sehen“, erklärt Johannes Bouman vom **Deutschen Geodätischen Forschungsinstitut der TU München** und Leiter der Projektgruppe „Goce/GeolExplore“.

Welcher An- oder besser Einblick der Erde sich auf diese Weise bietet, zeigt beispielsweise eine Karte des Nord-Ost-Atlantik, wo ein roter breiter Streifen die erhöhte Gravitation symbolisiert. Hervorgerufen wird sie durch den Aufstieg von dichten und schwerem Material aus dem Erdmantel entlang des Mittelzoanischen Rückens zwischen Grönland und Skandinavien. Auf diese Weise bildet sich neuer Meeresboden. „Wir haben deshalb uns auf diese Region konzentriert, obwohl die „Goce“-Karten die gesamte Erde zeigen, weil es für dieses Gebiet viele unabhängige Daten gibt, wie zum Beispiel seismische Daten“, begründet der Wissenschaftler. „Durch den Vergleich verschiedener Datensätze waren wir in der Lage, die Komplementarität der Datensätze zu bestimmen.“

Erdplatten im Fokus

So konnten mit den Schwerfeldmessungen wichtige Ergänzungen zum plattentektonischen Modell geliefert werden, indem Rückschlüsse auf die Dichte und Mächtigkeit der unterschiedlichen Platten gezogen wurden. „Was man mit „Goce“ jedoch nicht erkennen kann, ist die Plattenbewegung“, schränkt Institutsdirektor Professor Florian Seitz ein. „Dafür benötigt man andere Informationen wie zum Beispiel GPS-Beobachtungen.“

Allerdings gab es einige Hürden zu überwinden. Die „Goce“-Daten galten als schwer interpretierbar, denn die Höhe und Orientierung des Satelliten während seines Orbits schwankten. Zwar konnte seine augenblickliche Position mit Hilfe des GPS-Navigationssatellitensystems ständig bestimmt werden; aber – so Bouman – bei der Auswertung der Daten musste man jede Messung mit den gespeicherten Koordinaten korrelieren. Die Messwerte wurden nicht mit der tatsächlichen Flugbahn des Satelliten korreliert, sondern auf zwei Referenz-Ellipsoide umgerechnet. „Diese Ellipsoide, welche die Erde in 225 und 255 Kilometern Höhe umspan-



Nicht rund, sondern verbaut wie eine Kartoffel sieht die Erde aus, wenn aus Gravitations-sicht die Höhe überhöht dargestellt wird. Die Esa-Sonde Goce (unten) hat solche Bilder direkt aus dem All geliefert. Fotos: ESA

nen, haben eine konstante Höhe, und auch ihre geografische Orientierung ist festgelegt. Jedes Ellipsoid besteht aus 1,6 Millionen Gitterpunkten, die sich kombinieren lassen. „Auf diese Weise kann man, wie beim stereoskopischen Sehen mit zwei Augen, die dritte Dimension sichtbar machen. In Kombination mit einem geophysikalischen Modell erlauben diese Informationen einen Blick ins Erdinnere bis in 200 Kilometer Tiefe und darüber hinaus“, sagt Bouman.

Er nennt einige Forschungsziele in den Geowissenschaften, für die

die Gradientengitter als Grundlage dienen können, beispielsweise um die Struktur und Veränderung von Eisschichten noch genauer zu untersuchen, ebenso die Topografie der Landflächen. „Der Blick durch diese „Brille“ wird zu einem neuen Verständnis der Struktur der Erdkruste und der Lithosphäre führen sowie zu einem besseren Verständnis geodynamischer Prozesse wie der Mantelkonvektion. Was bis jetzt lokal und regional geschah, wird sich dann im globalen Rahmen abspielen und auf diese Weise den Beobachtungshorizont erweitern.“

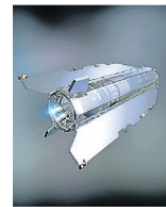


Fig. 3.14: Frankfurter Neue Presse, 24. März 2016, pp. 7 – BERNHARD MACKOWIAK.

- summing up the detail signals G_j from the lowest resolution level j' to the highest resolution level J in a MRR resulting in the total signal Z_J as

$$Z_J(x) = Z_{j'}(x) + \sum_{j=j'+1}^J G_j(x), \quad (3.4)$$

cf. Fig. 3.15 (c).

The here presented approach comprises regionally modelling the spectral domain of degree values $l = l_j + 1, \dots, l_J$; the low-resolution part $l \leq l_j + 1$ stems from an existing global SH model, which further is introduced as prior information up to degree l_j . At each resolution level j , an extended Gauß-Markov Model (GMM) is set up and variance component estimation (VCE) is used for the relative weighting of the heterogeneous observation groups, see Lieb (2017).

In general, two MRR strategies can be distinguished: the composition and the decomposition of $Z_J(x)$ up to, or down from a maximum level J . While the composition, cf. Fig. 3.15 (c), starts from the low-resolution signal $Z_{j'}(x)$ containing information up to level j' (in the following the minimum level j' of the MRR), adding a number of $J - j'$ detail signals $G_j(x)$, each representing one after another frequency band, i. e. level j , up to the total signal $Z_J(x)$. This bottom-up approach enables to react flexibly on any kind of data set by combining them in an optimal sense, i. e. introducing them level by level where they contain maximum spectral information. The decomposition, vice versa, starts from the high-resolution signal $Z_J(x)$ and sequentially splits it in $J - j'$ individual detail signals $G_j(x)$ down to the smoothed representation $Z_{j'}(x)$, by means of levels j .

SBFs are hereby suitable functions in order to extract specific frequency domains from both, measured signals, setting up the bottom-up composition, as well as from modelled signals

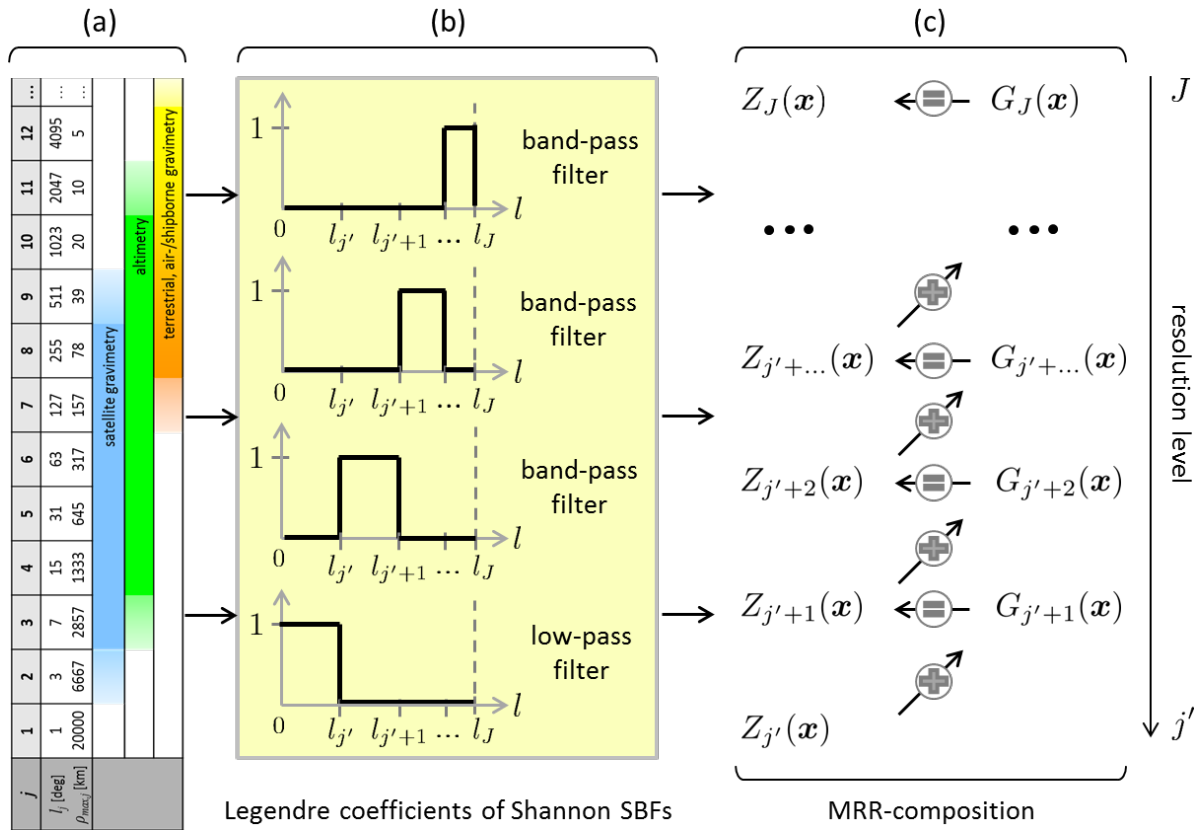


Fig. 3.15: Implementation and application of the MRR within DGFI's regional gravity modelling approach using SBFs: (a) spectral classification of observation types w.r.t. their resolution, (b) spectral representation of Legendre coefficients defining low- and band-pass filtering Shannon SBFs, (c) MRR composition following Eq. (3.4); for details see Lieb (2017).

applying the top-down decomposition. The composition is focused in the sequel for the spectral combination of real data; however, in order to overcome spectral gaps, the decomposition is also applied to resulting models. To set up DGFI's regional gravity field modelling approach, three criteria are formulated for selecting appropriate observation groups at each level; for details see Lieb (2017):

- (1) High sensitivity: Observation groups with smallest variance components are supposed to show the highest sensitivity and deliver the most spectral information at the corresponding level. It is the main criterion.
- (2) No correlations: The observation groups are assumed to be uncorrelated in the estimation model, i. e. their information should contribute only to one level.
- (3) Spectral range and spatial distribution (prior information not sufficient): The second criterion is not strictly kept, if spectral or spatial data gaps lead to singularity problems when solving the normal equations. Especially at higher resolution levels, the low spectral content of the prior information up to degree $l_{j'}$ might not be sufficient to overcome the gaps.

The third criterion requires the introduction of further observation groups, i. e. repeated contribution of the same data sets at different levels. Consequently, the modelling results (i. e. the detail signals $G_{j'}$) of neighbouring levels, obtained from the synthesis, are no longer independent of each other and contain superposing information when summing them up within the MRR, cf. step (c) in Fig. 3.15 and Eq. (3.4). Thus, it yields an iterative process of the steps (2) and (3) until no more singularities appear in the estimation models, trying to avoid as much correlations as possible.

MRR model in Northern Germany

In order to enrich the regional model at each resolution level as optimally as possible with information stemming from sensitive measurement techniques, a spectral combination via MRR is set up. From a reasonable choice of observation groups, the detail signals can be modelled and composed according to Fig. 3.15.

In a study area in Northern Germany, green bordered in Fig. 3.16 (b), cf. DGFITUM annual report 2015, 15 different observation groups are available: [1] terrestrial (yellow), airborne data sets over the [2] North and [3] Baltic Sea (orange flight tracks), [4] shipborne, [5] – [9] altimetry data sets (dark green) from five different satellite missions and GOCE measurements (not displayed), provided in terms of six gravity gradients (GG) [10] – [15]. The colours of the observation groups refer to the spectral classification in Fig. 3.15 (a). GOCO05s is introduced as prior information, i. e. as additional observation group for stabilizing the estimation models, and serves as background model up to $l_7 = 127$, which means it is subtracted from all observations so that the prior information can be introduced as zero-vector. Thus, $j' = 7$ defines the lowest level of the MRR; $J = 11$ is the highest level according to the maximum achievable spatial resolution of around 10 km, cf. Fig. 3.15 (a).

In the analysis of the extended GMMs, set up at each level $j = 8, \dots, 11$, Shannon kernels are used as SBFs for estimating the unknowns. The different observation groups are combined on normal equation level and VCE regulates the relative weighting. Thus, the observation groups of highest sensitivity relatively to each other are identified w.r.t. the different resolution levels. Following the three criteria defined above, two appropriate resolution levels are identified for a multi-level estimation: one extended GMM is set up at level $j = 8$, where the globally observed GOCE Gs [10] – [15] contribute valuable spectral information, and one is set up at highest level $J = 11$, where the “semi-global” altimetry [5] – [9], as well as the regional terrestrial [1], air-[2,3], and shipborne [4] data sets deliver appropriate gravitational content.

The estimated parameters then are used to model the referring detail signals G_8 and G_{11} at level 8 and level 11 within the synthesis steps of the estimation models. Further, the spectral information is transferred to the lower levels, in order to compute the low-resolution signal ΔZ_7 at $j' = 7$ (decomposition of the level-8 signal), and the detail signals G_9 and G_{10} at $j = 9, 10$ (decomposition of the level-11 signal). In the synthesis, the Shannon SBFs act as band-pass filters according to Fig. 3.15 (b). The composition of the signals at each resolution level, cf. Fig. 3.15 (c), finally delivers the spectrally combined level-11 signal ΔZ_{11} w.r.t. the background model. The “multi-level” combination, thus, becomes a “two-level” combination by applying a combination of MRR-composition and -decomposition.

According to $\Delta Z_J(x) = \Delta Z_{j'}(x) + \sum_{j=j'+1}^J G_j(x)$, following from Eq. (3.4) by substituting ΔZ for Z , the composition of the low-resolution signal $\Delta Z_{j'=7}$ and the detail signals G_8, G_9, G_{10}, G_{11} finally delivers the differential signal $\Delta Z_{11} =: \Delta Z_{11, \text{MRR}}$ up to level $J = 11$. It is displayed in Fig. 3.16 (c) in terms of gravity anomalies, the referring standard deviations $s\Delta Z_{11, \text{MRR}}$ are displayed in Fig. 3.16 (d). The statistics (mean difference and corresponding standard deviation) are given in the boxes in Fig. 3.16. For comparison, Fig. 3.16 (a) shows the differential signal ΔZ_{11} in terms of gravity anomalies from a single-level estimation at level $J = 11$. In both cases, $\Delta Z_{11, \text{MRR}}$ and ΔZ_{11} , the gravity anomalies vary between ± 30 mGal (outliers excluded) and the geographical patterns are very similar.

It is displayed in Fig. 3.16 (c) in terms of gravity anomalies, the referring standard deviations $s\Delta Z_{11, \text{MRR}}$ are displayed in Fig. 3.16 (d). The statistics (mean difference and corresponding standard deviation) are given in the boxes in Fig. 3.16. For comparison, Fig. 3.16 (a) shows the differential signal ΔZ_{11} in terms of gravity anomalies from a single-level estimation at level $J = 11$. In both cases, $\Delta Z_{11, \text{MRR}}$ and ΔZ_{11} , the gravity anomalies vary between ± 30 mGal (outliers excluded) and the geographical patterns are very similar.

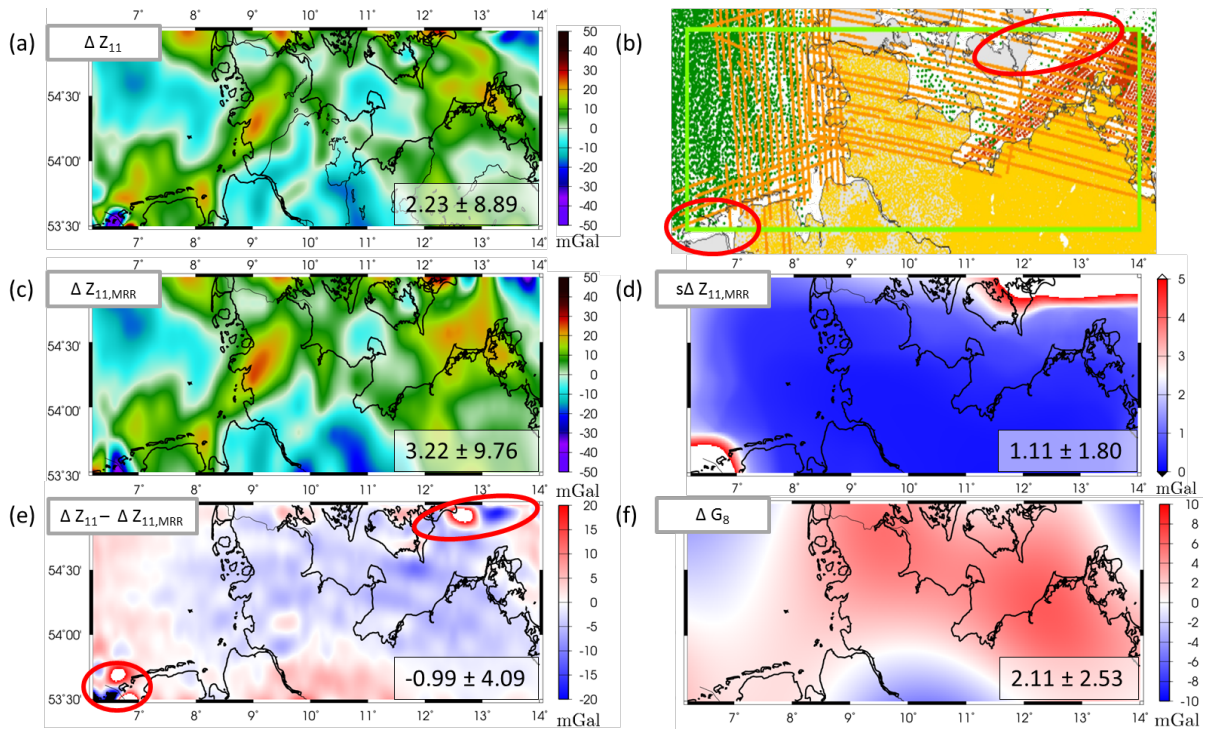


Fig. 3.16: (a) Differential signal ΔZ_{11} of a single-level estimation at level $j = 11$ in terms of gravity anomalies, (b) spatial distribution of the observations (yellow: terrestrial, orange: airborne, green: altimetry, red: ship-borne) covering the green bordered study area, (c) differential signal $\Delta Z_{11,MRR}$ of a MRR solution in terms of gravity anomalies, (d) referring standard deviations $s\Delta Z_{11,MRR}$, (e) difference $\Delta Z_{11} - \Delta Z_{11,MRR}$ between the single-level and the MRR solution in terms of gravity anomalies, and (f) difference ΔG_8 between the smoothed level-8 signal from ΔZ_{11} and the G_8 signal. The statistics (mean value \pm standard deviation) in the boxes are given in mGal.

In Fig. 3.16 (e) the differences $\Delta Z_{11} - \Delta Z_{11,MRR}$ between the single-level estimation ΔZ_{11} and the MRR solution $\Delta Z_{11,MRR}$ are visualized. They average -0.99 ± 4.09 mGal and are therefore not significant. However, they show largest amplitudes down to more than -50 mGal in the data gap area in the south-western corner, and up to around 40 mGal in the same region and further at the north-eastern borderline where high-resolution observations are missing, cf. Fig. 3.16 (b) and (e) red circled. Beside these small-scale variations, the differential pattern shows above all large-scale variations: In the western and southern areas the differences are positive (around $+5$ mGal), while in the middle, negative differences of around -5 mGal extend to wide parts. Similar large-scale structures are represented by the difference ΔG_8 of the detail signals G_8 and $Z_{11} \rightarrow G_8$ in Fig. 3.16 (f). Validating G_8 against the consistently filtered GOCO05s model yields an average difference of 0.02 ± 0.45 mGal, i. e. the remaining differences between the regional model and the global model are about one order of magnitude smaller than the differences of both regional level-8-models. Hence, the signal of G_8 is realistic.

In conclusion, the additional signal from GOCE at level 8 is represented in the MRR solution $\Delta Z_{11,MRR}$. Consequently, the enrichment of $\Delta Z_{11,MRR}$ in the medium wavelengths explains the large-scale differences in Fig. 3.16 (e) w.r.t. the single-level estimation ΔZ_{11} and the MRR solution $\Delta Z_{11,MRR}$ is stabilized. The MRR results are published by Lieb (2017); the single-level results are discussed by Lieb et al. (2016).

Related publications

Bouman J., Ebbing J., Fuchs M., Sebera J., Lieb V., Szwillus W., Haagmans R., Novak P.: Satellite gravity gradient grids for geophysics. *Nature Scientific Reports* 6, 21050, 2016, doi:[10.1038/srep21050](https://doi.org/10.1038/srep21050)

Lieb V., Schmidt M., Dettmering D., Börger K.: Combination of various observation techniques for regional modeling of the gravity field. *Journal of Geophysical Research*, 121(5), 3825–3845, 2016, doi:[10.1002/2015JB012586](https://doi.org/10.1002/2015JB012586)

Lieb V.: Enhanced regional gravity field modeling from the combination of real data via MRR. PhD thesis, German Geodetic Research Institute, Technical University of Munich, DGK Reihe C, 795, Verlag der Bayerischen Akademie der Wissenschaften, ISBN 978-3-7696-5207-9, 2017

Mackowiak B.: Blick durch die “Gravitationsbrille”. *Frankfurter Neue Presse*, 26. März 2016, pp.7

Weiner M., Reiffert S.: GOCE: Neues über den Aufbau der Erde. *TUMcampus Magazin*, Vol. 3/2016, pp.23

3.3 Standards and Conventions

The geodetic research and product generation is making use of various geodetic observation techniques such as VLBI, SLR/LLR, GNSS, DORIS, altimetry, gravity satellite missions, gravimetry, etc. In order to fully benefit from the ongoing technological improvements of these observing systems, it is essential that the analysis of the precise observations is based on the definition and application of common standards and conventions and a consistent representation and parameterization of the relevant quantities. This is of crucial importance for the establishment of highly accurate and consistent geodetic reference frames, needed for a reliable monitoring of the time-varying shape, rotation and gravity field of the Earth. These results are key contributions of global geodesy for Earth sciences and for quantifying global change phenomena, such as deformations and mass redistributions of the Earth system and global sea level rise (see Fig. 3.17).

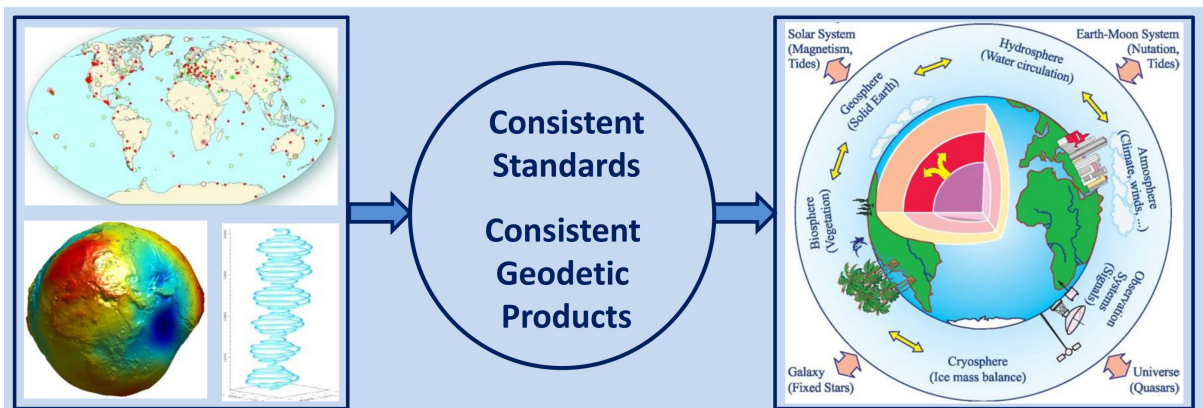


Fig. 3.17: The key role of standards and conventions for consistent geodetic products as the basis for Earth system research and for precisely quantifying global change phenomena.

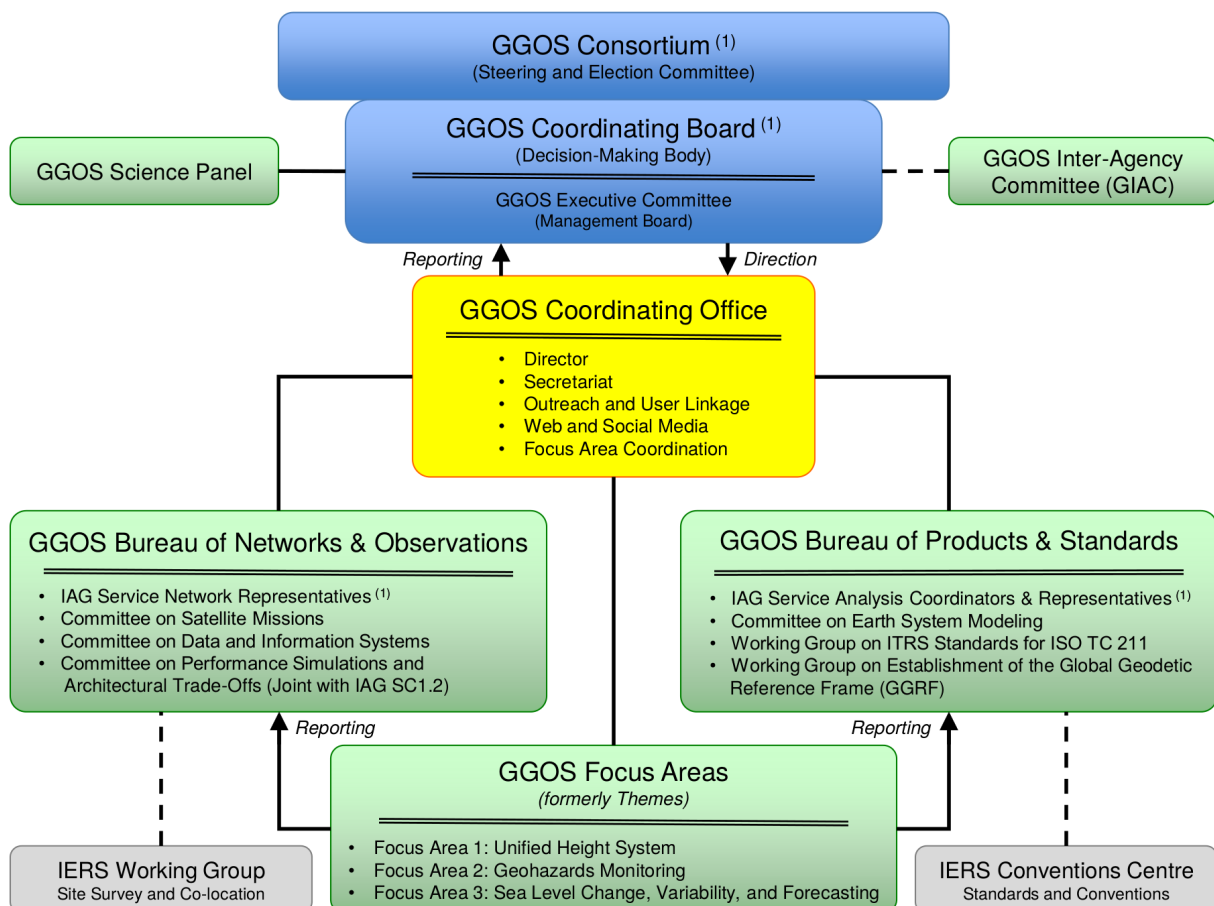
GGOS Bureau of Products and Standards

The Bureau of Products and Standards (BPS) has been established as a key component of IAG’s Global Geodetic Observing System (GGOS) in 2009. The present organizational structure of GGOS is shown in Fig. 3.18. The BPS is hosted and supported by the DGFI-TUM and the Institute for Astronomical and Physical Geodesy (IAPG) of the Technische Universität München, within the Forschungsgruppe Satellitengeodäsie (FGS).

The following GGOS entities are associated with the BPS:

- Committee “Contributions to Earth System Modelling”, Chair: M. Thomas (Germany),
- Joint Working Group “Establishment of the Global Geodetic Reference Frame (GGRF)”, Chair: U. Marti (Switzerland),
- Working Group “ITRS Standards for ISO TC211”, Chair: C. Boucher (France).

The Bureau comprises the staff members, the chairs of the associated GGOS components, the committee and the two working groups as listed above, as well as representatives of the IAG Services and other entities (see Fig. 3.19). As regards the development of standards, there is a link with the IERS Conventions Center, the IAU Working Group “Numerical Standards for Fundamental Astronomy”, BIPM, CODATA, NIST and ISO/TC211.



(1) GGOS is built upon the foundation provided by the IAG Services, Commissions, and Inter-Commission Committees

Fig. 3.18: Organizational structure of IAG’s Global Geodetic Observing System (GGOS).

Position	Representatives	Entity
IERS Conventions Center	Gerard Pétit	BIPM (France)
IERS Analysis Coordinator	Tom Herring	MIT (USA)
IGS Representative	Urs Hugentobler (BPS staff)	TUM (Germany)
ILRS Analysis Coordinator	Erricos Pavlis	UMBC/NASA (USA)
IVS Analysis Coordinator	John Gipson	GSFC/NASA (USA)
IDS Representatives	Frank Lemoine, John Ries, Jean-Michel Lemoine, Hugues Capdeville	GSFC/CSR (USA), CNES France
IGFS Chair	Riccardo Barzaghi	Politecnico, Milano (Italy)
ICGEM Chair	Franz Barthelmes	GFZ (Germany)
BGI Chair	Sylvain Bonvalot	IRD (France)
Gravity Comm. (Representat.)	Jürgen Kusche	Univ. Bonn (Germany)
IAG Representative to ISO	Johannes Ihde	BKG (Germany)
IAG Commun. and Outreach	József Ádám (Chair)	Univ. Budapest (Hungary)
Chair of Control Body for ISO Geodetic Registry	Mike Craymer (Chair), Larry Hothem (Vice-Chair)	NRCan (Canada), USA
IAU Representative, WG NSFA	Robert Heinkelmann (BPS staff)	GFZ (Germany)

Fig. 3.19: Associated members of the BPS representing the IAG Services, IAU and other entities (status: December 2016).

Mission and Objectives

The Bureau of Products and Standards (BPS) supports GGOS in its goal to obtain consistent products describing the geometry, rotation and gravity field of the Earth, along with its variations in time. The main purpose of the BPS is to keep track of adopted geodetic standards and conventions across all IAG components as a fundamental basis for the generation of consistent geometric and gravimetric products (Angermann et al., 2016a).

The work of the BPS is primarily focused on the IAG Services and the products they derive on an operational basis for Earth monitoring making use of various space geodetic observation techniques such as VLBI, SLR/LLR, GNSS, DORIS, altimetry, gravity satellite missions, gravimetry, etc. The Bureau builds upon existing observing and processing systems of the IAG and serves as a contact and coordinating point for the IAG analysis and combination services. The BPS also concentrates on the integration of geometric and gravimetric parameters and the development of new products required to address important geophysical questions and societal needs.

Inventory of standards and conventions

According to its charter, a key activity of the BPS is to assess the standards and conventions currently adopted and used by the IAG and its components for the processing of geometric and gravimetric observations as a basis for the generation of IAG products. The document entitled “GGOS Bureau of Products and Standards: inventory of standards and conventions used for the generation of IAG products” (Angermann et al., 2016b) has been published in the IAG Geodesist’s Handbook 2016:

- The present status regarding IAG Service products and related metadata information should be evaluated, gaps and deficiencies should be identified and recommendations should be provided. The work requires a close interaction between the BPS and the IAG Services as well as with the GGOS Portal. It is essential that well-defined procedures are defined to ensure effectiveness.
- In cooperation with the responsible IAG Services the accuracy requirements given in the GGOS 2020 document should be evaluated and should be updated in case of need. This activity will be supported by the GGOS Committee on “Satellite Missions”.
- If the current accuracy does not satisfy the user requirements, appropriate procedures and methods should be set up to improve the accuracy of the products. This task requires an optimal coordination, support and utilization of IAG Services, as well as leveraging existing IAG resources.
- The BPS should initiate steps to identify the user needs and requirements for products that are currently not provided by the IAG Services, required to address important geophysical questions and user needs. This task should be supported by the Science Panel and the Focus Areas.
- The BPS should work towards the development of new products derived from a combination of geometric and gravimetric observations. If such integrated products should be routinely provided, the establishment of new analysis and/or combination centers may become necessary.
- The BPS proposes to strengthen its role w.r.t. ISO/TC 211. The BPS acted as a proposer for the “New Work Item Proposal” ISO/TC 211: Revision of ISO 19111 “Geospatial Information – Spatial references by coordinates”.
- The BPS will continue the cooperation with the IAU concerning standards and conventions. A link has been established with the IAU Commission A3 “Fundamental Standards” and IAU’s Standards and Fundamental Astronomy (SOFA) service.
- The director of the BPS has been nominated by the IAG Executive Committee as the IAG Representative to the United Nations Global Geospatial Information Management (UN-GGIM) Working Group for a Global Geodetic Reference Frame (GGRF), Key Area “Data Sharing and Development of Geodetic Standards”. Thus, the BPS will be involved in the definition and the establishment of the GGRF.

Related publications

Angermann D., Gerstl M., Sánchez L., Gruber T., Hugentobler U., Steigenberger P., Heinkelmann R.: GGOS Bureau of Products and Standards: Inventory of standards and conventions for geodesy. In: Rizos C., Willis P. (Eds.) IAG 150 Years, IAG Symposia 143, 571–577, 2016a, doi:[10.1007/1345_2015_165](https://doi.org/10.1007/1345_2015_165)

Angermann D., Gruber T., Gerstl M., Heinkelmann R., Hugentobler U., Sánchez L., Steigenberger P.: GGOS Bureau of Products and Standards: Inventory of standards and conventions used for the generation of IAG products. In: Drewes H., Kuglitsch F., Adám J. (Eds.) The Geodesist’s Handbook 2016. Journal of Geodesy 90(10), 1095–1156, 2016b, doi:[10.1007/s00190-016-0948-z](https://doi.org/10.1007/s00190-016-0948-z)

4 Information Services and Scientific Transfer

The exchange of observation data, derived scientific data products and research results is a basic requirement to serve the scientific community and the public. DGFI-TUM is strongly cross-linked with other institutions and has continuously been involved in various national and international activities. Intensive collaborations exist in particular in the frame of the international scientific organizations IUGG, IAU and IAG. The international services of the IAG form the backbone for many disciplines of geosciences and the national and international spatial data infrastructure by coordinating and supporting geodetic research on the international level.

DGFI-TUM recognizes the outstanding role of the IAG services for science and practice and operates - mostly by long-term commitments - data centers, analysis centers, and research centers (cf. Section 1). In this context the institute operates various internet portals (Section 4.1), and scientists of DGFI-TUM have taken leading positions and supporting functions in IAG's Commissions, Services, Projects, Working and Study Groups, and in the Global Geodetic Observing System (GGOS). A complete list of memberships and functions of DGFI-TUM staff is given in Section 4.2. Publications in peer-reviewed scientific journals are still the most acknowledged way of scientific transfer. Section 4.3 provides a list of articles printed or published online in 2016. It is followed by a list of posters and oral presentations (Section 4.4) that were presented by DGFI-TUM staff at numerous international conferences, symposia and workshops (Section 4.5). DGFI-TUM's strong national and international scientific network is also reflected by various guests that visit DGFI-TUM every year in the frame of research co-operations or for a period of study or research (Section 4.6).

4.1 Internet representation

The internet is an indispensable medium for the exchange scientific information and data. DGFI-TUM maintains several independent internet sites to meet the growing demand for scientific information concerning different aspects. DGFI-TUM also maintains mailing lists to fulfill the requirements for information exchange within the International Laser Ranging Service (ILRS) and SIRGAS.

In 2016, DGFI-TUM maintained the following websites:

Deutsches Geodätisches Forschungsinstitut der Technischen Universität München (DGFI-TUM)

The website of DGFI-TUM at www.dgfi.tum.de highlights current research results and informs about the institute's structure and current research programme. Furthermore, it presents the national and international projects of DGFI-TUM as well as its contributions to various international scientific organizations. The web site (see Fig. 4.1) also provides a complete list of publications, reports and presentations since 1994. Annual Reports and DGFI Reports are available in electronic form.



Fig. 4.1: Web sites of DGFI-TUM (left) and SIRGAS (right)

Geocentric Reference System for the Americas (SIRGAS)

SIRGAS is the Geocentric Reference System for the Americas. The web site (www.sirgas.org) is operated by the IGS Regional Network Associate Analysis Centre for SIRGAS (IGS RNAAC SIRGAS), which is under the responsibility of DGFI-TUM since 1996.

The SIRGAS web site provides (see Fig. 4.1)

- a scientific description of definition, realization, and kinematics of the SIRGAS reference frame,
- an organizational overview (operational structure and functions of the different components of SIRGAS),
- a bibliographic compilation related to SIRGAS activities (articles, reports, presentations).

EUROLAS Data Centre (EDC)

The EUROLAS Data Center (EDC) provides access to the database of SLR observations and derived products (see Fig. 4.2). The web site at edc.dgfi.tum.de informs about the data flow within the Operation Center (OC) and the data holding of the Data Centre (DC).

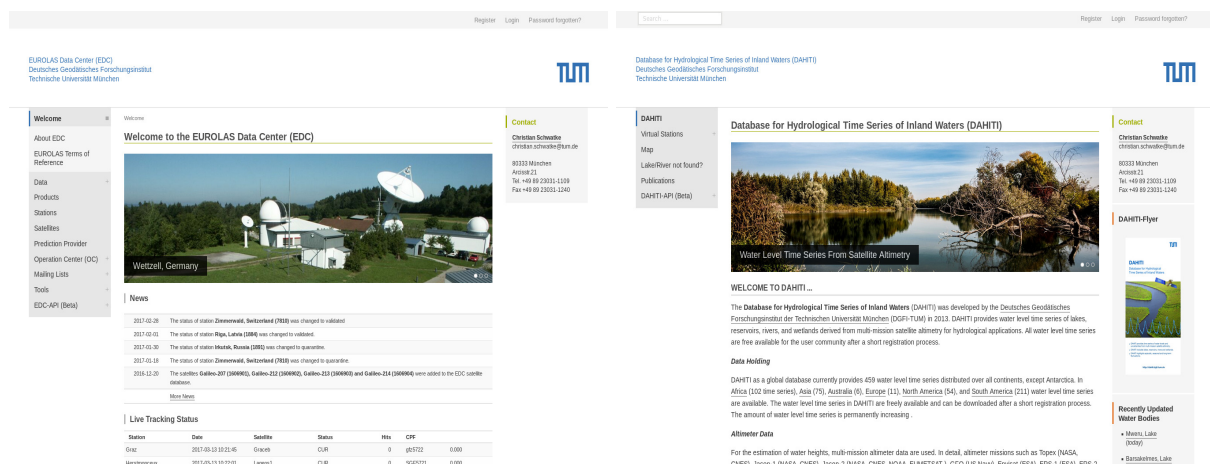


Fig. 4.2: Web sites of EDC (left) and DAHITI (right)

Database for Hydrological Time Series of Inland Waters (DAHITI)

The Database for Hydrological Time Series of Inland Waters (DAHITI) is a public repository of more than 450 water level time series of globally distributed lakes, rivers, reservoirs, and wetlands derived at DGFI-TUM from multi-mission satellite altimetry. The web site of DAHITI is available at dahiti.dgfi.tum.de (see Fig. 4.2)

Open Altimeter Database (OpenADB)

OpenADB is a database for multi-mission altimeter data and derived high-level products. It is designed for both non-expert users and scientific users who are interested in the analysis and application of altimetry data in order to determine new products, models and algorithms. OpenADB allows for fast parameter updates and for extracting data and parameters in user-defined formats. OpenADB is open to the public at no charge after registration. The web site is available at openadb.dgfi.tum.de.

GGOS Bureau of Products and Standards (BPS)

The GGOS Bureau of Products and Standards (BPS) was established as a component of IAG's Global Geodetic Observing System (GGOS) in 2009. The BPS is chaired by DGFI-TUM and operated jointly with partners from the Forschungsgruppe Satellitengeodäsie (FGS). The GGOS BPS web site is located at ggos-bps.dgfi.tum.de

GGOS Focus Area Unified Height System

DGFI-TUM chairs the GGOS Focus Area *Unified Height System* for the term 2015-2019. Its website is available at ihrs.dgfi.tum.de. The immediate objectives of this GGOS component are (1) the outlining of detailed standards, conventions, and guidelines to make the IAG Resolution on the International Height Reference System (IHRIS) applicable, and (2) to establish the realization of the IHRIS, i.e. the International Height Reference Frame (IHRF). The web page informs about current activities and achievements.

Office of the International Association of Geodesy (IAG)

Since the 24th General Assembly of the IUGG (2007) in Perugia, Italy, the DGFI has been hosting the Office of the International Association of Geodesy (IAG Office). For the same period, the former director of the DGFI has been holding the position of the IAG Secretary General. In this context, DGFI-TUM has taken the responsibility for the administration of the IAG budget. The web site of the IAG Office is available at iag.dgfi.tum.de

Project-Website: Wetland Dynamics (WLDYN)

The website of the DFG project WLDYN (Assessing the spatiotemporal dynamics of water volumes in large wetlands and lakes by combining remote sensing with macro-scale hydrological modeling) is available at wldyn.dgfi.tum.de. WLDYN is a joint project of DGFI-TUM, the GFZ Potsdam and the Johann Wolfgang Goethe-Universität in Frankfurt a.M. It aims at incorporating altimetry data into the global hydrological model WGHM for six globally distributed lakes and wetlands. The web page informs about the current status of the project and provides related publications, presentations and data.

4.2 Membership in scientific bodies

American Geophysical Union (AGU)

- Journal of Geophysical Research - Solid Earth,
Associate Editor: Bouman J.

Ausschuss Geodäsie der Bayerischen Akademie der Wissenschaften (DGK)

- *Member: Seitz F.*

Centre National d'Etudes Spatiales (CNES) / National Aeronautics and Space Administration (NASA)

- Ocean Surface Topography Science Team,
Member: Dettmering D.

Deutsche Gesellschaft für Geodäsie, Geoinformation und Landmanagement (DVW)

- Working Group 7: Experimentelle, Angewandte und Theoretische Geodäsie,
Member: Schmidt M., Seitz F.

European Union (EU)

- Coastal Waters Research Synergy Framework (CoReSyf) User Board,
Member: Passaro M.

European Geosciences Union (EGU)

- Geodesy Division,
President: Schmidt M.

European Space Agency (ESA)

- Organizing Committee for the Coastal Altimetry Workshop,
Member: Passaro M.

European Space Agency (ESA) / European Organisation for the Exploitation of Meteorological Satellites (EUMETSAT)

- Sentinel-3 Validation Team, Altimetry sub-group,
Member: Dettmering D.

Forschungsgruppe Satellitengeodäsie (FGS)

- *Deputy Speaker: Seitz F., Board member: Schmidt M.*

International Association of Geodesy (IAG)

- Commission 1, Sub-Commission 1.4: Interaction of celestial and terrestrial reference frames,
Member: Seitz M.
- Commission 1.2 / ICCT Joint Working Group Definition of next generation terrestrial reference frames,
Member: Bloßfeld M., Seitz M.
- Commission 1, Working Group 1.3.1 Time dependent transformations between reference frames,
Member: Sánchez L.

- Commission 4, Joint Working Group 4.3.3 Combination of Observation Techniques for Multi-dimensional Ionosphere Modelling,
Member: Erdogan E., Schmidt M.
- Commission 4, Sub-Commission 4.3 Atmosphere Remote Sensing,
Chair: Schmidt M.
- Commission 4, Working Group 4.3.1 Real Time Ionosphere Monitoring,
Member: Dettmering D., Erdogan E.
- Commission 4, Working Group 4.3.2 Ionosphere Predictions,
Vice-Chair: Erdogan E.
- Commission 4, Working Group 4.3.5 Ionosphere Scintillations,
Member: Schmidt M.
- Global Geodetic Observing System (GGOS) Bureau of Products and Standards,
Director: Angermann D., Member: Gerstl M., Sánchez L.
- Global Geodetic Observing System (GGOS) Coordinating Board,
Member: Angermann D., Sánchez L., Schmidt M.
- Global Geodetic Observing System (GGOS) Executive Committee,
Member: Angermann D.
- Global Geodetic Observing System (GGOS) Focus Area Unified Height System,
Lead: Sánchez L.
- Global Geodetic Observing System (GGOS) Joint Working Group 0.1.2 on the Realization of the International Height Reference System,
Chair: Sánchez L.
- Global Geodetic Observing System (GGOS) Working Group on Performance Simulations and Architectural Trade-Offs (PLATO),
Member: Seitz M.
- ICCT Joint Study Group 0.19 Time series analysis in geodesy,
Member: Schmidt M.
- ICCT Joint Study Group 0.20 Space weather and ionosphere,
Member: Erdogan E., Schmidt M.
- ICCT Study Group 5: Fusion of multi-technique satellite geodetic data,
Member: Bloßfeld M.
- Joint Working Group 1.1 Site Survey and Co-location,
Member: Angermann D., Schmid R., Seitz M.
- Symposia Series,
Assistant Editor-in-Chief: Sánchez L.
- Working Group for the establishment of the Global Geodetic Reference Frame (GGRF),
Member: Angermann D., Sánchez L.

International Astronomical Union (IAU)

- Commission A.2, Rotation of the Earth,
Vice-President: Seitz F.

- Division A Working Group: Third Realisation of International Celestial Reference Frame,
Member: Seitz M.

International DORIS Service (IDS)

- DORIS Analysis Working Group,
Member: Rudenko S.
- Scientific Committee for the IDS Workshop,
Member: Dettmering D.

International Earth Rotation and Reference Systems Service (IERS)

- Directing Board,
Associate member: Angermann D., Bloßfeld M.
- ITRS Combination Centre,
Chair: Seitz M., Member: Bloßfeld M.
- Working Group on Combination at the Observation Level,
Co-Chair: Seitz M., Member: Angermann D., Bloßfeld M.
- Working Group on SINEX Format,
Member: Seitz M.
- Working Group on Site Coordinate Time Series Format,
Member: Seitz M.

International GNSS Service (IGS)

- Antenna Working Group,
Chair: Schmid R.
- Governing Board,
Member: Schmid R., Network Representative: Sánchez L.
- GPS Tide Gauge Benchmark Monitoring - Working Group,
Member: Sánchez L.
- Regional Network Associate Analysis Centre for SIRGAS,
Chair: Sanchez L.

International Laser Ranging Service (ILRS)

- Analysis Standing Committee,
Member: Bloßfeld M., Müller H.
- Data Centre (EDC),
Chair: Schwatke C., Member: Müller H.
- Data Formats and Procedures Standing Committee,
Chair: Müller H., Member: Schwatke C.
- Governing Board,
Member: Müller H.
- LARGE (LAsER Ranging to GNSS s/c Experiment) Study Group,
Member: Müller H.
- Operations Centre (EDC),
Chair: Schwatke C.

- Quality Control Board,
Member: Müller H.
- Study Group on Data Format Update,
Member: Schwatke C.
- Study Group on ILRS Software Library,
Member: Schwatke C.

International Service for the Geoid (ISG)

- *Scientific advisor: Sánchez L.*

International Union of Geodesy and Geophysics (IUGG)

- *Representative to the Panamerican Institute for Geodesy and History (PAIGH):
Sánchez L.*

International VLBI Service for Geodesy and Astrometry (IVS)

- IVS Working Group on Satellite Observations with VLBI,
Member: Kwak Y.
- Operational Analysis Centre,
Member: Schmid R., Seitz M.

Sistema de Referencia Geocéntrico para las Américas (SIRGAS)

- Scientific Committee,
Member: Sánchez L.
- SIRGAS Analysis Centre,
Chair: Sánchez L.

4.3 Publications

- Abelen S.: *Signals of weather extremes in soil moisture and terrestrial water storage from multi-sensor Earth observations and hydrological modeling*. Dissertation, Technische Universität München, Deutsche Geodätische Kommission, C778, Munich, 2016
- Angermann D., Gerstl M., Sánchez L., Gruber T., Hugentobler U., Steigenberger P., Heinkelmann R.: *GGOS Bureau of Products and Standards: Inventory of standards and conventions for geodesy*. In: Rizos C., Willis P. (Eds.) IAG 150 Years, IAG Symposia 143, 571–577, 2016, doi:[10.1007/1345_2015_165](https://doi.org/10.1007/1345_2015_165)
- Angermann D., Gruber T., Gerstl M., Heinkelmann R., Hugentobler U., Sánchez L., Steigenberger P.: *GGOS Bureau of Products and Standards: Inventory of standards and conventions used for the generation of IAG products*. In: Drewes H., Kuglitsch F., Adám J. (Eds.) The Geodesist's Handbook 2016. Journal of Geodesy 90(10), 1095–1156, 2016, doi:[10.1007/s00190-016-0948-z](https://doi.org/10.1007/s00190-016-0948-z)
- Bentel K., Schmidt M.: *Combining different types of gravity observations in regional gravity modeling in spherical radial basis functions*. In: Sneeuw N., Novák P., Crespi M., Sansò F. (Eds.) VIII Hotine-Marussi Symposium on Mathematical Geodesy, IAG Symposia 142, 115–120, 2016, doi:[10.1007/1345_2015_2](https://doi.org/10.1007/1345_2015_2)
- Bergstrand S., Schmid R.: *Activities of the IERS Working Group on Site Survey and Co-location*. In: Behrend D., Baver K.D., Armstrong K.L. (Eds.) New Horizons with VGOS, International VLBI Service for Geodesy and Astrometry 2016 General Meeting Proceedings, NASA/CP-2016-219016, 113–117, 2016
- Bloßfeld M., Seitz M., Angermann D.: *Epoch reference frames as short-term realizations of the ITRS - datum stability versus sampling*. In: Rizos C., Willis P. (Eds.) IAG 150 Years, IAG Symposia 143, 26–32, 2016, doi:[10.1007/1345_2015_91](https://doi.org/10.1007/1345_2015_91)
- Bloßfeld M., Seitz M., Angermann D., Moreaux G.: *Quality assessment of IDS contribution to ITRF2014 performed by DGFI-TUM*. Advances in Space Research 58(12), 2505–2519, 2016, doi:[10.1016/j.asr.2015.12.016](https://doi.org/10.1016/j.asr.2015.12.016)
- Bloßfeld M., Stefka V., Müller H., Gerstl M.: *Satellite laser ranging – a tool to realize GGOS?* In: Rizos C., Willis P. (Eds.) IAG 150 Years, IAG Symposia 143, 540–547, 2016, doi:[10.1007/1345_2015_202](https://doi.org/10.1007/1345_2015_202)
- Boergens E., Buhl S., Dettmering D., Klüppelberg C., Seitz F.: *Combination of multi-mission altimetry data along the Mekong River with spatio-temporal kriging*. Journal of Geodesy, 2016, doi:[10.1007/s00190-016-0980-z](https://doi.org/10.1007/s00190-016-0980-z)
- Boergens E., Buhl S., Dettmering D., Schwatke C., Seitz F.: *The kriging method for combining multi-mission altimetry over the Mekong river*. In: Ouwehand L. (Ed.) Proceedings of the Living Planet Symposium 2016, Prague, Czech Republic, ESA SP-740, 2016
- Boergens E., Dettmering D., Schwatke C., Seitz F.: *Treating the hooking effect in satellite altimetry data: a case study along the Mekong River and its tributaries*. Remote Sensing 8(2), 91, 2016, doi:[10.3390/rs8020091](https://doi.org/10.3390/rs8020091)
- Bouman J., Ebbing J., Fuchs M., Sebera J., Lieb V., Szwillus W., Haagmans R., Novak P.: *Satellite gravity gradient grids for geophysics*. Nature Scientific Reports 6, 21050, 2016, doi:[10.1038/srep21050](https://doi.org/10.1038/srep21050)

- Dettmering D., Schwatke C., Boergens E., Seitz F.: *Potential of ENVISAT radar altimetry for water level monitoring in the Pantanal wetland*. Remote Sensing 8(7), 596, 2016, doi:[10.3390/rs8070596](https://doi.org/10.3390/rs8070596)
- Dettmering D., Strehl F., Schwatke C., Seitz F.: *Satellite altimetry and SAR remote sensing for monitoring inundation in the Pantanal wetland*. In: Ouwehand L. (Ed.) Proceedings of the Living Planet Symposium 2016, Prague, Czech Republic, ESA SP-740, 2016
- Fuchs M.J., Broerse T., Hooper A., Pietrzak J., Bouman J.: *GRACE gravity data to enhance the modeling of coseismic slip distribution for the 2011 Tohoku-Oki earthquake*. In: Rizos C., Willis P. (Eds.) IAG 150 Years, IAG Symposia 143, 477-483, doi:[10.1007/1345_2015_90](https://doi.org/10.1007/1345_2015_90), 2016
- Fuchs M.J., Hooper A., Broerse T., Bouman J.: *Distributed fault slip model for the 2011 Tohoku-Oki earthquake from GNSS and GRACE/GOCE satellite gravimetry*. Journal of Geophysical Research 121(2), 1114–1130, 2016, doi:[10.1002/2015JB012165](https://doi.org/10.1002/2015JB012165)
- Gómez-Enri J., Cipollini P., Passaro M., Vignudelli S., Tejedor B., Coca J.: *Coastal altimetry products in the Strait of Gibraltar*. IEEE Transactions on Geoscience and Remote Sensing 54(9), 5455–5466, 2016, doi:[10.1109/TGRS.2016.2565472](https://doi.org/10.1109/TGRS.2016.2565472)
- Göttl F., Dettmering D., Müller F.L., Schwatke C.: *Lake level estimation based on CryoSat-2 SAR altimetry and multi-looked waveform classification*. Remote Sensing 8(11), 885, 2016, doi:[10.3390/rs8110885](https://doi.org/10.3390/rs8110885)
- Göttl F., Schwatke C., Dettmering D.: *Combination of Envisat, CryoSat-2 and SARAL/AltiKa measurements for estimating water level variations of lakes*. In: Ouwehand L. (Ed.) Proceedings of the Living Planet Symposium 2016, Prague, Czech Republic, ESA SP-740, 2016
- Greff-Lefftz M., Métivier L., Panet I., Caron L., Pajot-Métivier G., Bouman J.: *Joint analysis of GOCE gravity gradients data of gravitational potential and of gravity with seismological and geodynamic observations to infer mantle properties*. Geophysical Journal International 205(1), 257–283, 2016, doi:[10.1093/gji/ggw002](https://doi.org/10.1093/gji/ggw002)
- Haberkorn C., Bloßfeld M., Bouman J., Fuchs M., Schmidt M.: *Towards a consistent estimation of the Earth's gravity field by combining normal equation matrices from GRACE and SLR*. In: Rizos C., Willis P. (Eds.) IAG 150 Years, IAG Symposia 143, 375–381, 2016, doi:[10.1007/1345_2015_76](https://doi.org/10.1007/1345_2015_76)
- Klopotek G., Artz T., Bellanger A., Bourda G., Gerstl M., Gordon D., Haas R., Halsig S., Hjelle G.A., Hobiger T., Hugentobler U., Iddink A., Kirkvik A.S., Lambert S., Plank L., Schmid R., Shu F., Titov O., Tong F., Wang G., Xu M., Zheng W.: *Results from the VLBI Analysis Software Comparison Campaign 2015*. In: Behrend D., Baver K.D., Armstrong K.L. (Eds.) New Horizons with VGOS, International VLBI Service for Geodesy and Astrometry 2016 General Meeting Proceedings, NASA/CP-2016-219016, 203-207, 2016
- Liang W., Limberger M., Schmidt M., Dettmering D., Hugentobler U.: *Combination of ground- and space-based GPS data for the determination of a multi-scale regional 4-D ionosphere model*. In: Rizos C., Willis P. (Eds.) IAG 150 Years, IAG Symposia 143, 751–758, 2016, doi:[10.1007/1345_2015_25](https://doi.org/10.1007/1345_2015_25)
- Lieb V., Schmidt M., Dettmering D., Börger K.: *Combination of various observation techniques for regional modeling of the gravity field*. Journal of Geophysical Research 121(5), 3825–3845, 2016, doi:[10.1002/2015JB012586](https://doi.org/10.1002/2015JB012586)

- López E., Dominguez J., Quijano B., Fernández-Prades C., Arribas J., Hernández-Pajares M., García-Rigo A., Schmidt M., Goss A., Spaltro E., Grosso J., Symeonidou M., Fountas S., Tsiropoulos Z., Van Evert F., Blok P., Roma D.: *Advanced multi-constellation EGNSS augmentation and monitoring network (AUDITOR)*. In: Proceedings of the Global Wireless Summit (GWS 2016), 2016
- Mueller F.L., Passaro M., Dettmering D., Bosch W.: *Sea ice leads and polynya detection using multi-mission altimetry in the Greenland Sea*. In: Ouwehand L. (Ed.) Proceedings of the Living Planet Symposium 2016, Prague, Czech Republic, ESA SP-740, 2016
- Panafidina N., Hugentobler U., Seitz M.: *Interaction between subdaily Earth rotation parameters and GPS orbits*. In: Rizos C., Willis P. (Eds.) IAG 150 Years, IAG Symposia 143, 159–167, 2016, doi:[10.1007/1345_2015_180](https://doi.org/10.1007/1345_2015_180)
- Passaro M., Dinardo S., Quartly G.D., Snaith H.M., Benveniste J., Cipollini P., Lucas B.: *Cross-calibrating ALES Envisat and CryoSat-2 Delay–Doppler: a coastal altimetry study in the Indonesian Seas*. *Advances in Space Research* 58(3), 289–303, 2016, doi:[10.1016/j.asr.2016.04.011](https://doi.org/10.1016/j.asr.2016.04.011)
- Rudenko S., Dettmering D., Esselborn S., Fagiolini E., Schöne T.: *Impact of Atmospheric and Oceanic De-aliasing Level-1B (AOD1B) products on precise orbits of altimetry satellites and altimetry results*. *Geophysical Journal International* 204(3), 1695–1702, 2016, doi:[10.1093/gji/ggv545](https://doi.org/10.1093/gji/ggv545)
- Sánchez L.: *SIRGAS Regional Network Associate Analysis Center Technical Report 2015*. In: Jean Y., Dach R. (Eds.) International GNSS Service Technical Report 2015, 111–121, 2016, doi:[10.7892/boris.80307](https://doi.org/10.7892/boris.80307)
- Sánchez L., Čunderlík R., Dayoub N., Mikula K., Minarechová Z., Šíma Z., Vátr V., Vojtíšková M.: *A conventional value for the geoid reference potential W_0* . *Journal of Geodesy* 90(9), 815–835, 2016, doi:[10.1007/s00190-016-0913-x](https://doi.org/10.1007/s00190-016-0913-x)
- Sánchez L., Drewes H.: *Crustal deformation and surface kinematics after the 2010 earthquakes in Latin America, links to crustal deformation model VEMOS2015 files*. PANGAEA, 2016, doi:[10.1594/PANGAEA.862536](https://doi.org/10.1594/PANGAEA.862536)
- Sánchez L., Drewes H.: *Crustal deformation and surface kinematics after the 2010 earthquakes in Latin America*. *Journal of Geodynamics* 102, 1–23, 2016, doi:[10.1016/j.jog.2016.06.005](https://doi.org/10.1016/j.jog.2016.06.005)
- Sánchez L., Drewes H., Brunini C., Mackern M.V., Martínez-Díaz W.: *SIRGAS core network stability*. In: Rizos C., Willis P. (Eds.) IAG 150 Years, IAG Symposia 143, 183–190, 2016, doi:[10.1007/1345_2015_143](https://doi.org/10.1007/1345_2015_143)
- Schlaffer S., Chini M., Dettmering D., Wagner W.: *Mapping wetlands in Zambia using seasonal backscatter signatures derived from ENVISAT ASAR time series*. *Remote Sensing* 8(5), 402, 2016, doi:[10.3390/rs8050402](https://doi.org/10.3390/rs8050402)
- Schlicht A., Bamann C., Marz St., Schwatke C., Schreiber U., Prochazka I.: *Status of the ELT data center*. Proceedings of the 20th International Workshop on Laser Ranging, Potsdam, Germany, 2016
- Schmid R.: *Antenna Working Group Technical Report 2015*. In: Jean Y., Dach R. (Eds.) International GNSS Service Technical Report 2015, 141–145, 2016, doi:[10.7892/boris.80307](https://doi.org/10.7892/boris.80307)
- Schmid R., Dach R., Collilieux X., Jäggi A., Schmitz M., Dilssner, F.: *Absolute IGS antenna phase center model igs08.atx: status and potential improvements*. *Journal of Geodesy* 90(4), 343–364, 2016, doi:[10.1007/s00190-015-0876-3](https://doi.org/10.1007/s00190-015-0876-3)

- Schöne T., Bingley R., Deng Z., Gravelle M., Griffiths J., Guichard M., Habrich H., Hansen D., Hunegnaw A., Jia M., King M., Merrifield M., Mitchum G., Neilan R., Noll C., Prouteau E., Sánchez L., Santamaría-Gómez A., Teferle N., Thaller D., Tregoning P., Williams S., Wöppelmann G.: *Tide Gauge Benchmark Monitoring Working Group Technical Report 2015*. In: Jean Y., Dach R. (Eds.) *International GNSS Service Technical Report 2015*, 195–196, 2016, doi:[10.7892/boris.80307](https://doi.org/10.7892/boris.80307)
- Schwatke C.: *EUROLAS Data Center (EDC) – Status Report 2014-2016*. Proceedings of the 20th International Workshop on Laser Ranging, Potsdam, Germany, 2016
- Schwatke C.: *EUROLAS Data Center (EDC) – Recent developments of the EDC*. Proceedings of the 20th International Workshop on Laser Ranging, Potsdam, Germany, 2016
- Seitz F., Müller J.: *Erdrotation*. In: Freeden W., Rummel R. (Eds.), *Handbuch der Geodäsie*, Springer, 1–29, 2016, doi:[10.1007/978-3-662-46900-2_12-2](https://doi.org/10.1007/978-3-662-46900-2_12-2)
- Seitz M., Angermann D., Bloßfeld M.: *Geometrische Referenzsysteme*. In: Freeden W., Rummel R. (Eds.), *Handbuch der Geodäsie*, Springer, 1–24, 2016, doi:[10.1007/978-3-662-46900-2_17-1](https://doi.org/10.1007/978-3-662-46900-2_17-1)
- Seitz M., Angermann D., Bloßfeld M., Gerstl M., Müller H.: *ITRS Combination Centres: Deutsches Geodätisches Forschungsinstitut (DGFI-TUM)*. In: Dick W.R., Thaller D. (Eds.), *IERS Annual Report 2015*, Verlag des Bundesamts für Kartographie und Geodäsie, 130–135, 2016
- Seitz M., Bloßfeld M., Angermann D., Schmid R., Gerstl M., Seitz F.: *The new DGFI-TUM realization of the ITRS: DTRF2014 (data)*. Deutsches Geodätisches Forschungsinstitut, Munich, 2016, doi:[10.1594/PANGAEA.864046i](https://doi.org/10.1594/PANGAEA.864046i)
- Singh A., Seitz F., Eicker A., Güntner A.: *Water budget analysis within the surrounding of prominent lakes and reservoirs from multi-sensor Earth observation data and hydrological models: case studies of the Aral Sea and Lake Mead*. *Remote Sensing* 8(11), 953, 2016, doi:[10.3390/rs8110953](https://doi.org/10.3390/rs8110953)
- Steigenberger P., Fritsche M., Dach R., Schmid R., Montenbruck O., Uhlemann M., Prange L.: *Estimation of satellite antenna phase center offsets for Galileo*. *Journal of Geodesy* 90(8), 773–785, 2016, doi:[10.1007/s00190-016-0909-6](https://doi.org/10.1007/s00190-016-0909-6)
- Yildiz H., Forsberg R., Tscherning C.C., Steinhage D., Eagles G., Bouman J.: *Upward continuation of Dome-C airborne gravity and comparison with GOCE gradients at orbit altitude in east Antarctica*. *Studia Geophysica et Geodaetica*, 2016, doi:[10.1007/s11200-015-0634-2](https://doi.org/10.1007/s11200-015-0634-2)

4.4 Posters and oral presentations

- Andersen O.B., Passaro M., Benveniste J., Piccioni G.: *A new Arctic 25-year Altimetric Sea-level Record (1992-2016) and Initial look at Arctic Sea Level Budget Closure*. AGU - Fall Meeting, New Orleans, USA, 2016
- Andersen O.B., Passaro M., Rose S.K., Svendsen P., Piccioni G.: *Arctic Sea Level Change over the altimetry era and reconstructed back to 1950*. Ocean Surface Topography Science Team Meeting 2016, La Rochelle, France, 2016 (Poster)

- Angermann D.: *GGOS Bureau of Products and Standards*. GGOS Coordinating Board Meeting, Vienna, Austria, 2016
- Angermann D.: *BPS overview of present activities and next steps*. GGOS Days 2016, Cambridge, USA, 2016
- Angermann D.: *Geodäsie – Die Vermessung der Erde im Wandel der Zeit*. Vortragsreihe am Ignaz-Günther-Gymnasium, Rosenheim, Germany, 2016
- Angermann D., Gruber T., Gerstl M., Hugentobler U., Sánchez L., Heinkelmann R., Steigenberger P.: *GGOS Bureau of Products and Standards: Recent activities and future work*. EGU General Assembly, Vienna, Austria, 2016 (Poster)
- Bergstrand S., Haas R., Saunier J., Schmid R., Pavlis E.C., Long J.: *Activities of the IERS Working Group on Site Survey and Co-location*. 9th IVS General Meeting, Johannesburg, South Africa, 2016
- Bloßfeld M.: *SLR research activities and products @ DGFI-TUM (invited)*. EGSIEM General Assembly, Luxembourg, Luxembourg, 2016
- Bloßfeld M.: *GGOS and the EOP – the key role of SLR for a stable estimation of highly accurate Earth orientation parameters (invited)*. EGU General Assembly, Vienna, Austria, 2016
- Bloßfeld M.: *Contribution of consistent laser observations to Earth system sciences*. 20th International Workshop on Laser Ranging, Potsdam, Germany, 2016
- Bloßfeld M., Angermann D., Müller H., Schmid R., Seitz M., Zeitlhöfler J.: *Ein Vergleich der aktuellsten ITRS-Realisierungen: ITRF2014, DTRF2014 und JTRF2014*. Geodätische Woche 2016, Hamburg, Germany, 2016
- Bloßfeld M., Angermann D., Schmid R., Seitz M.: *Report of the ITRS Combination Centre at DGFI-TUM*. IERS Directing Board Meeting, San Francisco, CA, USA, 2016
- Bloßfeld M., Angermann D., Seitz M., Schmid R.: *DTRF2014 products for station coordinates and EOP*. AGU Fall Meeting 2016, San Francisco, CA, USA, 2016 (Poster)
- Bloßfeld M., Müller H., Kehm A., Angermann D.: *A comparison of ITRF2014, DTRF2014 and JTRF2014 using SLR*. AGU Fall Meeting 2016, San Francisco, CA, USA, 2016 (Poster)
- Bloßfeld M., Panafidina N., Seitz M.: *Consistent dynamic satellite reference frames and terrestrial geodetic datum parameters - status report PN 6*. Projekttreffen der DFG-Forschergruppe FOR1503, Bonn, Germany, 2016
- Bloßfeld M., Schmidt M., Erdogan E.: *Thermospheric density estimation from SLR observations of LEO satellites - a case study with the ANDE-Pollux satellite*. AGU Fall Meeting 2016, San Francisco, CA, USA, 2016 (Poster)
- Bloßfeld M., Schmidt M., Panzetta F., Erdogan E.: *Interactions of Low-Orbiting Satellites with the Surrounding Ionosphere and Thermosphere (INSIGHT)*. DFG INSIGHT project meeting, Hannover, Germany, 2016
- Bloßfeld M., Seitz M., Angermann D., Schmid R.: *The most recent DGFI-TUM realization of the ITRS: DTRF2014*. Projekttreffen der DFG-Forschergruppe FOR1503, Bonn, Germany, 2016
- Boergens E., Buhl S., Dettmering D., Schwatke C., Seitz F.: *The kriging method for combining multi-mission altimetry over the Mekong River*. ESA Living Planet Symposia 2016, Prague, Czech Republic, 2016 (Poster)

- Boergens E., Buhl S., Dettmering D., Seitz F.: *River level monitoring based on multi-mission altimetry and spatio-temporal kriging - a case study in the Mekong river basin*. OSTST 2016, La Rochelle, France, 2016 (Poster)
- Börger K., Schmidt M., Dettmering D., Limberger M., Erdogan, E., Seitz F., Brandert S., Görres B., Kersten W., Bothmer V., Hinrichs J. Mrotzek N., Venzmer M.: *Global VTEC-modelling in near real-time based on space geodetic techniques, adapted B-spline expansions and Kalman-filtering including observations of the Sun's radiation*. EGU General Assembly, Vienna, Austria, 2016
- Cipollini P., Calafat F. M., Clarizia M. P., Gommenginger C., Passaro M., Snaith H.: *Advances in Satellite Altimetry and GNSS-Reflectometry for monitoring world's oceans and coasts*. SPIE Remote Sensing 2016, Edinburgh, Scotland, 2016
- Dettmering D., Schwatke C.: *Global multi-mission crossover analysis: performance of Jason-3 and other new data sets*. 2016 Ocean Surface Topography Science Team (OSTST) meeting, La Rochelle, France, 2016
- Dettmering D., Strehl F., Schwatke C., Seitz F.: *Satellite Altimetry and SAR remote sensing for monitoring inundation in the Pantanal Wetland*. ESA Living Planet Symposium, Prague, Czech Republic, 2016-05-09/13, 2016 (Poster)
- Drewes H., Sánchez L.: *The Velocity Model for SIRGAS 2010-2015 (VEMOS2015)*. Symposium SIRGAS 2016, Quito, Ecuador, 2016
- Erdogan E., Bloßfeld M., Schmidt M.: *Thermosphere - Ionosphere coupling: a data assimilation approach based on ionosphere measurements*. 1st colloquium of the SPP 1788 - Dynamic Earth, Bonn, Germany, 2016 (Poster)
- Erdogan E., Goss A., Schmidt M., Dettmering D., Seitz F., Börger K., Brandert S., Görres B., Bothmer V., Hinrichs J., Venzmer M., Mrotzek N.: *Using DORIS data in an Operational Tool for Ionospheric Mapping and Prediction*. International Doris Service Workshop (IDS), La Rochelle, France, 2016
- Erdogan E., Limberger M., Schmidt M., Seitz F., Dettmering D., Börger K., Brandert S., Görres B., Kersten W. Bothmer V., Hinrichs J., Venzmer M., Mrotzek N. : *The combination of satellite observation techniques for sequential ionosphere VTEC modeling* . EGU General Assembly, Vienna, Austria, 2016 (Poster)
- Erdogan E., Limberger M., Schmidt M., Seitz F., Dettmering D., Börger K., Brandert S., Görres B., Kersten W. F., Bothmer V., Hinrichs J., Venzmer M., Mrotzek N.: *VTEC Modelling Using Space Geodetic Techniques with Different Latencies and Sun Observations*. Beacon Satellite Symposium, Trieste, Italy, 2016 (Poster)
- Erdogan E., Limberger M., Schmidt M., Seitz F., Dettmering D., Börger K., Brandert S., Görres B., Kersten W. F., Bothmer V., Hinrichs J., Venzmer M., Mrotzek N.: *Estimation of Global Ionosphere VTEC Maps by the Combination of Satellite Observation Techniques based on Kalman-Filtering*. Beacon Satellite Symposium, Trieste, Italy, 2016
- Gómez-Enri J., Cipollini P., Passaro M., Vignudelli S., Coca J.: *Recomputed Sea State Bias Correction for coastal altimeter products*. ESA Living Planet 2016, Prague, Czech Republic, 2016 (Poster)
- Gómez-Enri J., Cipollini P., Passaro M., Vignudelli S., Coca J.: *Accurate coastal altimeter products in the Strait of Gibraltar: ready for exploitation*. Ocean Surface Topography Science Team Meeting 2016, La Rochelle, France, 2016 (Poster)

- Goss A., Erdogan E., Schmidt M.: *Daten- und signal-adaptive Darstellung von vertikalen TEC Werten unter Verwendung von B-Spline Basisfunktionen*. Geodätische Woche 2016, Hamburg, Germany, 2016
- Goss A., Schindelegger M., Seitz F. : *Numerical simulation of short period Earth rotation variations induced by ocean tides*. EGU General Assembly 2016, Vienna, Austria, 2016 (Poster)
- Göttl F., Schwatke C., Dettmering D.: *Combination of Envisat, CryoSat-2 and SARAL/ALTIKA measurements for estimating water level variations of lakes*. ESA Living Planet Symposia 2016, Prague, Czech Republic, 2016 (Poster)
- Hinrichs J., Bothmer V., Mrotzek N., Venzmer M., Erdogan E., Dettmering D., Limberger M., Schmidt M., Seitz F., Börger K., Brandert S., Görres B., Kersten W.: *Impacts of Space Weather Effects on the Ionospheric Vertical Total Electron Content* . EGU General Assembly, Vienna, Austria, 2016 (Poster)
- Kehm A., Bloßfeld M., Pavlis E., Seitz F.: *Future global SLR network evolution and its impact on the terrestrial reference frame*. EGU General Assembly, Vienna, Austria, 2016
- Kehm A., Bloßfeld M., Pavlis E., Seitz F.: *Future global SLR network evolution and its impact on the terrestrial reference frame*. GGOS PLATO Working Group Meeting, Vienna, Austria, 2016
- Kehm A., Bloßfeld M., Seitz F.: *Verbesserungspotential für die Realisierung geodätischer Referenzrahmen durch ein weiterentwickeltes globales SLR-Stationsnetz*. Geodätische Woche 2016, Hamburg, Germany, 2016
- Klopotek G., Artz T., Bellanger A., Bourda G., Gerstl M., Gordon D., Halsig S., Hjelle G.A., Hugentobler U., Iddink A., Kirkvik A.S., Lambert S., Plank L., Schmid R., Shu F., Titov O., Tong F., Wang G., Xu M., Zheng W.: *Results from the VLBI Analysis Software Comparison Campaign 2015 (VASCC2015)*. 9th IVS General Meeting, Johannesburg, South Africa, 2016
- Legeais J.-F., Cazenave A., Benveniste J., Ablain M., Larnicol G., Meyssignac B., Scharffenberg M., Johannessen J., Timms G., Rudenko S., Roca M., Andersen O., Cipollini P., Balmaseda M., Fernandes J., Quartly G., Fenoglio-Marc L., Passaro M., Ambrózio A., Restano M.: *A new ECV release (v2.0) to accurately measure the sea level change from the ESA Climate Change Initiative*. AGU Fall Meeting, San Francisco, CA, USA, 2016
- Legeais J.-F., Cazenave A., Benveniste J., Ablain M., Larnicol G., Meyssignac B., Scharffenberg M., Johannessen J., Timms G., Rudenko S., Roca M., Andersen O., Cipollini P., Balmaseda M., Fernandes J., Quartly G., Fenoglio-Marc L., Passaro M., Ambrózio A., Restano M.: *A New ECV Release (v2.0) to Accurately Measure the Sea Level Change from the ESA Climate Change Initiative*. Ocean Surface Topography Science Team Meeting 2016, La Rochelle, France, 2016 (Poster)
- Müller F., Passaro M., Dettmering D., Bosch W.: *Sea Ice Leads and Polynya Detection using Multi-Mission altimetry in the Greenland Sea*. ESA Living Planet Symposium 2016, Prague, Czech Republic, 2016
- Müller F., Passaro M., Schwatke C., Dettmering D., Bosch W.: *Unsupervised classification of multi-mission altimetry data for open water detection in the Greenland Sea*. OSTST 2016, La Rochelle, France, 2016 (Poster)
- Müller H., Bloßfeld M.: *Quality control and bias analysis at DGFI-TUM*. 20th International Workshop on Laser Ranging, Potsdam, Germany, 2016

- Panzetta F., Erdogan E., Bloßfeld M., Schmidt M.: *Studies on the ionospheric-thermospheric coupling mechanisms using SLR*. EGU General Assembly, Vienna, Austria, 2016
- Passaro M., Cipollini P., Fenoglio-Marc L.: *Measuring Coastal Significant Wave Height from Radar Altimetry with ALES Retracker*. Brazilian Symposium on Water Waves, Federal University of Rio de Janeiro, Brazil, 2016
- Passaro M., Cipollini P., Hausman J., Quartly G. D., Snaith H. M.: *Improved Multi-mission Coastal Altimetry from the ALES Global Dataset*. ESA Living Planet 2016, 2016 (Poster)
- Passaro M., Cipollini P., Quartly G. D., Snaith H. M., Dinardo S., Benveniste J., Lucas B.: *Coastal altimetry improves the understanding of sea level variability at regional scales*. 1st Joint Commission and IGFS Meeting International Symposium on Gravity, Geoid and Height Systems 2016, Thessaloniki, Greece, 2016
- Passaro M., Dinardo S., Quartly G. D., Snaith H. M., Benveniste J., Cipollini P., Lucas B.: *Cross-calibrating ALES Envisat and Cryosat-2 Delay-Doppler: a coastal altimetry study in the Indonesian Seas*. ESA Living Planet 2016, Prague, Czech Republic, 2016
- Passaro M., Müller F., Dettmering D.: *Exploring Cryosat-2 stack data for nadir-lead detection in sea-ice regions*. SAR Altimetry Workshop, La Rochelle, France, 2016
- Quartly G.D., Smith W., Passaro M.: *Intra-1 Hz Correlations*. Ocean Surface Topography Science Team Meeting 2016, La Rochelle, France, 2016 (Poster)
- Rebischung P., Schmid R.: *Preparations for the IGS realization of ITRF2014*. EGU General Assembly, Vienna, Austria, 2016 (Poster)
- Rebischung P., Schmid R.: *IGS transition to ITRF2014*. IERS Directing Board Meeting, San Francisco, CA, USA, 2016
- Rebischung P., Schmid R.: *IGS14/igs14.atx: a new framework for the IGS products*. AGU Fall Meeting 2016, San Francisco, CA, USA, 2016 (Poster)
- Riddell A., Moore M., Schmid R., Schmitz M.: *Insights into the IGS master antenna*. IGS Workshop 2016, Sydney, Australia, 2016 (Poster)
- Rudenko S., Esselborn S., Schöne T., Dettmering D., Neumayer K.-H.: *Assessment of ITRF2014 for precise orbit determination of altimetry satellites*. 2016 IDS Workshop, La Rochelle, France, 2016
- Rudenko S., Esselborn S., Schöne T., Dettmering D., Neumayer K.-H.: *Assessment of ITRF2014 for precise orbit determination of altimetry satellites*. Ocean Surface Topography Science Team Meeting 2016, La Rochelle, France, 2016
- Sánchez L.: *Working Group on the Strategy for the Realization of the International Height Reference System (IHRIS): Brainstorming and definition of action items*. Splinter meeting at the International Symposium on Gravity, Geoid and Height Systems 2016, Thessaloniki, Greece, 2016
- Sánchez L.: *GGOS Focus Area 1: Unified Height System, Present activities*. GGOS Coordinating Board Meeting, Vienna, Austria, 2016
- Sánchez L.: *Unified Height System: Required measurements and expected products (invited)*. GGOS Days 2016, Cambridge, MA, USA, 2016
- Sánchez L.: *Recent activities of the IGS Regional Network Associate Analysis Centre for SIR-GAS - IGS RNAAC SIRGAS*. Symposium SIRGAS 2016, Quito, Ecuador, 2016

- Sánchez L., Ihde J., Pail R., Barzaghi R., Marti U., Ågren J., Sideris M., Novák P.: *Strategy for the Realization of the International Height Reference System (IHR)* (invited). GGHS2016: International Symposium on Gravity, Geoid and Height Systems 2016, Thessaloniki, Greece, 2016
- Sánchez L., Ihde J., Pail R., Barzaghi R., Marti U., Ågren J., Sideris M., Novák P.: *Strategy for the Realization of the International Height Reference System (IHR)*. Symposium SIRGAS 2016, Quito, Ecuador, 2016
- Schlaffer S., Dettmering D., Chini M.: *Relationships between C-band SAR backscatter and wetland water height from altimeter*. ESA Living Planet Symposium, Prague, Czech Republic, 2016-05-09/13, 2016 (Poster)
- Schlicht A., Bamann Ch., Marz S., Schwatke C., Schreiber U., Prochazka I.: *Status of the ELT data center*. 20th International Workshop on Laser Ranging, Ootssdam, Germany, 2016
- Schlicht A., Reußner E., Marz S., Pail R., Xiong C., Lühr H., Stolle C., Bloßfeld M., Schmidt M., Erdogan E., Panzetta F., Svitlov S., Fluy J.: *Introducing the INSIGHT Project*. 1st colloquium of the DFG SPP 1788 Dynamic Earth, Bonn, Germany, 2016
- Schlicht A., Reußner E., Pail R., Lühr H., Stolle C., Xiong C., Schmidt M., Bloßfeld M., Panzetta F., Erdogan E., Flury J.: *INSIGHT (interaction of low-orbiting satellites with the surrounding ionosphere and thermosphere)*. EGU General Assembly, Vienna, Austria, 2016 (Poster)
- Schmid R.: *Splinter Meeting of the IGS Antenna Working Group*. IGS Workshop 2016, Sydney, Australia, 2016
- Schmid R., Bloßfeld M., Gerstl M., Angermann D.: *DGFI part of project PN 5 - status report*. Projekttreffen der DFG-Forschergruppe FOR1503, Bonn, Germany, 2016
- Schmidt M.: *Global Change Monitoring by Satellite Altimetry and Ionosphere Sounding at DGFI-TUM*. Technical Network Modern Geodetic Space Techniques for Global Change Monitoring, Shanghai, China, 2016
- Schmidt M.: *Global Change Monitoring by Satellite Altimetry and Ionosphere Sounding at DGFI-TUM*. Technical Network Modern Geodetic Space Techniques for Global Change Monitoring, Wuhan, China, 2016
- Schmidt M.: *Global Change Monitoring by Satellite Altimetry and Ionosphere Sounding at DGFI-TUM*. Thematic Network Modern Geodetic Space Techniques for Global Change Monitoring, Beijing, China, 2016
- Schmidt M., Bloßfeld M., Erdogan E., Müller H.: *Thermospheric density estimation using SLR observations to very low Earth orbiters*. IAG Commission 4 Symposium: Positioning and Navigation, Wroclaw, Poland, 2016
- Schmidt M., Bloßfeld M., Erdogan E., Panzetta F.: *Thermospheric density estimation from SLR observations to LEO satellites*. 1st Colloquium of the SPP 1788 Dynamic Earth, Bonn, Germany, 21, 2016
- Schmidt M., Erdogan E., Dettmering D., Goss A., Seitz F., Brandert S., Börger K., Bothmer V., Hinrichs J.: *Modelling the global vertical total electron content by adaptive approaches*. SGI Workshop 2016, Berlin, Germany, 2016
- Schmidt M., Erdogan E., Goss A., Seitz F., Dettmering D., Börger K., Brandert S., Görres B., Bothmer V., Hinrichs J., Venzmer M., Mrotzek N.: *Combination of Space Geodetic Observations in a Kalman Filter for an Estimation of the Global Vertical Total Electron Content*. IAG Commission 4 Symposium: Positioning and Navigation, Wroclaw, Poland, 2016

- Schwatke C.: *EUROLAS Data Center (EDC) – Status Report 2014-2016*. 20th International Workshop on Laser Ranging, Potsdam, Germany, 2016 (Poster)
- Schwatke C.: *EUROLAS Data Center (EDC) – Recent developments of the EDC*. 20th International Workshop on Laser Ranging, Potsdam, Germany, 2016 (Poster)
- Schwatke C., Dettmering D.: *DAHITI - An Innovative Approach for Estimating Water Level Time Series over Inland Water using Multi-Mission Satellite Altimetry*. EGU General Assembly, Vienna, Austria, 2016
- Schwatke C., Dettmering D.: *Database for Hydrological Time Series of Inland Waters (DAHITI)*. EGU General Assembly, Vienna, Austria, 2016 (Poster)
- Schwatke C., Dettmering D., Boergens E., Seitz F.: *DAHITI - Pegelstände aus dem Weltall. Aktuelles zu Wasserforschung - eine Ausstellung des TUM Wasser Cluster, TUM Science & Study Center Raitenhaslach, Burghausen, Germany, 2016* (Poster)
- Seitz F.: *Realization of global and regional geometrical reference systems of highest accuracy at DGFI-TUM*. First Workshop of DAAD Thematic Network Modern Geodetic Space Techniques for Global Change Monitoring, Stuttgart, 2016
- Seitz M., Angermann D., Bloßfeld M.: *Combination of techniques at CC DGFI*. COL final meeting, Frankfurt, Germany, 2016
- Seitz M., Angermann D., Bloßfeld M., Schmid R.: *Report of the ITRS Combination Centre at DGFI-TUM*. IERS Directing Board Meeting, Vienna, Austria, 2016
- Seitz M., Bloßfeld M., Angermann D., Schmid R.: *Non-linear station motions in the DGFI realization of the ITRF2014*. EGU General Assembly, Vienna, Austria, 2016
- Seitz M., Bloßfeld M., Angermann D., Schmid R.: *DTRF2014: the new DGFI realization of the ITRS*. IGS Workshop 2016, Sydney, Australia, 2016
- Steigenberger P., Montenbruck O., Fritsche M., Uhlemann M., Dach R., Prange L., Schmid R.: *Estimation of satellite antenna phase center offsets for Galileo*. IGS Workshop 2016, Sydney, Australia, 2016
- Talpe J., Nerem R., Lemoine F., Bloßfeld M.: *Influence of SLR Solutions on Reconstructions of Polar Ice Sheet Melt from Time-Variable Gravity using GRACE*. ESA Living Planet Symposia, Prague, Czech Republic, 2016 (Poster)
- Talpe M., Nerem S., Lemoine F. G., Forootan E., Bloßfeld M., Schmidt M.: *Extending the record of terrestrial water storage (TWS) in major continental basins from time-variable gravity*. AGU Fall Meeting 2016, San Francisco, CA, USA, 2016 (Poster)

4.5 Participation in meetings, symposia, conferences

- 2016-01-15 : **Kick-off meeting, H2020 project AUDITOR, Santander, Spain**
Schmidt M.
- 2016-01-18/19 : **EGSIEM General Assembly, Luxemburg, Luxemburg**
Bloßfeld M.
- 2016-01-20/21 : **ADAPIO final meeting, Bonn, Germany**
Erdogan E., Limberger M., Schmidt M.
- 2016-01-29/30 : **Retreat of the Faculty of Civil, Geo and Environmental Engineering of the TUM, Hohenkammer, Germany**
Seitz, F.
- 2016-02-07 : **46th IGS Governing Board Meeting, Sydney, Australia**
Schmid R.
- 2016-02-08/12 : **IGS Workshop 2016, Sydney, Australia**
Schmid R.
- 2016-02-18 : **Project meeting DFG-INSIGHT, Hannover, Germany**
Bloßfeld M.
- 2016-02-19 : **IERS Working Group COL and E-GRASP Meeting, Frankfurt a. M., Germany**
Angermann D.
- 2016-03-02 : **Review of DFG SPP 1889 Sea Level and Society, Hamburg, Germany**
Seitz, F.
- 2016-03-14/16 : **Brazilian Symposium on Water Waves, Rio de Janeiro, Brasil**
Passaro M.
- 2016-04-05 : **Annual meeting of DGK Section Geodesy, Hanover, Germany**
Seitz, F.
- 2016-04-16 : **GGOS Coordinating Board Meeting, Vienna, Austria**
Angermann D., Sánchez L.
- 2016-04-17 : **IERS Directing Board Meeting, Vienna, Austria**
Angermann D.
- 2016-04-17/22 : **EGU General Assembly, Vienna, Austria**
Angermann D., Bloßfeld M., Kehm A., Panzetta F., Schmidt M., Schwatke C.
- 2016-04-21 : **Annual meeting of the GGOS Standing Committee PLATO, Vienna, Austria**
Bloßfeld M., Kehm A.
- 2016-04-21 : **E-GRASP/Eratosthenes meeting, Vienna, Austria**
Bloßfeld M., Kehm A.
- 2016-04-22 : **ILRS Analysis Standing Committee Meeting, Vienna, Austria**
Bloßfeld M., Kehm A.

- 2016-04-26 : **Midterm Meeting of the IGSSE Focus Area Water, Freising, Germany**
Börgens E., Seitz F.
- 2016-05-09/13 : **ESA Living Planet Symposium 2016, Prague, Czech Republic**
Boergens E., Dettmering D., Müller F., Passaro M.
- 2016-05-10/12 : **OPTIMAP project meeting and milestone review, Munich, Germany**
Dettmering D., Erdogan E., Goss A., Schmidt M., Seitz F.
- 2016-05-14/22 : **DAAD Delegation Journey to CAS Beijing, Wuhan University, and Tongji University Shanghai, China**
Schmidt M.
- 2016-05-23/24 : **WLDYN project meeting, Munich, Germany**
Börgens E., Dettmering D., Schwatke C., Seitz F.
- 2016-06-13/14 : **Status seminar, DFG Research Unit FOR1503 Reference Systems, Bonn, Germany**
Angermann D., Bloßfeld M., Schmid R.
- 2016-06-17 : **FGS Board Meeting, Frankfurt a. M., Germany**
Schmidt M., Seitz F.
- 2016-06-27/29 : **1st Colloquium for the DFG-SPP "Dynamic Earth", Bonn, Germany**
Schmidt M.
- 2016-06-28/30 : **Sentinel-3 Expert User Meeting, Franscati, Italy (via Webex)**
Dettmering D., Passaro, M.
- 2016-07-05/06 : **DFG-Rundgespräch SPP 2017: Mountain Building Processes in 4D, Potsdam, Germany**
Seitz F., Sánchez L.
- 2016-07-06 : **Interactive Workshop to develop Research Strategies for Resilient Water Systems, TUM Water Cluster, Garching, Germany**
Dettmering D.
- 2016-07-13 : **First EC H2020 Co-ReSyF User Board meeting, Cork, Ireland**
Passaro M.
- 2016-07-20 : **System Definition Review Meeting, H2020 project AUDITOR, Castelldefels, Spain**
Schmidt M., Goss A.
- 2016-07-21 : **1st Workshop of DAAD Thematic Network "Modern Geodetic Space Techniques for Global Change Monitoring", Stuttgart, Germany**
Seitz F.
- 2016-08-08 : **SGI Workshop 2016, Berlin, Germany**
Schmidt M.
- 2016-09-04/07 : **IAG Commission 4 Symposium: Positioning and Navigation, Wroclaw, Poland**
Schmidt M.

- 2016-09-19/23 : **International Symposium on Gravity, Geoid and Height Systems GGHS 2016, Thessaloniki, Greece**
Sánchez L., Passaro M.
- 2016-09-30 : **FGS Board Meeting, Munich, Germany**
Schmidt M., Seitz F.
- 2016-10-09 : **ILRS Governing Board Meeting, Potsdam, Germany**
Müller, H.
- 2016-10-09/14 : **20th International Workshop on Laser Ranging, Potsdam, Germany**
Bloßfeld M., Müller H., Schwatke C.
- 2016-10-11/13 : **INTERGEO/Geodätische Woche, Hamburg, Germany**
Seitz F., Bloßfeld M., Goss A., Kehm A.
- 2016-10-21 : **Strategy meeting, DGK Section Geodesy, Munich, Germany**
Seitz, F.
- 2016-10-24/27 : **GGOS Days 2016, Cambridge, USA**
Angermann D., Sánchez L.
- 2016-10-27 : **INSIGHT project meeting, GFZ Potsdam, Germany**
Bloßfeld M., Schmidt M.
- 2016-10-31 : **SAR Altimetry Workshop, La Rochelle, France**
Passaro M., Müller F.
- 2016-10-31/11-01 : **International DORIS Service Workshop (IDS), La Rochelle, France**
Dettmering D., Rudenko S.
- 2016-11-01 : **IDS Governing Board Meeting, La Rochelle, France**
Dettmering D.
- 2016-11-01/04 : **2016 Ocean Surface Topography Science Team (OSTST) meeting, La Rochelle, France**
Dettmering D., Müller F., Passaro M., Rudenko S.
- 2016-11-16/18 : **Symposium SIRGAS 2016, Quito, Ecuador**
Sánchez L.
- 2016-11-16/18 : **DGK Annual Meeting, Munich, Germany**
Seitz, F.
- 2016-11-21/25 : **SIRGAS Workshop on Vertical Datum Unification and Realization of the IHRs en Latin America, Quito, Ecuador**
Sánchez L.
- 2016-11-22/24 : **OPTIMAP project meeting and milestone review, Göttingen, Germany**
Goss A., Schmidt M.
- 2016-12-7/8 : **WLDYN project meeting, Frankfurt, Germany**
Börgens E., Seitz F.
- 2016-12-10 : **IERS Directing Board Meeting, San Francisco, USA**
Bloßfeld M.

- 2016-12-12/15 : **AGU Fall Meeting, San Francisco, USA**
Bloßfeld M.
- 2016-12-13 : **GGOS Bureau for Networks and Observations meeting, San Francisco, USA**
Bloßfeld M.

4.6 Guests

- 2016-01-01/08-31 : Talpe M., University of Colorado, Boulder, USA
- 2016-02-01 : Dr. Eicker A., University of Bonn, Germany
- 2016-02-17 : Piccioni G., DTU Space - National Space Institute, Lyngby, Denmark
- 2016-06-08 : Roggenbuck O. with a group of students, Jade University, Oldenburg, Germany
- 2016-06-29 : 21 heads of Chinese research institutions, Delegation of the Chinese Academy of Sciences (CAS), Beijing, China
- 2016-11-08 : Prof. Otsubo T., Hitotsubashi University, Tokyo, Japan
- 2016-11-24 : Natsiopoulou D., Aristotle University of Thessaloniki, Greece
- 2016-12-15 : Prof. Deng X., University of Newcastle, Australia

5 Projects

A large part of DGFI-TUM's research activities is financed through third-party funds from various sources. Funding of the following projects is gratefully acknowledged (in alphabetic order):

ADAPIO Development of a novel adaptive model to represent global ionosphere information from combining space geodetic measurement systems (DLR)

ArcticSea High latitude sea level record (CLS/ESA)

AUDITOR Advanced multi-constellation EGNSS Augmentation and Monitoring Network (EU Horizon2020)

CIEROT Combination of space geodetic observations for the determination of mass transports in the cryosphere and their impact on Earth rotation (DFG)

CLIVAR-Hydro Signals of climate variability in continental hydrology from multi-sensor space and in-situ observations and hydrological modeling (DFG/IGSSE)

DAAD Thematic Network Modern Geodetic Space Techniques for Global Change Monitoring (DAAD)

DIGERATI Direct geocentric realisation of the American reference frame by combination of geodetic observation techniques (DFG)

EXTREMES Signals of weather extremes in soil moisture and continental water storage from multi-sensor Earth observation and hydrological modeling (TUM.Diversity/Laura Bassi-Award)

FOR 584, P6 Integration of Earth rotation, gravity field and geometry using space geodetic observations (DFG)

FOR 1503, PN5-2 Consistent celestial and terrestrial reference frames by improved modeling and combination-2 (DFG)

FOR 1503, PN6-1 Consistent dynamic satellite reference frames and terrestrial geodetic datum parameters-1 (DFG)

FOR 1503, PN6-2 Consistent dynamic satellite reference frames and terrestrial geodetic datum parameters-2 (DFG)

GOCE+ WaterStorage GRACE/GOCE water storage changes over the Amazon region (ESA)

MULTIGRAV Multi-resolution representation for regional gravity field modelling (TUM.Diversity/Laura Bassi-Award)

NEG-OCEAN Variations in ocean currents, sea ice concentration and sea surface temperature along the North-East coast of Greenland (DFG)

OPTIMAP Operational Tool for Ionospheric Mapping And Prediction (ZGeoBw)

ORG4Heights Optimally combined regional geoid models for the realization of height systems in developing countries (DFG)

REWAP Monitoring and Prediction of Regional Water Availability for Agricultural Production under the Influence of Climate Anomalies and Weather Extremes (DFG/IGSSE)

SPP 1788, INSIGHT Interactions of low-orbiting satellites with the surrounding ionosphere and thermosphere (DFG)

SWARM+Innovations SLIM Swarm Magnetic Gradients for Lithospheric Modelling (ESA)

UHR-GravDat Consistent estimate of ultra-high resolution Earth surface gravity data (DFG)

WLDYN Assessing the spatiotemporal dynamics of water volumes in large wetlands and lakes by combining remote sensing with macro-scale hydrological modelling (DFG)

6 Personnel

6.1 Lectures and courses at universities

- Bloßfeld M.** Lecture “Realisierung und Anwendungen globaler geodätischer Referenzsysteme”, TUM, SS 2016
- Bloßfeld M.** Lecture “Earth System Dynamics”, TUM, WS 2016/17
- Bosch W.** Lecture “Oceanography and Satellite Altimetry”, TUM, WS 2015/16 and WS 2016/17
- Bouman J.** Lecture “Gravity and Magnetic Field from Space”, TUM, WS 2015/16
- Sánchez L.** Lecture “Vertiefende Aspekte der Höhensysteme”, TUM, WS 2016/17
- Schmidt M.** Lecture “Numerical Modelling”, TUM, WS 2015/16 and WS 2016/17
- Schmidt M.** Lecture “Numerische Methoden in der Satellitengeodäsie”, TUM, SS 2016
- Schmidt M.** Lecture “Höhere Geodäsie”, HCU, SS 2016
- Schmidt M.** Lecture “Ionosphärenmonitoring und -modellierung”, TUM, WS 2016/17
- Seitz F.** Lecture “Earth System Dynamics”, TUM, WS 2015/16
- Seitz F.** Lecture “Seminar ESPACE”, TUM, SS 2016
- Seitz F.** Doktorandenseminar des Deutschen Geodätischen Forschungsinstituts, TUM, WS 2015/16, SS 2016 and WS 2016/17
- Seitz F.** Lecture “Erdrotation”, TUM, WS 2016/17

6.2 Lectures at seminars and schools

- Seitz F.:** Lecture “Realization of global and regional geometrical reference systems of highest accuracy at DGFI-TUM”. Summer School: 1st Workshop of DAAD Thematic Network “Modern Geodetic Space Techniques for Global Change Monitoring”, Stuttgart, Germany, 2016-07-21
- Angermann D.:** Lecture “Geodäsie – Die Vermessung der Erde im Wandel der Zeit”. Ignaz-Günther-Gymnasium, Rosenheim, Germany, 2016-11-10
- Sánchez L.:** Lecture “Vertical reference systems”. Summer School: SIRGAS Workshop on Vertical Datum Unification and Realization of the IHRS in Latin America, Quito, Ecuador, 2016-11-21/25

6.3 Thesis supervision

Master and Diploma Theses

- Seitz F., Dettmering D.:** Master Thesis Kirsch S., TUM (prepared in co-operation with the German Federal Institute of Hydrology, BfG): Regionaler Meeresspiegeltrend in der Deutschen Bucht – Vergleich zwischen Satellitenaltimetrie und Pegelmessungen. 2016-02-03

Seitz F., Schmidt M. : Master Thesis Goss A., TUM (prepared in co-operation with TU Wien, Austria): Hochfrequente Variationen der Erdrotation: Physikalischer Hintergrund und numerische Simulation. 2016-02-29

Seitz F., Dettmering D. (co-supervisors): Diploma Thesis Strehl F., TU Wien, Austria (prepared in co-operation with DGFI-TUM): Berechnung von zeitlichen Variationen der Wasservolumina in Feuchtgebieten aus der Kombination von Satellitenaltimetrie und Fernerkundung – Beispielregion Pantanal. 2016-08-23

Seitz F., Dettmering D. : Master Thesis Putnam A., TUM: Pulse-limited altimeter waveform simulator. 2016-09-14

Doctoral Theses

Seitz F. (supervisor): Doctoral Thesis Abelen S., TUM: Signals of weather extremes in soil moisture and terrestrial water storage from multi-sensor Earth observations and hydrological modeling. 2016-06-27

Schmidt M. (co-supervisor): Doctoral Thesis Lieb V., TUM: Enhanced regional gravity field modeling from the combination of real data via MRR. 2016-12-22

6.4 Conferral of Doctorates

Abelen S. : *Title:* Signals of weather extremes in soil moisture and terrestrial water storage from multi-sensor Earth observations and hydrological modeling. *Supervisors:* Prof. Dr.-Ing. F. Seitz (TUM), Prof. Dr.-Ing. U. Stilla (TUM), Prof. Dr.techn. W. Wagner (TU Wien, Austria). *Day of defense:* 2016-06-27. *Institution:* TUM

Lieb V. : *Title:* Enhanced regional gravity field modeling from the combination of real data via MRR. *Supervisors:* Prof. Dr.techn. R. Pail (TUM), apl. Prof. Dr.-Ing. M. Schmidt (TUM), Prof. F. Simons, PhD (Princeton University, USA). *Day of defense:* 2016-12-22. *Institution:* TUM

6.5 TUM Graduate School

International Research Phase

Ressler G. : Academic Institution: ESA/ESTEC, Netherlands.
Duration: 2016-01-01 until 2016-12-31. Supervisor: Dr. R. Haagmans

Börgens E. : Academic Institution: Technical University of Denmark.
Duration: 2016-10-01 until 2016-12-23. Supervisor: Dr. O. Andersen

6.6 Scientific Awards

Limberger M. : Award of the Johannes B. Ortner-Stiftung of the Technical University of Munich